Gaussian-3 Studies of the Structures, Bonding, and Energetics of Selected Chemical Systems

LAW Chi–Kin

A Thesis Submitted in Partial Fulfilment

of the Requirements for the Degree of

Master of Philosophy

in

Chemistry

July 2002


香港中文大學
THE CHINESE UNIVERSITY OF HONG KONG
大學
圖書館系統
07 MAR 2003
LIBRARY SYSTEM

Gaussian-3 Studies of the Structures, Bonding, and Energetics of Selected Chemical Systems

Abstract

The Gaussian–3 (G3) and Gaussian–3X (G3X) models of theory have been applied in the following investigations: (i) Heats of formation for $(CH)_6$ isomers; (ii) Structures, stability, and nature of bonding of isomeric N_7 nitrogen clusters and their singly charged cations and anions; (iii) The dissociative photoionization channels of dimethyl sulfide; (iv) The thermochemistry of chlorine fluorides, ClF_n, n = 1–7, and their singly charged cations and anions. Furthermore, the electronic structures of carbon and silicon nanotubes, carbon and silicon nanowires have been investigated using the semi-empirical PM3 and other ab initio methods.

Our calculated results generally are in good to excellent agreement with the available experimental data. Such a good accord lends confidence and reliability to those results with no available experimental data.

Submitted by LAW Chi–Kin

for the Degree of Master of Philosophy in Chemistry

at The Chinese University of Hong Kong in (July 2002)

利用 Gaussian–3 理論研究化學體系之結構，化學鍵及能量

論文摘要

本論文採用 Gaussian–3 (G3) 和 Gaussian–3X (G3X) 理論對以下的課題進行研究：(i) $(CH)_6$ 及其同分異構物的組合熱；(ii) 氮原子簇合物 N_7 及其單電荷陽離子和陰離子的結構、穩定性和化學鍵；(iii) 二甲硫的光電離分解通道；(iv) 氟化氯 ClF_n, n = 1–7 及其單電荷陽離子和陰離子的結構與熱化學。此外，又利用半經驗的 PM3 法及其他從頭計算的理論研究納米碳管、納米矽管、納米碳綫和納米矽綫的電子結構。

與文獻列出的實驗值相比較下，我們的計算結果令人滿意。本論文的研究表明：對於某些缺乏實驗數據的反應和體系，我們可通過類似的理論取得可靠的數值結果。這些結果對反應途徑的設計和熱化學數據的測量具有指導作用。

Acknowledgments

I would like to sincerely express my gratitude to my supervisor, Professor Wai–Kee Li, for his guidance, supervision, and invaluable advises, as well as his encouragement has made this thesis possible. I have gained more than the knowledge of doing a research from him.

I also wish to thank: Professor R. Q. Zhang, at the City University of Hong Kong, who collaborate with me in the project of nanotubes and nanowires; Mr. Xin Wang, at the Sichuan University, who collaborate with me in the project of nitrogen clusters.

My thanks also goes to Mr. Chi–Lun Li, who has been work with me for two years; Mr. Justin, Kai–Chi Lau, who has been a constant source of advices and inspirations in carrying out the calculations. Furthermore, I would like to thanks all my colleagues in Room 225A and 333, Science Center (North Block), the Chinese University of Hong Kong.

Finally, I remain deeply grateful to my family. They provided me with indispensable support and wisdom during these two years.

Table of Contents

Abstract		i
Acknowledgements		iii
Table of Contents		iv
List of Tables		vi
List of Figures		viii
Chapter 1	**Introduction**	1
	1.1 The Gaussian–3 Method	1
	1.2 The G3 Method with Reduced Mϕller–Plesset Order and Basis Set	2
	1.3 The Gaussian–3X Method	2
	1.4 Calculation of Thermodynamical Data	3
	1.5 Remark on the Location of Equilibrium and Transition Structures	3
	1.6 Natural Bond Orbital (NBO) Analysis	4
	1.7 Scope of the Thesis	4
	1.8 References	5
Chapter 2	**Gaussian–3 Heats of Formation for $(CH)_6$ Isomers**	6
	2.1 Introduction	6
	2.2 Methods of Calculation and Results	7
	2.3 Discussion	9
	2.4 Conclusion	11
	2.5 Publication Note	12
	2.6 References	12
Chapter 3	**A Gaussian–3 Investigation of N_7 Isomers**	14
	3.1 Introduction	14
	3.2 Computational Method and Results	16
	3.3 Discussion	16
	3.4 Conclusion	24
	3.5 Publication Note	24
	3.6 References	24
Chapter 4	**A Gaussian–3 Study of N_7^+ and N_7^- Isomers**	27
	4.1 Introduction	27
	4.2 Computational Method and Results	29
	4.3 Discussion	30
	4.3.1 The N_7^+ isomers	30
	4.3.2 The N_7^- isomers	37
	4.4 Conclusion	41
	4.5 Publication Note	41
	4.6 References	41
Chapter 5	**Thermochemistry of Chlorine Fluorides ClF_n, n = 1–7, and Their Singly Charged Cations and Anions: A Gaussian–3 and Gaussian–3X**	45

	Study	
	5.1 Introduction	45
	5.2 Methods of Calculations	47
	5.3 Results and Discussion	48
	5.3.1 Comparison of the G3 and G3X methods	48
	5.3.2 Assessments of the experimental results	54
	5.3.3 Bond dissociation energies of ClF_n, ClF_n^+, and ClF_n^-	57
	5.3.4 Summary of the thermochemical data.	58
	5.4 Conclusion	59
	5.5 Publication Note	60
	5.6 References	60
Chapter 6	**A Gaussian–3 Study of the Photoionization and Dissociative Photoionization Channels of Dimethyl Sulfide**	63
	6.1 Introduction	63
	6.2 Methods of Calculations	64
	6.3 Results and Discussion	64
	6.3.1 Bond cleavage reactions	67
	6.3.2 Dissociation channels involving transition structures	68
	6.4 Conclusion	70
	6.5 Publication Note	70
	6.6 References	70
Chapter 7	**Theoretical Study of the Electronic Structures of Carbon and Silicon Nanotubes, Carbon and Silicon Nanowires**	72
	7.1 Introduction	72
	7.2 Models and Computational Methods	74
	7.3 Results and Discussion	75
	7.4 Conclusion	87
	7.5 Publication Note	87
	7.6 References	87
Chapter 8	**Conclusion**	90
Appendix A		91
Appendix B		93

List of Tables

Chapter 2

Table 1	Total energies (in hartrees) at 0 K (E_0) and enthalpies at 298 K (H_{298}) for the $(CH)_6$ isomers calculated at various G2 and G3 levels	9
Table 2	Heats of formation (kJ mol^{-1}) at 0 K (ΔH_{f0}) and 298 .K (ΔH_{f298}) for the $(CH)_6$ isomers calculated at various G2 and G3 levels using the atomizatiom scheme	10
Table 3	Heats of formation (kJ mol^{-1}) at 0 K (ΔH_{f0}) and 298 K (ΔH_{f298}) for the $(CH)_6$ isomers calculated at various G2 and G3 levels using isodesmic bond separation reactions	11

Chapter 3

Table 1	The G3 energies at 0 K (E_0), enthalpies at 298 K (H_{298}), heats of formation at 0 K (ΔH_{f0}), and at 298 K (ΔH_{f298}) of the twelve N_7 isomers	14
Table 2	Some significant donor-acceptor natural bond orbital interactions and their second-order perturbation stabilization energies, $\Delta E_{(2)}$ (kJ mol^{-1}), calculated at the MP2(FU)/6–31G(d) level	14

Chapter 4

Table 1	The G3 total energies (E_0) and enthalpies (H_{298}), and the standard heats of formation at 0 and 298 K (ΔH_{f0} and ΔH_{f298}) of N_7^+ and N_7^- isomers	31
Table 2	Significant donor-acceptor natural bond orbital interactions in N_7^+ and N_7^- isomers and their second-order perturbation stabilization energies, $\Delta E_{(2)}$ (kJ mol^{-1}), calculated at the MP2(FU)/6–31G(d) level	34
Table 3	The G3 IEs and EAs of N_7 isomers	36

Chapter 5

Table 1	G3 and G3X total energies (E_0), enthalpies (H_{298}), standard heats of formation at 0 K (ΔH_{f0}), and 298 K (ΔH_{f298}) of chlorine fluorides	51
Table 2	G3 and G3X total energies (E_0), enthalpies (H_{298}), standard heats of formation at 0 K (ΔH_{f0}), and 298 K (ΔH_{f298}) of chlorine fluorides cations	52
Table 3	G3 and G3X total energies (E_0), enthalpies (H_{298}), standard heats of formation at 0 K (ΔH_{f0}), and 298 K (ΔH_{f298}) of chlorine fluorides anions	53
Table 4	G3 and G3X IEs and EAs of chlorine fluorides.	54

Table 5 G3X and G3 bond dissociation energies (in kJ mol^{-1}) at 0 K for chlorine fluorides and their ions 57

Chapter 6

Table 1 Appearance energies (AEs) and E_{ex}-onset values for CH_2SH^+ (CH_3S^+), CH_2S^+, CHS^+, and CH_3^+ determined in the CID of $CH_3SCH_3^+$ + Ar and photoionization of CH_3SCH_3, respectively. 65

Table 2 G3 total energies (E_0), enthalpies (H_{298}), and standard heats of formation at 0 K ($\Delta H°_{f0}$) and 298 K ($\Delta H°_{f298}$) of the species involved in the dissociation of dimethyl sulfide and its cation 66

Table 3 Experimental and calculated $\Delta H°_0$ (eV) of the dissociation of the dimethyl sulfide 67

Chapter 7

Table 1 Electronic energy levels for a C atom and a Si atom obtained from PM3 calculations 78

List of Figures

Chapter 3

Figure 1	The structures of twelve N_7 isomers optimized at the MP2(FU)/6–31G(d) level, bond distance in Å and angle in degree (bold font)	18
Figure 2	NBO description for the twelve N_7 isomers identified in this work. The dotted line represents a one-electron bond (see text)	21

Chapter 4

Figure 1	The structures of one N_7 (**XIII**), four N_7^+, and seven N_7^- isomers optimized at the MP2(FU)/6–31G(d) level, bond distances are in Å and bond angles in degrees (bold font)	32
Figure 2	NBO description for the eleven N_7^+ and N_7^- isomers identified in this work	35

Chapter 5

Figure 1	Theoretical equilibrium structures of chlorine fluorides and their singly charged cations and anions optimized at the levels of MP2(Full)/6–31G(d) (normal font) and B3LYP/6–31G(2df,p) (bold font)	49
Figure 2	Summary of the G3X thermochemical data of the chlorine fluorides and their ions, illustrating the alternating patterns of the data	59

Chapter 6

Figure 1	Structural formula of the stable species involved in the dissociation of dimethyl sulfide, along with their symmetry point groups and electronic states	65
Figure 2	Potential energy surface showing the possible mechanism for dissociation $CH_3SCH_3^+ \rightarrow CH_2SH^+ + CH_3$	68
Figure 3	Potential energy surface showing the possible mechanism for dissociation $CH_3SCH_3^+ \rightarrow CH_2S^+ + CH_4$	69

Chapter 7

Figure 1	Four model compounds: a diamond nanowire $C_{54}H_{60}$ (1), a silicon nanowire $Si_{54}H_{60}$ (2), a carbon nanotube $C_{54}H_{12}$ (3), and a silicon nanotube $Si_{54}H_{12}$ (4)	76
Figure 2(a)	The TDOS and PDOS of diamond nanowire $C_{54}H_{60}$ (1)	79
Figure 2(b)	The TDOS and PDOS of silicon nanowire $Si_{54}H_{60}$ (2)	80
Figure 2(c)	The TDOS and PDOS of carbon nanotube $C_{54}H_{12}$ (3)	81

Figure 2(d)	The TDOS and PDOS of silicon nanotube $Si_{54}H_{12}$ (4)	82
Figure 3(a)	The PDOS and ODOS of one representative atom (the circled one) for each structure shown in Figure 1: diamond nanowire $C_{54}H_{60}$ (1)	83
Figure 3(b)	The PDOS and ODOS of one representative atom (the circled one) for each structure shown in Figure 1: silicon nanowire $Si_{54}H_{60}$ (2)	84
Figure 3(c)	The PDOS and ODOS of one representative atom (the circled one) for each structure shown in Figure 1: carbon nanotube $C_{54}H_{12}$ (3)	84
Figure 3(d)	The PDOS and ODOS of one representative atom (the circled one) for each structure shown in Figure 1: silicon nanotube $Si_{54}H_{12}$ (4)	85

Chapter 1
Introduction

Accurate calculation of molecular energies is one of the major tasks of quantum chemistry. At present, quantum mechanical methods for the calculation of thermochemical data have developed beyond the reproduction of experimental results; these methods are now able to make reliable predictions where experimental data appear to be uncertain or do not exist at all. It is now certain that the future of quantum chemistry and the future of chemistry are inextricably linked. In the past decade or so, Pople and his co–workers proposed a series of ab initio methods, the Gaussian–n (Gn) models,[1–11] in order to achieve the goal of accurate calculation of molecular energies. They have now developed a general procedure for accurate energies applicable for a variety of molecular systems. The Gn models, based on a series of additivity approximations,[8,9] consist of a sequence of single–point calculations to provide an accurate prediction on the energetics of a given molecular system. Up to now, there are three main Gn models: Gaussian–1 (G1),[1,2] Gaussian–2 (G2),[3,4] and Gaussian–3 (G3)[5–7]. In addition, there are less expensive variants of these models (*vide infra*). These methods have now been shown to be able to determine the energetics for molecular systems of various sizes with an average absolute deviation from experiment to be within 10 kJ mol^{-1} (or ~2 kcal mol^{-1}).

Since the G1 and G2 models in general yield results less accurate than G3, these methods have not been applied to the projects presented in this thesis. In this thesis, we mainly employ the G3 method and its variants including G3(MP2)[6] and G3X[7] to study the structures and energetics of some selected chemical systems.

1.1 The Gaussian–3 Method

The G3 energy is an approximation of the molecular energy at the QCISD(T)/G3large level, where G3large is a modified 6–311+G(3df,2p) basis set. In the G3 model, structures are optimized at the second–order Møller–Plesset theory (MP2) using the 6–31G(d) basis set with all electrons included, i.e., at the MP2(Full)/6–31G(d) level. Based on these optimized structures, single–point

calculations at QCISD(T)/6–31G(d), MP4/6–31G(d), MP4/6–31+G(d), MP4/6–31G(2df,p), and MP2(Full)/G3large levels are required. Also, this model requires higher level correction (HLC) in the calculation of total electronic energies (E_e). The HLC is $-6.386 \times 10^{-3} n_\beta - 2.977 \times 10^{-3}(n_\alpha - n_\beta)$ for molecules and $-6.219 \times 10^{-3} n_\beta - 1.185 \times 10^{-3}(n_\alpha - n_\beta)$ for atoms, in which n_α and n_β are the number of α and β electrons, respectively, with $n_\alpha \geq n_\beta$. The MP2(Full)/6–31G(d) harmonic vibrational frequencies, scaled by 0.9661,[13] are applied for the zero–point vibrational energy (ZPVE) correction at 0 K ($E_0 = E_e + \text{ZPVE}$).

The G3 theory has been used to calculate molecular energies, such as atomization energies,[2–9] ionization energies,[2,10] proton affinities,[2,10] and electron affinities[2] of 125 molecules for which these quantities have been well established experimentally. The average absolute deviation is about 1.02 kcal mol^{-1} (or ~4 kJ mol^{-1}).[5] Detailed methodology of the G3 theory is given in Appendix A.

1.2 The G3 Method with Reduced Mϕller–Plesset Order and Basis Set

An economical variant of the G3 theory, G3(MP2), has been introduced by Pople et al. recently.[6] The G3(MP2) model involves only two single–point energy calculations at the QCISD(T)/6–31G(d) and MP2/G3MP2large levels, based on the geometry optimized at the MP2(Full)/6–31G(d) level. The G3MP2large basis set is the same as the aforementioned G3large basis set, except the core polarization functions have been removed.[6] HLC is also included to yield the E_e of the molecule, where HLC = $-9.729 \times 10^{-3} n_\beta - 4.471 \times 10^{-3}(n_\alpha - n_\beta)$ for molecules and $-9.345 \times 10^{-3} n_\beta - 2.021 \times 10^{-3}(n_\alpha - n_\beta)$ for atoms. Similar to the G3 method, the MP2(Full)/6–31G(d) vibrational frequencies, scaled by 0.9661,[13] are applied for the ZPVE correction at 0 K to give the total energy of (E_0) for the molecule.

It is noted that the G3(MP2) method is able to yield results with average absolute deviations of 1.3 kcal mol^{-1} (or ~5.4 kJ mol^{-1}), when compared with the 299 energies determined by experiments.[5]

1.3 The Gaussian–3X Method

Since the G3 theory still does poorly for some of the larger non–hydrogen systems containing second–row atoms such as the hypervalent molecules SF_6 and

PF_5, etc., a modification of the G3 theory, called Gaussian–3X (G3X), has been developed in 2001.[7] This new method shows an improvement for the energetics of non–hydrogen systems over the G3 theory: the G3 mean absolute deviation is 2.11 kcal mol^{-1} (or ~8.8 kJ mol^{-1}) for the 47 non–hydrogen species in the G3/99 test set,[12] while the corresponding deviation for the G3X method is 1.49 kcal mol^{-1} (or ~6.2 kJ mol^{-1}).

In the G3X model, all the structures are now optimized at the B3LYP/6–31G(2df,p) level. In the energy calculations, apart from the five single–points in the G3 model, an additional one, HF/G3Xlarge, is required. Comparing the G3Xlarge and the G3large basis sets, there is an additional g polarization function in the former for second–row elements Al–Cl. In other words, there is no g function for Na and Mg. HLC is also included to account for the remaining basis set deficiencies: HLC = $-6.783 \times 10^{-3} n_\beta - 3.083 \times 10^{-3}(n_\alpha - n_\beta)$ for molecules and $-6.877 \times 10^{-3} n_\beta - 1.152 \times 10^{-3}(n_\alpha - n_\beta)$ for atoms. In this model, all optimized structures are characterized by vibrational frequencies calculations at the B3LYP/6–31G(2df,p) level. A scaling factor[13] of 0.9854 was used for the ZPVE corrections. The mathematical details of the G3X theory are described in Appendix A.

1.4 Calculation of Thermodynamical Data

The heats of formation at temperature T (ΔH°_{fT}) in this work were calculated in the following manner. For molecule AB, its Gn ΔH°_{fT} was calculated from the corresponding heat of reaction $\Delta H^\circ_{rT}(A + B \rightarrow AB)$ and the respective experimental $\Delta H^\circ_{fT}(A)$ and $\Delta H^\circ_{fT}(B)$ for elements A and B. In the calculations of ΔH°_{rT} for anions, we set the ΔH°_{rT} value of a free electron to be zero.

1.5 Remark on the Location of Equilibrium and Transition Structures

In this thesis, all stationary points on the potential energy surface were characterized by vibrational frequency calculations. In other words, equilibrium structures have only real vibrational frequencies, while transition structures (TSs) have one and only one imaginary frequency. In addition, for each TS located, the "reactant(s)" and "product(s)" were verified by intrinsic reaction coordinate (IRC) calculations. In addition, for the dissociation channels which we claim to involve

only bond breaking and no TSs, we did try to locate the TS(s) for them and found none.

1.6 Natural Bond Orbital (NBO) Analysis

The Natural Bond Orbital (NBO) analysis is carried out in order to study the bonding and interactions in the various identified N_7, N_7^+, and N_7^- isomers in Chapters 3 and 4. The bond interaction in the various isomers is discussed in terms of stabilization energies, $\Delta E_{(2)}$, which is calculated by the second-order perturbation analysis of Fock matrix obtained in the NBO analysis.[14] By this perturbational approach, the donor-acceptor interactrion involving a filled orbital φ (donor) and an unfilled antibonding orbital φ^* (acceptor) can be quantitatively described. Specifically, this stabilization energy is calculated by the following expression:

$$\Delta_{\varphi\varphi^*}E_{(2)} = -2\frac{(<\varphi \mid F \mid \varphi^* >)^2}{\varepsilon_{\varphi^*} - \varepsilon_{\varphi}}$$

where F is the Fock operator and ε_{φ} and ε_{φ^*} are the NBO energies of the donor and acceptor orbitals.[15]

1.7 Scope of the Thesis

In the following chapters, the calculation results of a number of molecular systems will be discussed. In Chapter 2, the heats of formation of $(CH)_6$ isomer are studied. The structures, stability, and nature of bonding of isomeric N_7 nitrogen clusters and their singly charged ions will be discussed in Chapters 3 and 4, respectively. The method empolyed in these three chapters was the G3 model of theory. In Chapter 5, the structures and energetics of chlorine fluorides ClF_n, n = 1–7, as well as their singly charged cations and anions are investigated with the G3 and G3X methods. The relative merits of these two methods are then assessed in this work as well. The dissociation mechanisms of dimethyl sulfide (CH_3SCH_3) with the G3 model of theory will be discussed in Chapters 6. In Chapter 7, the electronic structures of carbon and silicon nanotubes, carbon and silicon nanowires are investigated with the semi-empirical PM3 and other ab initio methods. Finally, a conclusion will be given in Chapter 8.

Editorial Note: Each chapter of this thesis should be treated as separate entity. In

other words, it has its own numbering system for molecular species, equations, tables, figures, and references.

1.8 References

1. Pople, J. A.; Head-Gordon, M.; Fox, D. J.; Raghavachari, K.; Curtiss, L. A. *J. Chem. Phys.* **1989**, *90*, 5622.
2. Curtiss, L. A.; Jones, C.; Trucks, G. W.; Raghavachari, K.; Pople, J. A. *J. Chem Phys.* **1990**, *93*, 2537.
3. Curtiss, L. A.; Raghavachari, K.; Trucks, G. W.; Pople, J. A. *J. Chem. Phys.* **1991**, *94*, 7221.
4. Curtiss, L. A.; Raghavachari, K.; Pople, J. A. *J. Chem. Phys.* **1993**, *98*, 1293.
5. Curtiss, L. A.; Raghavachari, K.; Redfern, P. C.; Rassolov, V. R.; Pople, J. A. *J. Chem. Phys.* **1998**, *109*, 7764.
6. Curtiss, L. A.; Redfern, P. C.; Raghavachari, K.; Rassolov, V. R.; Pople, J. A. *J. Chem. Phys.* **1999**, *110*, 4703.
7. Curtiss, L. A.; Redfern, P. C.; Raghavachari, K.; Pople, J. A. *J. Chem. Phys.* **2001**, *114*, 108.
8. Curtiss, L. A.; Carpenter, J. E.; Raghavachari, K.; Pople, J. A. *J. Chem. Phys.* **1992**, *96*, 9030.
9. Curtiss, L. A.; Raghavachari, K.; Pople, J. A. *Chem. Phys. Lett.* **1993**, *214*, 183.
10. Curtiss, L. A.; Raghavachari, K.; Redfern, P. C.; Pople, J. A. *J. Chem. Phys.* **1997**, *106*, 1063.
11. Curtiss, L. A.; Raghavachari, K.; Redfern, P. C.; Pople, J. A. *J. Chem. Phys.* **1998**, *109*, 42.
12. Curtiss, L. A.; Raghavachari, K.; Redfern, P. C.; Pople, J. A. *J. Chem. Phys.* **2000**, *112*, 7374.
13. Scott, A. P.; Radom, L. *J. Phys. Chem.* **1996**, *100*, 16502.
14. Reed, A. E.; Curtiss, L. A.; Weinhold, F. *Chem. Rev.* **1988**, *88*, 899.
15. Klaptke, T. M.; Schulz, A. *Quantum Chemical Methods in Main-Group Chemistry*, Chichester, John Wilay & Sons, **1998**.

Chapter 2

Gaussian–3 Heats of Formation for $(CH)_6$ Isomers

Abstract

The heats of formation for the five $(CH)_6$ valence isomers have been calculated using both the atomization and isodesmic bond separation schemes with the G3 and G3(MP2) methods of theory. The results obtained suggest that the accumulated small component errors found in the G2–based methods are significantly reduced in the G3 methods. Also, a combination of either the G2 or G3 with the isodesmic scheme affords accurate thermochemical data for relative large hydrocarbon systems such as benzene and its isomers.

At the G3 level, using the isodesmic bond separation scheme, we obtain the following ΔH_{f0} values (in kJ mol^{-1}) for the following five $(CH)_6$ isomers: 100.8 for benzene (**1**) (compared to the experimental value of 100.4 ± 1), 423.9 for Dewar benzene (**2**), 580.0 for prismane (**3**), 405.5 for benzvalene (**4**), and 600.7 for 3,3'-bicyclopropenyl (**5**). At the same level with the same scheme, the calculated ΔH_{f298} values for isomers **1** to **5** are, respectively, 82.3 (compared to experimental value of 82.9 ± 0.3), 405.2, 559.8, 386.3, and 586.0 kJ mol^{-1}.

2.1 Introduction

In a previous work,[1] four Gaussian–2 (G2) based methods, namely, G2,[2] G2(MP2),[3] G2(MP3),[3] and G2(MP2,SVP),[4,5] were applied to calculate the heats of formation for five $(CH)_6$ isomers, using both the atomization[5] and isodesmic bond separation[6] schemes. The five $(CH)_6$ isomers studied included benzene (**1**), Dewar benzene (**2**), prismane (**3**), benzvalene (**4**), and 3,3'-bicyclopropenyl (**5**) (*Chemical Abstracts* name: bi-2-cyclopropen-1-yl). Upon analyzing the results obtained, several interesting observations may be made. First, with the atomization scheme, the four G2–based methods can lead to ΔH_f values that differ by as much as 30 kJ mol^{-1}. Moreover, for benzene, the only isomer whose listed experimental data are suitable for comparison

with ab initio results, even the "best" method, G2(MP2,SVP), yields ΔH_f values that are 5–7 kJ mol^{-1} off the experimental results. On the other hand, with the isodesmic scheme, the G2–based methods lead to ΔH_f values that are within 5 kJ mol^{-1} of each other. Also, using this scheme, the "best methods", G2 and G2(MP2,SVP) in this case, lead to ΔH_f values for benzene that are within 1 kJ mol^{-1} of the experimental results. Based on these observations, it may be concluded that the G2 methods suffer from "an unfavorable accumulation of small component errors" when applied to relatively large systems, a conclusion previously drawn by Nicolaides and Radom.[5] However, such a deficiency may be circumvented by the isodesmic scheme. Also, the accumulation of errors in the G2–based methods is reflected in the relatively large difference (10–20 kJ mol^{-1}) between the ΔH_f values obtained using the atomization and isodesmic schemes.

Recently, Pople and coworkers proposed the Gaussian–3 (G3)[7] method, which is believed to be superior to G2. With the G3 method, using the atomization scheme, the average absolute deviation from experimental ΔH_f values for 148 species is 4 kJ mol^{-1}, as compared to 7 kJ mol^{-1} for G2. Within the past two years, we have applied the G3 model to study the thermochemistry of hydrochlorofluoromethanes[8] and hydrochlorofluoro-silanes[9] and it is found that the G3 method yields very satisfactory ΔH_f values for these fairly large systems. [It should be noted that halomethanes are one of the systems that G2 does not treat very well.] In addition, we also applied the more recently developed G3(MP2)[10] method to the aforementioned silanes.[9] The G3(MP2) method is a computationally less expensive variant of the G3 protocol.

In the present work, we apply both the G3 and G3(MP2) methods to calculate the heats of formation for the five $(CH)_6$ valence isomers. In addition to arriving at reliable results for these thermochemical quantities, this project is also an attempt to determine whether the accumulation of errors found in the G2–based methods is eliminated, or at least reduced.

2.2 Methods of Calculation and Results

All calculations were carried out on DEC500au, COMPAQ XP900 and SGI10000 workstations, as well as on an SGI Origin 2000 High Performance Server,

using the Gaussian 98 package of programs.[11] The computational methods we employed were the aforementioned G3 and G3(MP2) levels of theory.

The total energies at 0 K (E_0) and enthalpies at 298 K (H_{298}) for the five $(CH)_6$ isomers calculated at the G3 and G3(MP2) levels are tabulated in Table 1. Also included in this table are the E_0 and H_{298} values for the five isomers calculated at the G2 and G2(MP2) levels of theory; these results have already been reported in Ref 1.

The result in Table 1 can then be transformed into the heats of formation ΔH_{f0} and ΔH_{f298} for the isomers using either the atomization or isodesmic bond separation schemes. In the former,[1,5] ΔH_{f0} was obtained from theoretical atomization energies in conjunction with standard ΔH_{f0} value for the atom. Furthermore, ΔH_{f298} was obtained using theoretical enthalpy temperature corrections for the species under consideration, evaluated with statistical thermodynamics formulas in combination with literature values of enthalpy temperature corrections for elements in their standard states. The G3 and G3(MP2) heats of formation at 0 K and 298 K calculated with the atomization scheme are summarized in Table 2. For easy comparison, the ΔH_{f0} and ΔH_{f298} values of the $(CH)_6$ isomers calculated with the G2 and G2(MP2) methods using same scheme are also included in this table; these results are taken from our previous studies.[1]

In addition to the atomization scheme, the G3 and G3(MP2) ΔH_{f0} values for the $(CH)_6$ isomers were also calculated with the following isodesmic bond separation reaction:[1,6]

$$\mathbf{1} + 6CH_4 \rightarrow 3C_2H_6 + 3C_2H_4 \quad (1)$$

$$\mathbf{2} + 8CH_4 \rightarrow 5C_2H_6 + 2C_2H_4 \quad (2)$$

$$\mathbf{3} + 12CH_4 \rightarrow 9C_2H_6 \quad (3)$$

$$\mathbf{4} + 10CH_4 \rightarrow 7C_2H_6 + C_2H_4 \quad (4)$$

$$\mathbf{5} + 8CH_4 \rightarrow 5C_2H_6 + 2C_2H_4 \quad (5)$$

The G3 and G3(MP2) ΔH_{f0} and ΔH_{f298} values calculated with this scheme are listed in Table 3, along with those results obtained with two G2–based methods taken from our previous studies .[1]

Table 1: Total energies (in hartrees) at 0 K (E_0) and enthalpies at 298 K (H_{298}) for the $(CH)_6$ isomers calculated at various G2 and G3 levels[a]

	Benzene (1)	Dewar benzene (2)	Prismane (3)	Benzvalene (4)	3,3'–Bicyclo-propenyl (5)
E_0 values					
G2(MP2)	–231.77625	–231.65581	–231.59778	–231.66265	–231.58811
G2	–231.78053	–231.66023	–231.60179	–231.66677	–231.59240
G3(MP2)	–231.82975	–231.70596	–231.64539	–231.71225	–231.63825
G3	–232.05220	–231.92893	–231.86887	–231.93554	–231.86145
H_{298} values					
G2(MP2)	–231.77080	–231.65023	–231.59273	–231.65736	–231.58116
G2	–231.77508	–231.65465	–231.59673	–231.66147	–231.58545
G3(MP2)	–231.82430	–231.70038	–231.64038	–231.70695	–231.63130
G3	–232.04675	–231.92336	–231.86381	–231.93024	–231.85451

[a] The G2(MP2) and G2 results are taken from Ref 1.

2.3 Discussion

Before discussing the G3 and G3(MP2) results, it is noted that experimental heats of formation for **1**, **2**, and **4** are also listed in Tables 2 and 3 for comparison. However, among these experimental results, only those of benzene (**1**) are gas-phase measurements, which may be compared directly with high-level computational results. Meanwhile, the experimental heats of formation for **4** was determined by its heats of isomerization to **1** *in solution*,[12] and those of **2** were estimated from the heat of rearrangement of hexamethyl Dewar benzene to hexamethylbenzene.[13] Hence, strictly speaking, the experimental results for **2** and **4** should not be compared directly with our G3/G3(MP2) results; they are included in Table 2 and 3 for reference only.

Examining the results for **1** listed in Table 2, it is seen that the accumulated small component errors of the G2–based methods are eliminated to a significant extent in the G3 and G3(MP2) methods. For the ΔH_{f0} of **1**, the G2 and G2(MP2) values are off by 16.5 and 21.1 kJ mol^{-1}, respectively, while the errors of these methods for the ΔH_{f298} of **1** are even larger. On the other hand, these errors (in the order of 15–20 kJ mol^{-1}) are reduced to 2–5 kJ mol^{-1} in the G3 and G3(MP2) results. Such a significant reduction is indeed noteworthy. At the same time, employing the isodesmic scheme to circumvent

the accumulation of errors, both the G2– and G3–based methods lead to excellent results for **1**, with errors of about 3 kJ mol^{-1} or even less.

Table 2: Heats of formation (kJ mol^{-1}) at 0 K (ΔH_{f0}) and 298 K (ΔH_{f298}) for the $(CH)_6$ isomers calculated at various G2 and G3 levels using the atomizatiom scheme[a]

	Benzene (**1**)	Dewar benzene (**2**)	Prismane (**3**)	Benzvalene (**4**)	3,3'–Bicyclo-propenyl (**5**)
ΔH_{f0} values [b]					
G2(MP2)	121.5	437.7	590.1	419.8	615.5
G2	116.9	432.6	586.2	415.6	610.8
G3(MP2)	95.1	420.2	579.1	403.6	597.9
G3	102.5	426.1	583.8	408.8	603.9
Experimental [c]	100.4±1	382	–	382	–
ΔH_{f298} values [d]					
G2(MP2)	105.7	422.7	573.7	404.1	604.2
G2	101.1	417.6	569.8	399.9	599.5
G3(MP2)	80.1	405.5	563.0	388.2	586.8
G3	87.4	411.4	567.7	393.3	592.2
Experimental [c]	82.9±0.3	364	–	363	–

[a] The G2(MP2) and G2 results are taken from Ref 1. [b] To obtain these ΔH_{f0} values, in addition to the E_0 values given in Table 1, we also require the E_0 values for the C and H atoms. In the order of G2(MP2), G2, G3(MP2) and G3, the E_0 values for C are –37.78390, –37.78432, –37.78934 and –37.82772 hartrees. The corresponding E_0 values for H are –0.50000, –0.50000, –0.50184 and –0.50100 hartree. [c] Experimental values are taken from Ref 14. [d] To obtain these ΔH_{f298} values, in addition to the H_{298} values in Table 1, we also require the H_{298} values for the C and H atoms. We can obtain these quantities by adding $E_{trans} + PV$ (=2.5RT = 0.00236 hartree at 298 K) to their E_0 values.

For the remaining four isomers, to assess the performance of the G3–based methods, we no longer have the advantage of making direct comparison between the calculated and experimental results. However, if we hold the view that errors in the atomization scheme are reduced in the isodesmic scheme, we may use the difference in ΔH_{f0} values obtained with these two schemes as an indicator of the degree to which the accumulated errors are lowered. For **1**, these differences are in the range of 16–21 kJ mol^{-1} for the G2–based methods; they are reduced to 2–8 kJ mol^{-1}. For isomers **2–5**, the differences for the G3–based methods remain fairly constant, ranging from 2–3 kJ mol^{-1} for most of them to 6–8 kJ mol^{-1} for a few. These differences represent very significant

reduction from those of the G2–based methods. For the G2–based methods, the aforementioned differences for isomers **2–5** are in the range of 17–24 kJ mol^{-1}.

Table 3: Heats of formation (kJ mol^{-1}) at 0 K (ΔH_{f0}) and 298 K (ΔH_{f298}) for the $(CH)_6$ isomers calculated at various G2 and G3 levels using isodesmic bond separation reactions[a]

	Benzene (**1**)	Dewar benzene (**2**)	Prismane (**3**)	Benzvalene (**4**)	3,3'–Bicyclo-propenyl (**5**)
ΔH_{f0} values [b]					
G2(MP2)	102.8	418.7	570.5	400.4	596.5
G2	100.5	415.5	567.5	397.5	593.6
G3(MP2)	103.5	426.0	580.2	407.2	603.9
G3	100.8	423.9	580.0	405.5	600.7
Experimental [c]	100.4±1	382	–	382	–
ΔH_{f298} values [d]					
G2(MP2)	84.2	400.2	549.9	380.8	581.5
G2	82.0	397.1	547.0	378.1	578.8
G3(MP2)	85.1	407.8	560.0	387.9	589.1
G3	82.3	405.2	559.8	386.3	586.0
Experimental [c]	82.9±0.3	364	–	363	–

[a] The G2(MP2,SVP), G2(MP2) and G2 results are taken from Ref 1. [b] To obtain these ΔH_{f0} values, in addition to the E_0 values given in Table 1, we also require the E_0 values for CH_4, C_2H_4 and C_2H_6. In the order of G2(MP2), G2, G3(MP2) and G3, the E_0 values for CH_4 are –40.40968, –40.41091, –40.42210 and –40.45762 hartrees . The corresponding E_0 values for C_2H_4 are –78.41428, –78.41592, –78.43477 and –78.50741 hartrees. Those for C_2H_6 are –79.62893, –79.63088, –79.65120 and –79.72339 hartrees. [c] Experimental values are taken from Ref 14. [d] To obtain these ΔH_{f298} values, in addition to the H_{298} values given in Table 1, we also require the H_{298} values for CH_4, C_2H_4 and C_2H_6. In the order of G2(MP2), G2, G3(MP2) and G3, the H_{298} values for CH_4 are –40.40587, –40.40709, –40.41828 and –40.45380 hartrees . The corresponding quantities for C_2H_4 are –78.41028, –78.41191, –78.43077 and –78.50341 hartrees. Those for C_2H_6 are –79.62445, –79.62640, –79.64671 and –79.71890 hartrees.

2.4 Conclusion

Based on the G3 and G3(MP2) results obtained for relatively large system such as the $(CH)_6$ isomers, it is found that the accumulated small error components found in G2–based methods are reduced to a large extent in the G3–based methods. At the same

time, both the G2 and G3 methods combined with the isodesmic scheme should lead to accurate thermochemical data for relatively large hydrocarbon compounds.

2.5 Publication Note

An article based on the results reported in this Chapter has now appeared in *J. Mol. Struct. (Theochem)* **2001**, *572*, 243.

2.6 References

(1) Cheung, Y.-S.; Wong, C.-K.; Li, W.-K. *J. Mol. Struct. (Theochem)* **1998**, *454*, 17.

(2) Curtiss, L.A.; Raghavachari, K.; Trucks, G.W.; Pople, J.A. *J. Chem. Phys.* **1991**, *94*, 7221.

(3) Curtiss, L.A.; Raghavachari, K.; Trucks, G.W.; Pople, J.A. *J. Chem. Phys.* 98 (1993) 1293.

(4) Curtiss, L.A.; Redfern, P.C.; Smith, B.J.; Radom, L. J. *Chem. Phys.* **1996,** *104*, 5148.

(5) Nicolaides, A.; Radom, L. *Mol. Phys.* **1996**, *88*, 759.

(6) Raghavachari, K.; Stefanor, B. B.; Curtiss, L.A. *J. Chem. Phys.* **1997**, *106*, 6764.

(7) L.A. Curtiss, L. A.; Raghavachari, K.; Redfern, P.C.; Rassolov, V.; Pople, J. A. *J. Chem. Phys.* **1998**, *109*, 7764.

(8) Ma, N. L.; Lau, K.-C.; Chien, S.-H.; Li, W.-K. *Chem. Phys. Lett.* **1999**, *311*, 275.

(9) Chien, S.-H.; Li, W.-K.; Ma, N.-L. *J. Phys. Chem. A* **2000**, *104*, 11398.

(10) Curtiss, L. A.; Raghavachari, K.; Redfern, P. C.; Rassolov, V.; Pople, J. A. *J. Phys. Chem A* **1999**, *110*, 4703.

(11) Frisch, M. J.; Trucks, G. W.; Schlegel, H. B.; Scuseria, G. E.; Robb, M. A.; Cheeseman, J. R.; Zakrzewski, V. G.; Montgogery, J. A.; Jr.; Stratmann, R.E.; Burant, J. C.; Dapprich, S.; Millam, J. M.; Daniels, A. D.; Kudin, K. N.; Strain, M. C.; Farkas, O.; Tomasi, J.; Barone, V.; Cossi, M.; Cammi, R.; Mennucci, B.; Pomelli, C.; Adamo, C.; Clifford, S.; Ochterski, J.; Petersson, G. A.; Ayala, P. Y.; Cui, Q.; Morokuma, K.; Malick, D. K.; Rabuck, A. D.; Raghavachari, K.; Foresman, J. B.; Cioslowski, J.; Ortiz, J. V.; Baboul, A. G.; Stefanov, B. B.; Liu, G.; Liashenko, A.; Piskorz, P.; Komaromi, I.; Gomperts, R.; Martin, R. L.; Fox, D.

J.; Keith, T.; Al-Laham, M. A.; Peng, C. Y.; Nanayakkara, A.; Gonzalez, C.; Challacombe, M.; Gill, P. M. W.; Johnson, B.; Chen, W.; Wong, M. W.; Andres, J. L.; Gonzalez, C.; Head-Gordon, M.; Replogle, E. S.; Pople, J. A. *GAUSSIAN 98*, Revision A.7; Gaussian, Inc., Pittsburgh PA, 1998.

(12) Turro, N. J.; Renner, C. A.; Katz, T. J.; Wiberg, K. B.; Cannon, H. A. *Tetrahedron Lett.* **1976**, 4133.

(13) H.M. Rosenstock, H. M.; Dannacher, J.; Liebman, Radiat. J. F. *Phys. Chem.* **1982**, *20*, 7.

(14) Lias, S.G.; Bartmess, J. E.; Liebman, J. F.; Holmes, J. F.; Levin, R. E.; Mallard, W. J. *J. Phys. Chem. Ref. Data Suppl 1*, **1988**, 231.

Chapter 3

A Gaussian–3 Investigation of N_7 Isomers

Abstract

A Gaussian–3 (G3) investigation has been carried out to examine twelve (low-spin) isomers of N_7 clusters. Of these twelve species, five are reported for the first time. All of them are identified as local minima on the MP2(FU)/6–31G(d) potential energy surface. The most stable N_7 isomer is **I**, which consists of a five-membered ring and a side chain with C_s symmetry. This is one of the isomers that are reported for the first time. Natural bond orbital analysis is also carried out in order to study the bonding of the isomers. Some non-classical structures are found. The stability of some of the more stable isomers is enhanced by conjugation or hyperconjugation.

3.1 Introduction

Chemists have long been interested in finding new materials that can be used to store large amounts of energy. The crucial characteristic of these materials is the ratio between energy released in a fragmentation reaction and the specific weight. The compounds with a high value of this ratio are called high-energy-density materials (HEDMs). Nitrogen clusters, the most studied among these systems, have received considerable attention for a long time.[1-10] Many hypothetical stable structures have been predicted theoretically for the nitrogen clusters, such as N_4,[1-3] N_6,[2-5] N_8,[2,3,6,7] N_{10},[3,8] and N_{20}.[9,10] These theoretical investigations show that many N_{2n} ($n \geq 2$) clusters have much higher energy than the energy of n N_2 molecules. If synthesized, these clusters would be HEDMs. But most of these molecules still await experimental confirmation.

Recently, the N_5^+ cation, a cluster with an odd-number of nitrogen atoms, was synthesized.[11] The novel N_5^+ cation, first predicted to be stable theoretically by Pyykkö in 1991,[12] is the first polynitrogen species containing more than three nitrogen atoms. Since the synthesis of the N_5^+ cation, intensive interests on nitrogen clusters are aroused again.[13-22] Li et al.[13] carried out ab initio and DFT investigations on the mechanism of the formation of the N_5^+ cation. Nguyen and Ha[14] studied the

structures, energetics, and properties of the N_5^+ cation using DFT, coupled-cluster, and many-body perturbation theory. A triplet structure corresponding to a weak complex between linear triplet N_3^+ and N_2 was found by them. Recently, we reported our isomeric study of fifteen N_5, N_5^+, and N_5^- isomers using the Gaussian–3 method (G3).[15] Zheng and co-workers[16] used microwave or electrical discharge method to prepare tetrahedral tetrazetes (N_4). A weak infrared transition at 936.7 cm^{-1} was observed, which is very compatible with their quantum chemical calculation result. This experimental study provides new evidence for the isolation of tetrazete, the neutral polynitrogen compound N_4. Gagliardi et al.[17] studied the dissociation mechanism of open-chain N_6 into $3N_2$ molecules. The computed barrier is 120.1 kJ mol^{-1} at the CASPT2 level, which shows that the open-chain N_6 can form stable molecules. Very recently, Gagliardi et al.[18] also reported the dissociation reaction of N_8 azapentalene to $4N_2$ molecules. Schmidt and co-workers[19] studied the potential energy surface for cubic N_8. Recently, Chung et al.[20] performed an ab initio study of potential energy surfaces for three N_8 isomers.

Based on the existence of the N_5^+ cation, which is the only N_n ($n > 3$) species with synthetic and spectroscopic evidence, it appears that it is also important to investigate odd-number nitrogen clusters. Prior to this work, there have been only two reports on the N_7 clusters. In 1998, Li et al.[21] carried out an isomeric study for N_7 and eight isomers were found. Among them, an open-chain structure was found to be the most stable. Subsequently, we also carried an ab initio study of N_7 clusters.[22] Five new structures were found, and the open-chain N_7 radical with C_{2v} symmetry is still the most stable among the isomers. These results suggest that odd-number nitrogen clusters are likely to be stable and potential HEDMs if they could be synthesized, even though N_7 clusters have properties different from those of even-number nitrogen clusters. For instance, the N_7 clusters are radicals with an unpaired electron, while N_8 clusters are closed-shell systems. Clearly, the bonding in the N_7 clusters is more complex and interesting. In the present note, all the N_7 isomers are examined by the G3 method. Also, natural bond orbital (NBO) analysis is carried out to study the bonding of the N_7 isomers. In this work, twelve (low-spin) isomers of N_7 clusters are identified as local minima on the MP2(FU)/6–31G(d) potential energy surface. Of these twelve species, five are reported for the first time. A new structure, which is more stable (by almost 100 kJ mol^{-1}) than the aforementioned open-chain N_7 radical with C_{2v} symmetry, is also found.

3.2 Computational Method and Results

All calculations were carried out on DEC 500au, COMPAQ XP900, and XP1000 workstations, as well as an SGI Origin 2000 High Performance Server, using the Gaussian 98 package of programs.[23] The computational method we employed was the G3 model.[24] In addition to the structural and energetics results, the bonding in the various isomers identified will also be discussed based on their NBO analysis.[25, 26]

The structures of the twelve isomers optimized at the MP2(FU)/6–31G(d) level are shown in Figure 1. The G3 total energies, enthalpies and the heats of formation ΔH_{f0} and ΔH_{f298} of all isomers are listed in Table 1. The pictorial bonding description of various isomers obtained by NBO analysis is shown in Figure 2. The second-order perturbation stabilization energy $\Delta E_{(2)}$ obtained by NBO analysis are summarized in Table 2. The stabilization energy $\Delta E_{(2)}$ is calculated by second-order perturbation theory analysis of the Fock matrix.[27] If stablization energy $\Delta E_{(2)}$ for a donor bond orbital transferred to an acceptor bond orbital is large, it indicates that there is strong interaction between the two bonds. The larger the $\Delta E_{(2)}$, the stronger interaction.[28] In Table 2, only the stabilization energies for donor π orbital transferred to acceptor π^* orbital or donor lone pair orbital transferred to acceptor π^* orbital are listed. The $\Delta E_{(2)}$ values smaller than 41.8 kJ mol^{-1} (or 10 kcal mol^{-1}) are not included in Table 2, as these interactions may be deemed as not strong.

3.3 Discussion

The twelve isomers identified in this work have been characterized as local minima on the MP2(FU)/6–31G(d) potential energy surface by vibrational frequency calculations. Those structures with one or more imaginary frequencies at the MP(FU)/6–31G(d) level are not reported in the present paper. We will now discuss the structures, energetics, and bonding of the isomers.

Isomer **I** is a new structure reported for the first time. As shown in Table 1, the energy of **I** is much lower than those of the other isomers. It is about 86 kJ mol^{-1} more stable than the open-chain N_7 (isomer **II**), which has been suggested as the most stable N_7 isomer prior to this work.

Table 1: The G3 energies at 0 K (E_0), enthalpies at 298 K (H_{298}), heats of formation at 0 K (ΔH_{f0}), and at 298 K (ΔH_{f298}) of the twelve N_7 isomers

Isomer	Symmetry	E_0 (hartree)	H_{298} (hartree)	ΔH_{f0} (kJ mol^{-1})	ΔH_{f298} (kJ mol^{-1})
I	(C_s)	–382.86366	–382.85689	897.8	885.5
II	(C_{2v})	–382.83075	–382.82335	984.2	973.5
III	(C_s)	–382.77066	–382.76467	1142.0	1127.6
IV	(C_s)	–382.75851	–382.75220	1173.9	1160.3
V	(C_s)	–382.74922	–382.74311	1198.2	1184.2
VI	(D_{2d})	–382.68289	–382.67642	1372.4	1359.3
VII	(C_s)	–382.66074	–382.65497	1430.5	1415.6
VIII	(C_s)	–382.65444	–382.64829	1447.1	1433.2
X	(C_{2v})	–382.64567	–382.63988	1470.1	1455.2
IX	(C_{2v})	–382.64448	–382.63868	1473.2	1458.4
XI	(C_1)	–382.62993	–382.62391	1511.4	1497.2
XII	(C_s)	–382.60881	–382.60333	1566.9	1551.2

Table 2: Some significant donor-acceptor natural bond orbital interactions and their second-order perturbation stabilization energies, $\Delta E_{(2)}$ (kJ mol^{-1}), calculated at the MP2(FU)/6–31G(d) level

Isomer	Doner NBO	Acceptor NBO	$\Delta E_{(2)}$	Doner NBO	Acceptor NBO	$\Delta E_{(2)}$
I	αBD [a] π N^2–N^3	αBDπ* N^4–N^5	79.1	αBDπ N^4–N^5	αBDπ* N^2–N^3	77.4
	αLP [c] N^1	αBDπ* N^2–N^3	142.3	αLP N^1	αBDπ* N^4–N^5	139.7
	βBD [b] π N^2–N^3	βBDπ* N^4–N^5	86.2	βBDπ N^4–N^5	βBDπ* N^2–N^3	78.7
	βLP [d] N^1	βBDπ* N^2–N^3	206.3	βLP N^1	βBDπ* N^4–N^5	189.5
II	αLP N^1	αBDπ* N^2–N^3	685.8	αLP N^7	αBDπ* N^5–N^6	685.8
	βLP N^3	βBDπ* N^1–N^2	173.2	βLP N^5	βBDπ* N^6–N^7	173.2
III	αBDπ N^1–N^2	αBDπ* N^2N^4	267.8	αBDπ N^2N^4	αBDπ* N^1–N^2	267.8
	βLP N^3	βBDπ* N^1N^2	62.8	βLP N^4	βBDπ* N^1–N^2	47.7
V	αLP N^3	αBDπ* N^1N^2	159.4	αLPN^4	αBDπ* N^1–N^2	159.4
	βBDπ N^1–N^3	βBDπ* N^2–N^4	51.5	βBDπ N^2N^4	βBDπ* N^1–N^3	51.5
VI	βLP N^3	βBDπ* N^2–N^6	258.2			
XI	αLP N^4	αBDπ* N^1–N^2	68.6	αLPN^6	αBD*N^1–N^2	61.5

[a] α BD represents bond orbital occupied by α spin electron.
[b] β BD represents bond orbital occupied by β spin electron.
[c] α LP represents α spin lone pair electron.
[d] β LP represents β spin lone pair electron.

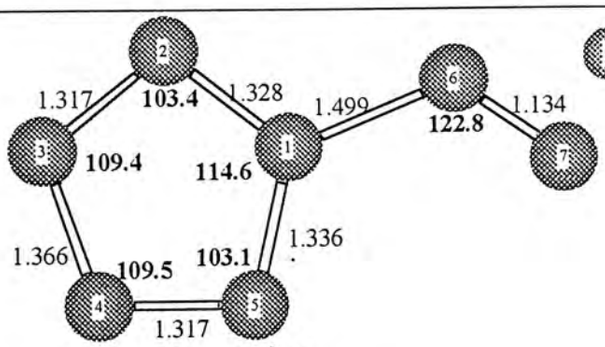

I (C_s; ^{2}A′)

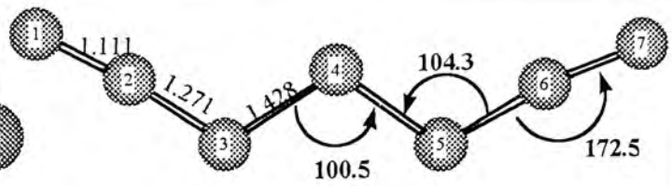

II (C_{2v}; ^{2}B$_1$)

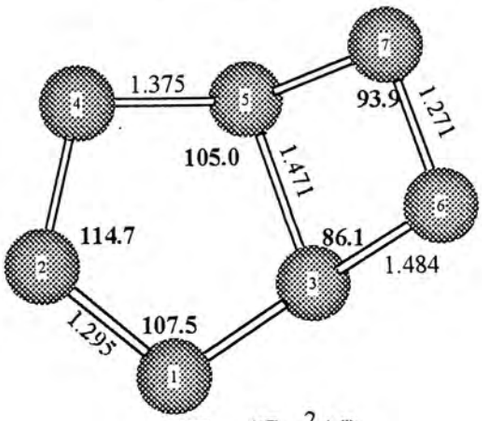

III (C_s; ^{2}A″)

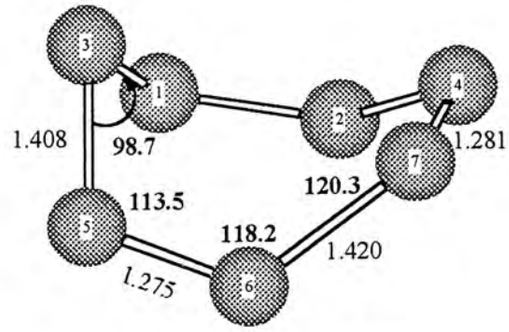

IV (C_s; ^{2}A′)

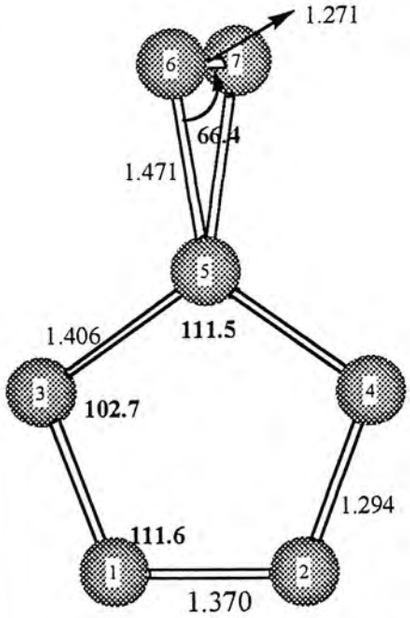

V (C_{2v}; ^{2}B$_1$)

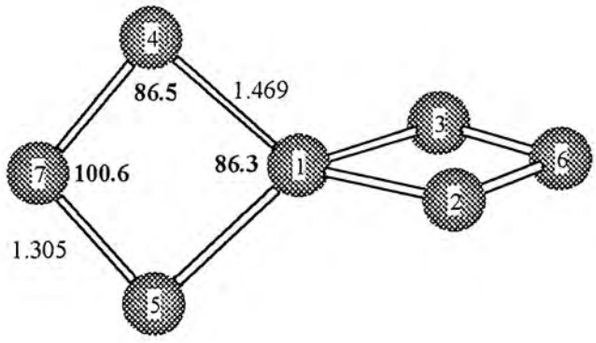

VI (D_{2d}; ^{2}A$_2$)

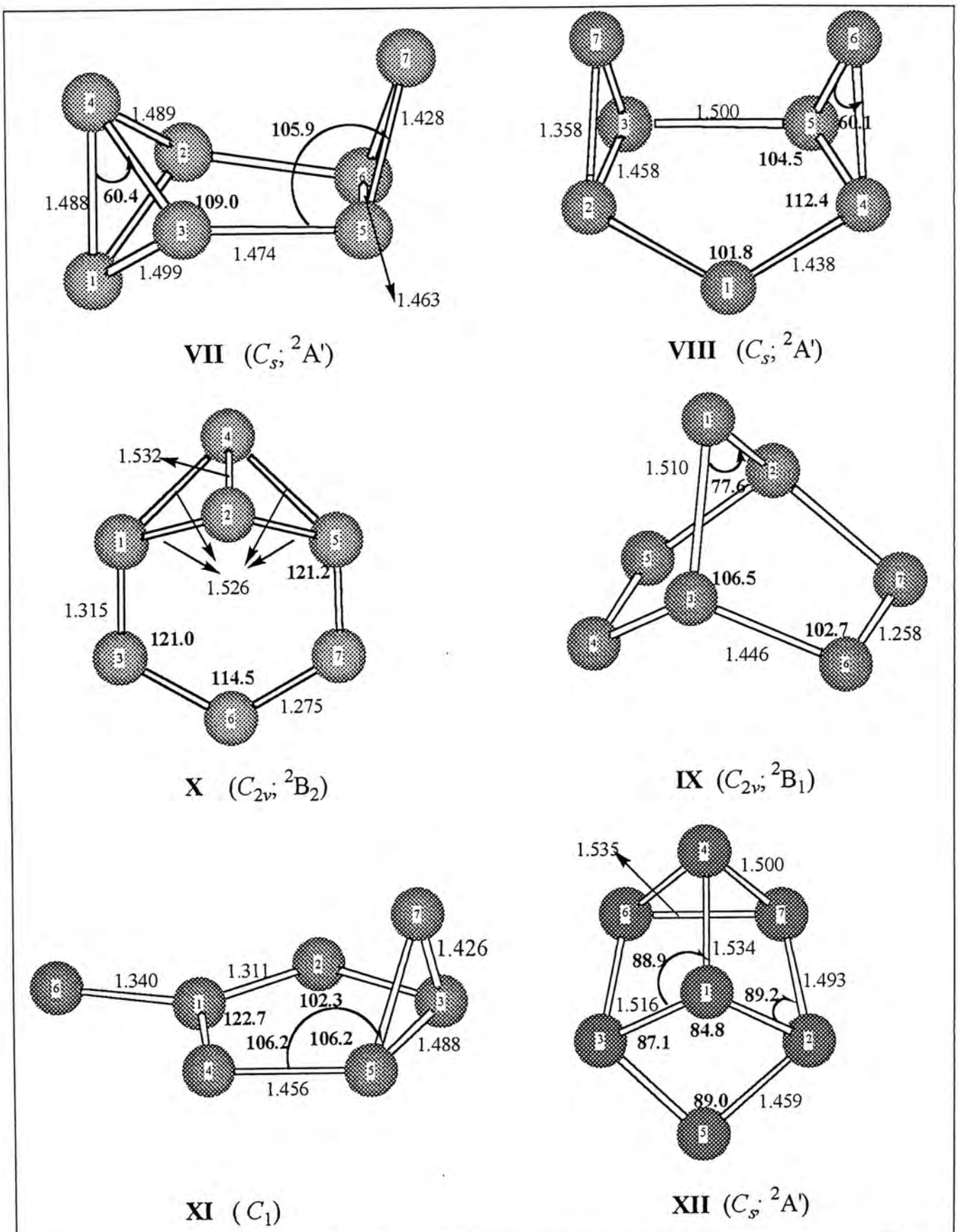

Figure 1. The structures of twelve N_7 isomers optimized at the MP2(FU)/6–31G(d) level, bond distance in Å and angle in degree (bold font).

From Figure 1, it can be seen that isomer **I** is planar radical, with a five-membered ring and a side chain connected by a N–N single bond (1.499 Å). This structure is similar to the azidopentazole N_8 (a five-membered ring with an azide side chain), which is the most stable structure among the N_8 isomers.[7] In the five-membered ring, the lengths of the five bonds are between 1.317 and 1.366 Å,

indicating a high degree of conjugation. The experimental N=N double bond has a length of 1.252 Å (in diimide). The aromatic bond length between two nitrogen atoms is about 1.35 Å. These results indicate there is strong conjugation in the five-membered ring of **I**, as confirmed by the NBO results.

As shown in Figure 2 and in Table 2, the NBO results suggest that the bonds of N^2-N^3 (the atom numbering is shown in Figs. 1 and 2), N^4-N^5 and N^6-N^7 are double bonds, while the other bonds are single bonds. Also, the lone electron is mainly resided at N^7. According to Table 2, the $\Delta E_{(2)}$ values for donor π orbitals transferred to acceptor π^* orbitals are large, about 77–86 kJ mol^{-1}. The $\Delta E_{(2)}$ values for donor lone pair orbitals transferred to acceptor π^* orbitals are even larger, about 142–206 kJ mol^{-1}. So there is strong conjugation between the two double bonds in the five-membered ring and also there is strong donor-acceptor interactions (negative hyperconjugation) between the lone pair orbitals on N^1 and the π^* orbitals of the two double bonds in the five-membered ring. These results suggest the stability of this isomer is enhanced by conjugation and hyperconjugation, as noted by Klapötke[5] for N_6 isomers previously.

Before leaving isomer **I**, it is noted that its structure is similar to that of the pentazoles, which are experimentally known. So far only arylpentazoles have been isolated. However, even the most stable derivative will decompose explosively above 50 °C.[29, 30]

Isomer **II** has been reported by Li[21] and by us[22] previously. It was taken to be the most stable N_7 isomer. But, with the discovery of **I** in the present work, it can no longer make such a claim. Even so, its energy is much lower than those of the remaining ten isomers. As shown in Figure 1, **II** is a "W–shaped" open-chain radical. The bond length (1.111Å) of N^1-N^2 and N^6-N^7 is only slightly longer than that (1.094Å) of N_2, but much shorter than a typical N=N double bond length (1.252Å). The bond length (1.271Å) of N^2-N^3 and N^5-N^6 is little longer the N=N double bond length. Examining the NBO analysis results summarized in Figure 2, in addition to the σ–bond skeleton, on the left half of the radical, there is a one-electron bond[22] (denoted by a dotted line) between N^1 and N^2, and another one between N^2 and N^3, as well as a single electron localized at N^1 and N^3. This same description is repeated on the right half of the radical. Thus, it may be concluded that the formal bond order between N^1 and N^2 (or N^6 and N^7) is 2½, while that between N^2 and N^3

(or N^5 and N^6) is 1½. Furthermore, the lone electron of the radical is mainly localized at N^4.

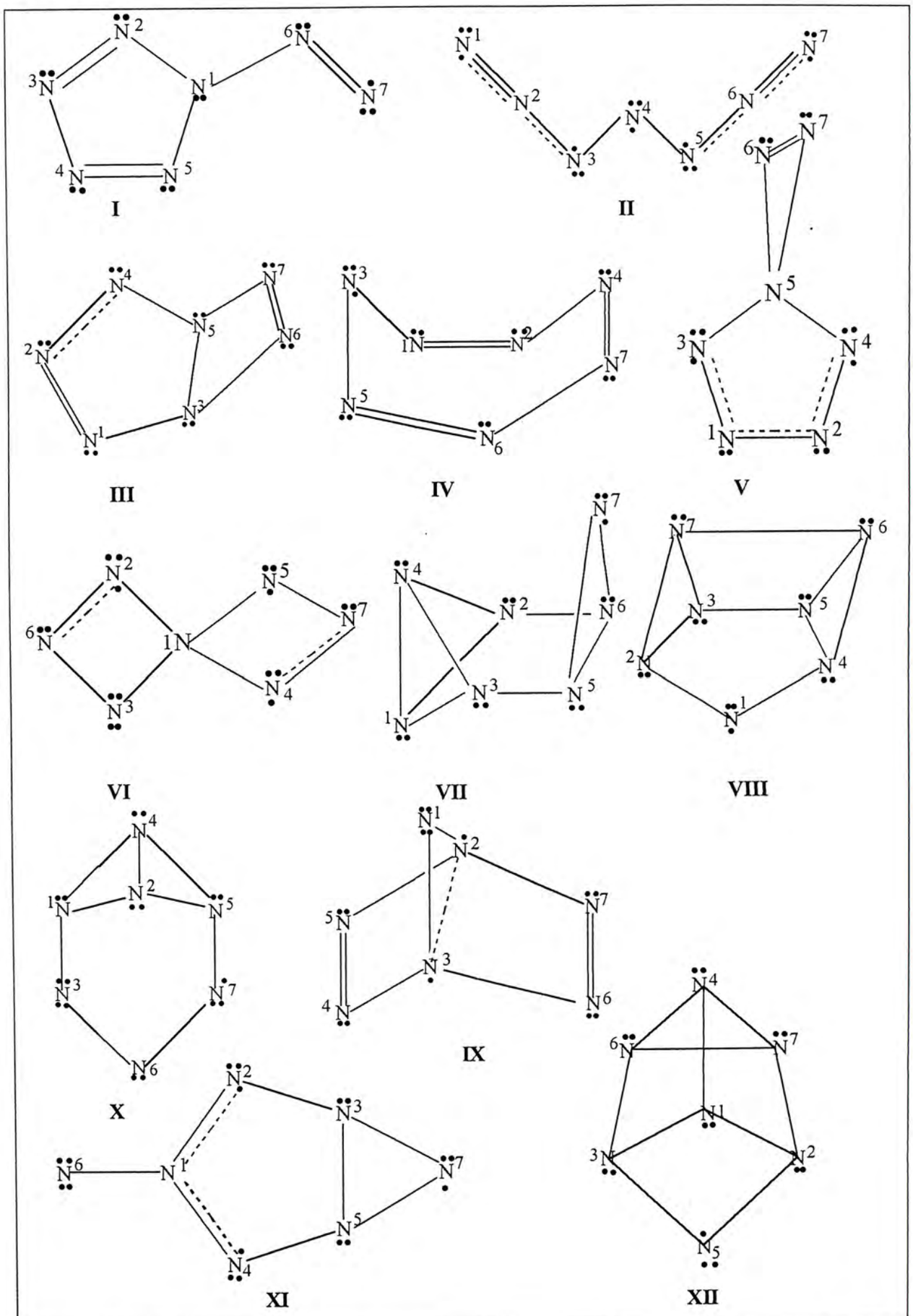

Figure 2. NBO description for the twelve N_7 isomers identified in this work. The dotted line represents a one-electron bond (see text).

Quantitatively, from Table 2, it can be seen that there are also very strong donor-acceptor interactions (negative hyperconjugation) between the lone pair orbital on N^1 and the π^* orbital of bond N^2-N^3. Conversely, there is interaction between the lone pair orbital on N^3 and the π^* orbital of bond N^1-N^2. [There are identical interactions on the other side of the radical.] The $\Delta E_{(2)}$ values for these interactions are 685.6 and 173.2 kJ mol^{-1}, respectively. A similar hyperconjuation was also found in the open-chain N_6 by Klapötke[5] based on NBO analysis. In other words, the stability of **II** is also enhanced by hyperconjugation.

About 244, 276 and 300 kJ mol^{-1} less stable than **I** are, respectively, isomers **III**, **IV**, and **V**. It is noted that these three N_7 isomers possess formal N=N double bonds and they are more stable than the remaining seven isomers, which do not. Additionally, **III** has a five-membered ring fused with a four-membered ring; **IV** has the cyclic structure of a seven-membered ring; **V** has structure consisting of a five-membered ring and three-membered ring. For **III**, there is strong donor-acceptor interaction between the π orbital of bond N^1-N^2 and the π^* orbital of bond N^2-N^4, as well as the reciprocal interaction between the π orbital of bond N^2-N^4 and the π^* orbital of bond N^1-N^2. In addition, there is less interaction between lone pair orbital on N^3 and the π^* orbital of bond N^1–N^2 (or between lone pair orbital on N^4 and the π^* orbital of bond N^1–N^2). As **III** has C_s symmetry, the pictorial description given in Figure 2 for this isomer may be taken as a contributing resonance structure. In another equivalent structure, we may have a π bond between N^2 and N^4 and a one-electron bond between N^1 and N^2. So the lone electron of the radical is extensively delocalized among atoms N^1, N^2, and N^4. This delocalization also extends as to N^3 and N^5, albeit to a lesser extent. For **IV**, there is no strong interaction among the three double bonds around the seven-membered ring. In other words, they are isolated double bonds, and the lone electron is localized at N^3. For **V**, there is donor-acceptor interaction among the lone pair orbitals on N^3 and N^4 and the π^* orbital of bond N^1-N^2. The $\Delta E_{(2)}$ value for these interactions is 159.4 kJ mol^{-1}. There is also conjugation between the double bonds N^1-N^3 and N^2-N^4, with the $\Delta E_{(2)}$ value being 51.5 kJ mol^{-1}.

Isomer **VI** is a highly symmetric molecule, which is reported for the first time. But its energy is very high. It is about 475 kJ mol^{-1} less stable than **I**.

According to the NBO results, there is strong interaction (258.2 kJ mol^{-1}) between the lone pair orbital on N^3 and the π^* orbital on bond N^2–N^6. As the two rings in **VI** (with D_{2d} symmetry) are equivalent to each other, we may picture another resonance structure with two lone pairs at N^5 and 1½ lone pairs at N^3. In other words, the lone electron of the radical is delocalized between N^3 and N^5.

About 533, 549, 572, and 669 kJ mol^{-1} less stable than **I** are, respectively, isomers **VII**, **VIII** (reported for the first time), **X**, and **XII**. Isomer **XII** is the most unstable N_7 radical found so far. In three of these four radicals, the lone electron is found to be localized on a single nitrogen atom: N^7 in **VII**, N^1 in **VIII**, and N^5 in **XII**. In **X**, the lone electron is delocalized between N^3 and N^7 (only one resonance structure is shown in Figure 2 for this isomer). According to the NBO analysis of **VIII**, there is a weak bond between N^6 and N^7, which are 2.088 Å apart. Also, there is no conjugation or hyperconjugation in any of these four isomers.

Isomers **IX** and **XI** are also high-energy N_7 radicals; both are reported for the first time. Isomer **IX** was optimized at MP2(FC)/6–31G(d) by Li et al.[21] But their structure may be better described as three dissociated fragments, two N_2 molecules ($N^4{\equiv}N^5$ and $N^6{\equiv}N^7$) and an N_3 radical. In **IX**, each of the two five-membered rings is not planar. So there is no conjugation in the rings. Thus the N^4-N^5 and N^6-N^7 bonds are isolated double bonds. The distance between N^2 and N^3 is 1.894 Å, and the NBO results suggest there is a weak one-electron bond between the two atoms. So the lone electron of the radical is delocalized between N^2 and N^3. For **XI**, the five-membered ring is now planar. There is donor-acceptor interactions between lone pair orbitals on N^4 and N^6 and the π^* orbital of bond N^1-N^2 (or between the lone pair orbitals on N^2 and N^6 and the π^* orbital of bond N^1-N^4). But most bonds in **XI** are single bonds, and its energy is still very high. The lone electron of this radical is localized at N^7.

Finally, it is noted that among the eight isomers reported by Li et al.[21], two (their **1** and **7**) are also discussed here (our **II** and **XII**, respectively). Also, they report two open-chain structures, both called **7**, which have the same energy. As mentioned earlier, our **IX** is an undissociated version of their **5** (N_2 + N_3 + N_2). As for the remaining four isomers (**2**, **3**, **4**, and **6** in their notation): **2** has one imaginary vibrational frequency at the MP2(FU)/6–31G(d) level; **3** has two imaginary vibrational frequencies; **4** dissociates into N_2 and N_5 fragments; **6** is a high-spin

(quartet) cluster which is not considered in this work.

3.4 Conclusion

Applying the G3 method, we have carried out an isomeric study for N_7 clusters. Twelve low-spin isomers of N_7 clusters are identified as local minima on the MP2(FU)/6–31G(d) potential energy surfaces. Out of these twelve species, five of them are introduced for the first time.

The most stable N_7 isomer is **I**. It is 86 kJ mol^{-1} more stable than the open-chain **II**, which was taken as the most stable in N_7 isomer previously. The NBO analysis gives an explicit and clear bonding description for these isomers. The NBO results suggest that the stability of **I, II, III**, and **V** is enhanced by conjugation and hyperconjugation.

When an electron is added to or taken from an N_7 isomer, closed-shell systems are resulted. The isomeric studies for the N_7^+ cations and N_7^- anions will be discuss in chapter 4.

3.5 Publication Note

An article based on the results reported in this Chapter has now appeared in *Chem. Phys. Lett.* **2001**, *338*, 367.

3.6 References

(1) Wright, J. S. *J. Am. Chem. Soc.* **1974**, *96*, 4753.

(2) Lauderadle, W. J.; Stanton, J. F.; Bartlett, R. J. *J. Phys. Chem.* **1992**, *96*, 1173.

(3) Glukhovtsev, M. N.; Jiao, H.; Schleyer, P. v. R. *Inorg. Chem.* **1996**, *35*, 7124.

(4) Glukhovtsev, M. N.; Schleyer, P. R. *Chem. Phys. Lett.* **1992**, *198*, 547.

(5) Klapötke, T. M. *J. Mol. Structure. (THEOCHEM)* **2000**, *499*, 99.

(6) Tian, A.; Ding, F.; Zhang, L.; Xie, Y.; Schaefer, H. F. *J. Phys. Chem. A* **1997**, *101*, 1946.

(7) Gagliardi, L.; Evagelisti, S.; Roos, B.O.; Widmark, P.-O. *J. Mol. Struct. (THEOCHEM)* **1998**, *428*, 1.

(8) Chen, C.; Sun, K.; Shyu, S. *J. Mol. Structure. (THEOCHEM)* **1999**, *459*, 113.

(9) Wright, J. S.; McKay, D. J.; DiLabio, G. A. *J. Mol. Structure. (THEOCHEM)* **1998**, *424*, 47.

(10) Ha, T. K.; Suleimenov, O.; Nguyen, M. T. *Chem. Phys. Lett.* **1999**, *315*, 327.

(11) Christe, K. O.; Wilson, W. W.; Sheehy, J. A.; Boatz, J. A. *Angew. Chem. Int. Ed.*

1999, *38*, 2004.

(12) Pyykkö, P.; Runeberg, N. *J. Mol. Structure. (THEOCHEM)* **1991**, *234*, 279.

(13) Xu, W.; Li, G.; Wang, L.; Li, S.; Li, Q. *Chem. Phys. Lett.* **1999**, *314*, 300.

(14) Nguyen, M. T.; Ha, T.-K. *Chem. Phys. Lett.* **2000**, *317*, 135.

(15) Wang, X.; Hu, H.-r.; Tian, A.; Wong, N. B.; Chien, S.-H.; Li, W.-K. *Chem. Phys. Lett.* **2000**, *329*, 483

(16) Zheng, J.; Waluk, J.; Spanget-Larsen, J.; Blake, D. M.; Radziszewski, J. G. *Chem. Phys. Lett.* **2000**, *328*, 227.

(17) Gagliardi, L.; Evangelisti, S.; Barone, V.; Roos, B. O. *Chem. Phys. Lett.* **2000**, *320*, 518.

(18) Gagliardi, L.; Evangelisti, S.; Bernhardsson, A.; Lindh, R.; Barone, V.; Roos, B. O. *Int. J. Quant. Chem.* **2000**, *77*, 315.

(19) Schmidt, M. W.; Gordon, M. S.; Boatz, J. A. *Int. J. Quant. Chem.* **2000**, *76*, 434.

(20) Chung, G.; Schmidt, M. W.; Gordon, M. S. *J. Phys. Chem. A* **2000**, *104*, 5647.

(21) Li, Q.; Hu, X.; Xu, W. *Chem. Phys. Lett.* **1998**, *287*, 94.

(22) Wang, X.; Ren, Y.; Shuai, M.-B.; Wong, N.-B.; Li, W.-K.; Tian, A.-M. *J. Mol. Struct. (THEOCHEM)* **2001**, *538*, 145.

(23) Frisch, M. J.; Trucks, G. W.; Schlegel, H. B.; Scuseria, G. E.; Robb, M. A.; Cheeseman, J. R.; Zakrzewski, V. G.; Montgogery, J. A.; Jr.; Stratmann, R.E.; Burant, J. C.; Dapprich, S.; Millam, J. M.; Daniels, A. D.; Kudin, K. N.; Strain, M. C.; Farkas, O.; Tomasi, J.; Barone, V.; Cossi, M.; Cammi, R.; Mennucci, B.; Pomelli, C.; Adamo, C.; Clifford, S.; Ochterski, J.; Petersson, G. A.; Ayala, P. Y.; Cui, Q.; Morokuma, K.; Malick, D. K.; Rabuck, A. D.; Raghavachari, K.; Foresman, J. B.; Cioslowski, J.; Ortiz, J. V.; Baboul, A. G.; Stefanov, B. B.; Liu, G.; Liashenko, A.; Piskorz, P.; Komaromi, I.; Gomperts, R.; Martin, R. L.; Fox, D. J.; Keith, T.; Al-Laham, M. A.; Peng, C. Y.; Nanayakkara, A.; Gonzalez, C.; Challacombe, M.; Gill, P. M. W.; Johnson, B.; Chen, W.; Wong, M. W.; Andres, J. L.; Gonzalez, C.; Head-Gordon, M.; Replogle, E. S.; Pople, J. A. *GAUSSIAN 98*, Revision A.7; Gaussian, Inc., Pittsburgh PA, 1998.

(24) Curtiss, L. A.; Raghavachari, K.; Redfern, P. C.; Pople, J. A. *J. Chem. Phys.* **2000**, *112*, 7374.

(25) Carpenter, J. E.; Weinhold, F. *J. Mol, Struct. (THEOCHEM)* **1998**, *169*, 41.

(26) Carpenter, J. E. Ph. D. *Thesis*, University of Wisoconsin, Madison, **1987**.

(27) Reed, A. E.; Curtiss, L. A.; Weinhold, F. *Chem. Rev.* **1988**, *88*, 899.

(28) Lin, J.-F.; Wu, C.-C.; Lien, M.-H. *J. Phys.Chem.* **1995**, *99*, 16903.

(29) Müller, R.; Wallis, J. D.; Philpsborn, W. v. *Angew. Chem.* **1985**, *97*, 515.

(30) Janoschek, R. *Angew. Chem.* **1993**, *105*, 242.

Chapter 4

A Gaussian–3 Study of N_7^+ and N_7^- Isomers

Abstract

A Gaussian–3 study is carried out to investigate the isomers of N_7^+ and N_7^-. At MP2(FU)/6–31G(d) level, four N_7^+, and seven N_7^- isomers are identified. Of these eleven species, nine are reported for the first time. The most stable N_7^+ isomer is $\mathbf{1}^+$, it has a "W–shape" open-chain structure with C_{2v} symmetry, while the most stable N_7^- isomer is $\mathbf{5}^-$, which is a weak $N_2 \cdot \cdot \cdot N_5^-$ complex with C_1 symmetry. Natural bond orbital (NBO) analysis suggests that the stability of some of the more stable isomers is enhanced by conjugation or hyperconjugation.

4.1 Introduction

Polynitrogen compounds N_n have attracted considerable interest for a long time because of their potential use as high energy density materials (HEDMs) for propulsion or explosive application.[1–4] There have been many theoretical studies at various levels for nitrogen clusters such as N_4,[1,2,5,6] N_6,[1,2,7–9] N_8,[1,2,10–14] N_{10},[2,15,16] N_{12},[14,17] N_{18},[18] N_{20},[19–24] N_{28},[25] and N_{60}.[26] These computational investigations show that many N_{2n} ($n \geq 2$) clusters have much higher energy than the energy of n N_2 molecules. All of these clusters are potential HEDMs, even though most, if not all, of them still await experimental confirmation. Experimentally, and very recently, tetranitrogen N_4 has been prepared and detected by Cacace et al.[27] These authors suggested their N_4 molecule may have "an open-chain geometry with two distinct, closely bound N_2 units joined by a longer weaker bond." However, further theoretical analysis of this system is required.

On the other hand, for odd-numbered nitrogen clusters N_{2n+1} ($n \geq 1$), only a few studies have been carried out: N_3,[28,29] N_5,[6,29–35] N_7,[36–39] N_9,[40,41] and N_{13}.[36] Very recently, the N_5^+ cation, a cluster with an odd number of nitrogen atoms was synthesized by Christe et al.[42] This N_5^+ cation was first predicted to be stable theoretically by Pyykkö et al.[31] in 1991, which is the first polynitrogen species containing more than three

nitrogens. With the existence of the N_5^+ cation, which is the only N_n ($n > 3$) species with synthetic and spectroscopic evidence, it appears that it is important to investigate odd-numbered nitrogen clusters as well. Subsequently, an intense interest on the odd-numbered nitrogen clusters has been aroused.[9,29,30,32–35,38,39,41] Xu et al.[32] carried out ab initio and DFT investigations on the mechanism of the formation of the N_5^+ cation. Nguyen and Ha[33] studied the structures, energetics, and properties of the N_5^+ cation using DFT, coupled cluster and many-body perturbation theory. They reported a triplet structure corresponding to a weak complex between linear triplet N_3^+ and N_2. In addition, they have reported the decomposition mechanism of the N_5 and N_6 clusters and their ions recently.[9] We also reported our isomeric study of fifteen N_5, N_5^+, and N_5^- isomers using the Gaussian–3 method (G3) in 2000.[34] Very recently, Ponec et al.[35] studied the nature of bonding in the open-chain N_5^+ ion.

Despite continuing efforts to prepare such species, the only known polynitrogen compounds are molecular dinitrogen (N_2), the azide ion (N_3^-), the open-chain N_5^+ cation, and the recently prepared tetranitrogen N_4. From the chronological discovery of the known polynitrogen compounds: N_2 (1772), N_3^- (1956), N_5^+ (1999), and N_4 (2002), we may consider that the existence of N_2 and N_3^- would elicit the emergence of the N_5^+ cation. Hence, the next polynitrogen species may be the N_7^+ cation ($N_5^+ + N_2$) or the N_7^- anion ($N_3^- + N_4$). In the present work, the structures, bonding and energetics of the N_7^+ cations and the N_7^- anions are studied computationally. Prior to this work, there have been one report each on the N_7^+ cations [41] and the N_7^- anions,[37] and three studies on the N_7 clusters.[38–40] In their study of the dissociation pathways of N_9 and N_9^+ clusters by ab initio and DFT methods,[42] Li et al. reported an N_7^+ cation, which has an open-chain "W–shape" structure with C_{2v} symmetry. A theoretical prediction of the structures and stabilities of several azidamines using the ab initio and DFT methods was reported by Michels et al.[36] in 1995. Their results suggest that azidamines could be synthetically accessible. In 1998, Li et al.[37] carried out an isomeric study for N_7 and eight isomers were found. Among them, an open-chain structure was found to be the most stable. Afterwards, we have also carried out theoretical studies of N_7 clusters.[38,39] In our previous G3 studies,[39] we were interested in the open-shell N_7 clusters and an isomeric study was carried out. Twelve low-spin isomers of N_7 clusters were identified as local

minima and out of these 12 species, five were reported for the first time. The most stable N_7 isomer, called **I** and with C_s symmetry, consists of a five-membered ring and an N_2 side-chain. In addition, according to the natural bond orbital (NBO) analysis, the stability of some of the more stable N_7 isomers is enhanced by conjugation or hyperconjugation.

Since the N_7 clusters are radicals with an unpaired electron, their singly charged N_7^+ cations and N_7^- anions are closed-shell systems. Clearly, the bonding in the N_7^+ and N_7^- isomers is much different from that in the N_7 isomers. In the present note, we will concentrate on the structures and energies of the N_7^+ and N_7^- isomers. Furthermore, we will determine the ionization energies (IEs) and the electron affinities (EAs) of the N_7 isomers. The theoretical model we employ is again the recently proposed G3 model of theory.[43] Also, NBO analysis[44,45] is carried to study the bonding of the N_7^+ and N_7^- isomers. In this work, four N_7^+, and seven N_7^- isomers are identified as local minima on the MP2(FU)/6–31G(d) potential energy surface. Out of these 11 species, nine are reported for the first time. The most stable N_7^+ isomer is $\mathbf{1}^+$ and it has a "W–shape" open-chain structure with C_{2v} symmetry, while the most stable N_7^- isomer is $\mathbf{5}^-$, which is a weak $N_2 \cdots N_5^-$ complex with C_1 symmetry.

4.2 Method of Calculation and Results

All calculations were carried out on DEC 500au, COMPAQ XP900, and XP1000 workstations, as well as an SGI Origin 2000 High Performance Server, using the Gaussian 98 package of programs.[46] The computational method we employed was the G3 model.[43] In addition to the structural and energetics results, the bonding in the various isomers identified will also be discussed based on their NBO analysis.[44,45]

In our notation, numerals with superscript + or – such as $\mathbf{1}^+$ and $\mathbf{5}^-$ refer to stable N_7^+ cations and N_7^- anions, respectively. Roman numerals **I, II,** ..., etc. refer to stable N_7 isomers reported in our previous work.[39] All structures identified have only real vibrational frequencies. Those structures with one or more imaginary frequencies at the MP2(FU)/6–31G(d) level are not reported in the present letter.

The structures of one N_7 (**XIII**), various N_7^+ ($\mathbf{1}^+$–$\mathbf{4}^+$), and N_7^- ($\mathbf{5}^-$–$\mathbf{11}^-$) isomers optimized at the MP2(FU)/6–31G(d) level are displayed in Figure 1. The G3 total energies, enthalpies and the heats of formation ΔH_{f0} and ΔH_{f298} of all isomers are listed in Table 1. The pictorial bonding description of various isomers obtained by NBO analysis is shown in Figure 2. For easy reference, in both Figures 1 and 2, each atom in every isomer is numbered. The second-order perturbation stabilization energy $\Delta E_{(2)}$ obtained by NBO analysis are summarized in Table 2. The stabilization energy $\Delta E_{(2)}$ is calculated by second-order perturbation theory analysis of the Fock matrix.[47] If stablization energy $\Delta E_{(2)}$ for a donor bond orbital transferred to an acceptor bond orbital is large, there is strong interaction between the two bonds: the larger the $\Delta E_{(2)}$, the stronger interaction.[48] In Table 2, only the stabilization energies for donor π orbital transferred to acceptor π^* orbital or donor lone pair orbital transferred to acceptor π^* orbital are listed. The $\Delta E_{(2)}$ values smaller than 41.8 kJ mol^{-1} (or 10 kcal mol^{-1}) are not included in Table 2, as these interactions may be deemed as weak. With the aid of Table 1, the ionization energies (IEs) and electron affinities (EAs) of all the N_7 isomers can be easily calculated and they are tabulated in Table 3.

4.3 Discussion

As shown in Figure 1 and Table 1, four N_7^+ isomers, and seven N_7^- isomers have been identified. We will partition the discussion of the results into two sections: one for the cationic isomers and one for the anionic ones.

4.3.1 The N_7^+ isomers

The most stable N_7^+ isomer is $\mathbf{1}^+$, which has a "W–shaped" open-chain structure, with C_{2v} symmetry, which is similar to the structure of N_7 isomer **II**.[39] It has been reported by Li et al.[41] previously. At the G3 level, the ionization energy of **II** is calculated to be 7.45 eV. In any event, the general shapes of $\mathbf{1}^+$ and **II** are quite similar, as $\mathbf{1}^+$ is formed by ionizing a nonbonding electron located at N^4 of **II**. The bond length of N^1–N^2 and N^6–N^7 (1.143 Å) is only slightly longer than that of N_2 (1.094 Å), or the bond length of N^1–N^2 (and N^6–N^7) of **II** (1.111 Å), but much shorter than a typical N=N double bond length (1.252 Å). The bond length (1.325 Å) of N^2–N^3 and N^5–N^6 is much

longer than the N=N double bond length and bond length of N^2–N^3 (and N^5–N^6) of **II** (1.271 Å). Examining the NBO results in Table 2, it can be seen that there is strong interaction ($\Delta E_{(2)}$ = 202.7 kJ mol^{-1}) between the π orbital of bond N^3–N^4 and the π^* orbital of bond N^1–N^2. In addition, there is very strong donor-accepter interaction (negative hyperconjugation) between the lone pair orbital on N^5 and the π^* orbital of bond N^3–N^4, some interaction between the lone pair orbital on N^5 and the π^* orbital of bond N^6–N^7, as well as a small amount of interaction between the lone pair orbital on N^3 and the π^* orbital of bond N^1–N^2. The $\Delta E_{(2)}$ values for these interactions are 752.4, 293.4 and 60.9 kJ mol^{-1}, respectively. In other words, the stability of $\mathbf{1}^+$ is enhanced by both conjugation and hyperconjugation.

Table 1: The G3 total energies (E_0)[a] and enthalpies (H_{298}), and the standard heats of formation at 0 and 298 K (ΔH_{f0} and ΔH_{f298}) of N_7^+ and N_7^- isomers

Species		Symmetry	E_0 (Hartrees)	H_{298} (Hartrees)	ΔH_{f0} (kJ mol^{-1})	ΔH_{f298} (kJ mol^{-1})
N_7^+	$\mathbf{1}^+$	C_{2v}	–382.55693	–382.54968	1703.1	1692.1
	$\mathbf{2}^+$	C_{2v}	–382.51905	–382.51222	1802.6	1790.4
	$\mathbf{3}^+$	C_{2v}	–382.36909	–382.36201	2196.3	2184.8
	$\mathbf{4}^+$	C_{3v}	–382.16984	–382.16451	2719.4	2703.3
N_7^-	$\mathbf{5}^-$	C_1	–383.10523	–383.09721	263.5	254.5
	$\mathbf{6}^-$	C_2	–382.89779	–382.88961	808.2	799.6
	$\mathbf{7}^-$	C_s	–382.88246	–382.87652	848.4	833.9
	$\mathbf{8}^-$	C_{2v}	–382.88133	–382.87454	851.4	839.1
	$\mathbf{9}^-$	C_2	–382.87957	–382.87380	856.0	841.1
	$\mathbf{10}^-$	D_{2d}	–382.83727	–382.83068	967.1	954.3
	$\mathbf{11}^-$	C_s	–382.75125	–382.74526	1192.9	1178.6

[a] The G3 electronic energy reported is corrected with MP2(FU)/6–31G(d) frequencies, scaled by 0.9661.

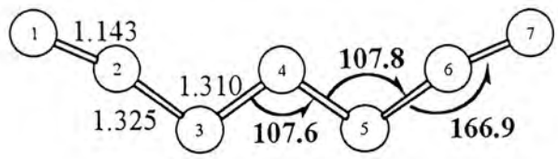

$\mathbf{1}^{+}$ (C_{2v}; $^{1}A_{1}$)

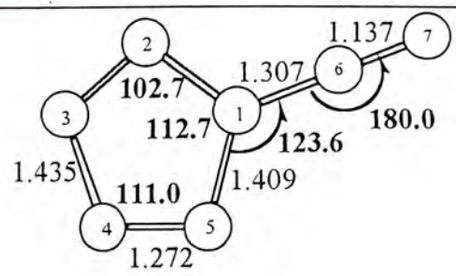

$\mathbf{2}^{+}$ (C_{2v}; $^{1}A_{1}$)

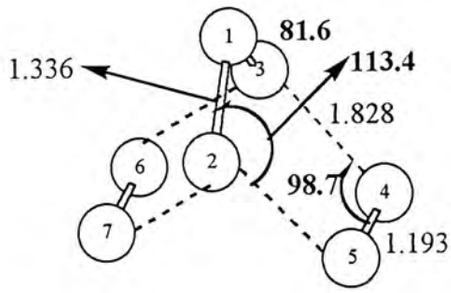

$\mathbf{3}^{+}$ (C_{2v}; $^{1}A_{1}$)

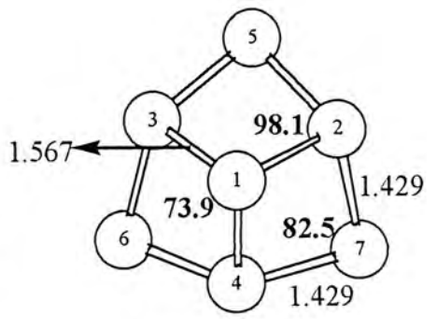

$\mathbf{4}^{+}$ (C_{3v}; $^{1}A_{1}$)

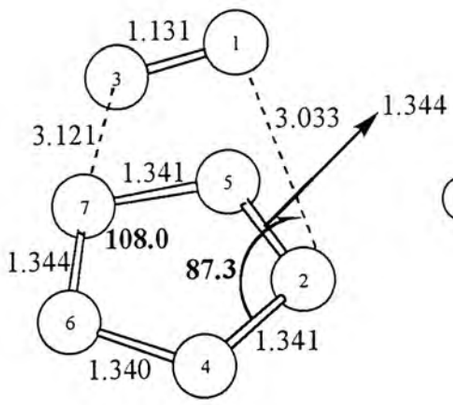

$\mathbf{5}^{-}$ (C_{1}; ^{1}A)

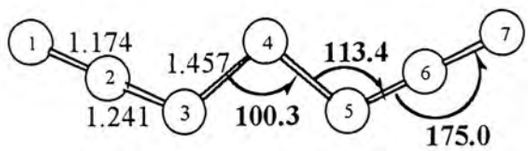

$\mathbf{6}^{-}$ (C_{2}; ^{1}A)

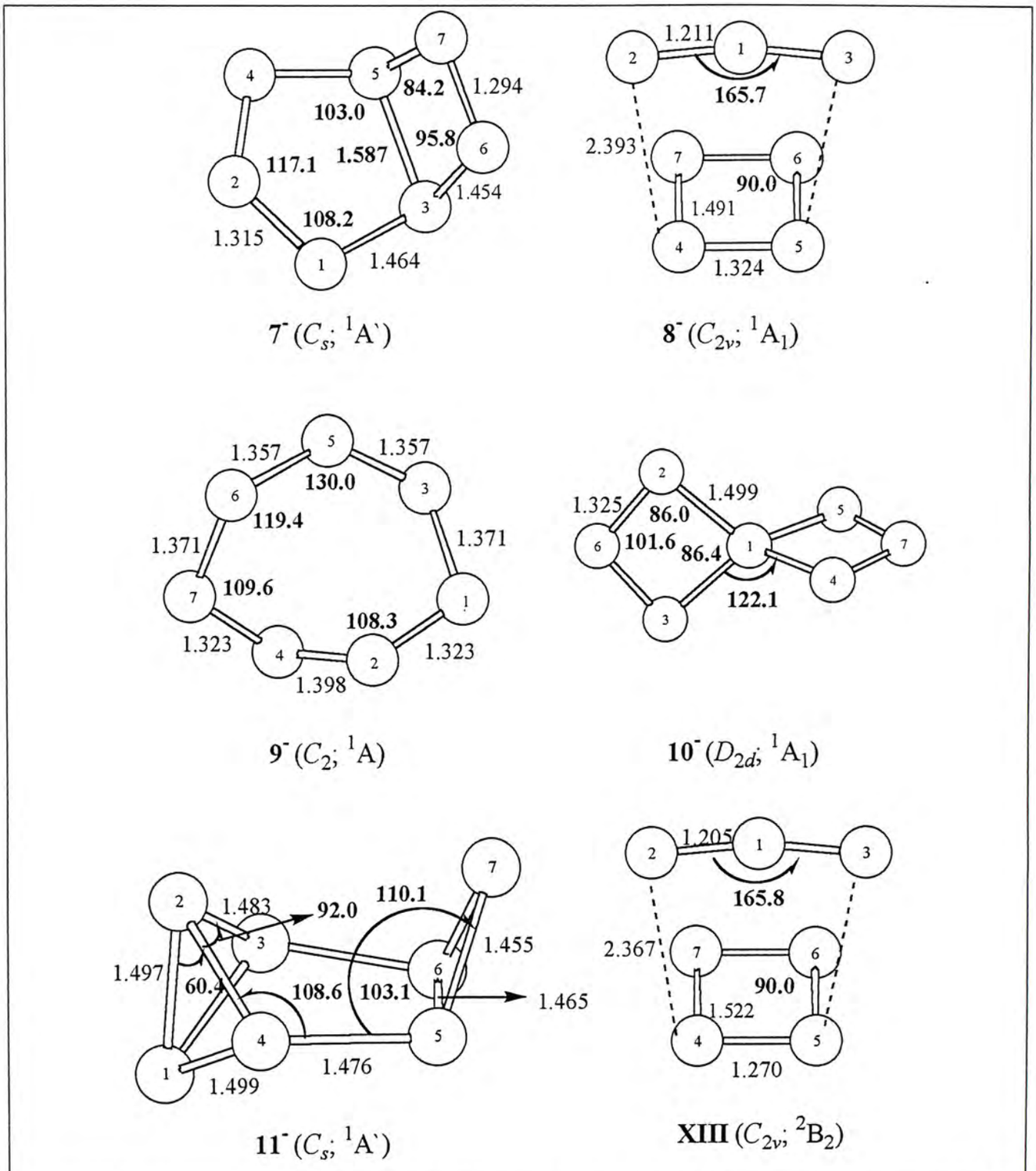

Figure 1. The structures of one N_7 (**XIII**), four N_7^+, and seven N_7^- isomers optimized at the MP2(FU)/6–31G(d) level, bond distances are in Å and bond angles in degrees (bold font).

Table 2: Significant donor-acceptor natural bond orbital interactions[a] in N_7^+ and N_7^- isomers and their second-order perturbation stabilization energies, $\Delta E_{(2)}$ (kJ mol^{-1}), calculated at the MP2(FU)/6–31G(d) level

Species	Donor NBO	Acceptor NBO	$\Delta E_{(2)}$	Donor NBO	Acceptor NBO	$\Delta E_{(2)}$
1$^+$	BDπ N^3–N^4	BDπ* N^1–N^2	202.7	LP N^5	BDπ* N^3–N^4	752.4
	LP N^3	BDπ* N^1–N^2	60.9	LP N^5	BDπ* N^6–N^7	293.4
2$^+$	BD π N^2–N^3	BDπ* N^4–N^5	88.2	BDπ N^4–N^5	BDπ* N^2–N^3	88.2
	LP N^1	BDπ* N^2–N^3	131.2	LP N^1	BDπ* N^4–N^5	131.2
	LP N^1	BDπ* N^6–N^7	295.2			
3$^+$	LP N^2	BDπ* N^4–N^5	95.9	LP N^3	BDπ* N^4–N^5	116.0
5$^-$	BD π N^2–N^4	BDπ* N^5–N^7	155.4	BDπ N^5–N^7	BDπ* N^2–N^4	155.0
	LP N^6	BDπ* N^2–N^4	683.1	LP N^6	BDπ* N^5–N^7	675.9
6$^-$	LP N^4	BDπ* N^5–N^6	102.2	LP N^4	BDπ* N^2–N^3	102.2
	LP N^5	BDπ* N^6–N^7	75.1	LP N^3	BDπ* N^1–N^2	75.1
	LP N^7	BDπ* N^5–N^6	970.5	LP N^1	BDπ* N^2–N^3	970.5
7$^-$	LP N^4	BDπ* N^1–N^2	901.1			
8$^-$	LP N^2	BDπ* N^1–N^3	89.5	LP N^3	BDπ* N^1–N^2	1404.9
	LP N^3	BDπ* N^4–N^5	56.4	LP N^3	BDπ* N^6–N^7	56.4
9$^-$	BD π N^5–N^6	BDπ* N^4–N^7	151.0	BDπ N^4–N^7	BDπ* N^5–N^6	97.9
	BD π N^4–N^7	BDπ* N^1–N^2	52.5	BDπ N^1–N^2	BDπ* N^4–N^7	52.5
	LP N^3	BDπ* N^5–N^6	691.5	LP N^3	BDπ* N^1–N^2	587.7
	LP N^4	BDπ* N^1–N^2	53.0	LP N^2	BDπ* N^4–N^7	53.0
10$^-$	LP N^5	BDπ* N^4–N^7	944.8	LPN^3	BD*N^2–N^6	944.8

[a] BD represents bond orbital, while LP represents lone pair electrons.

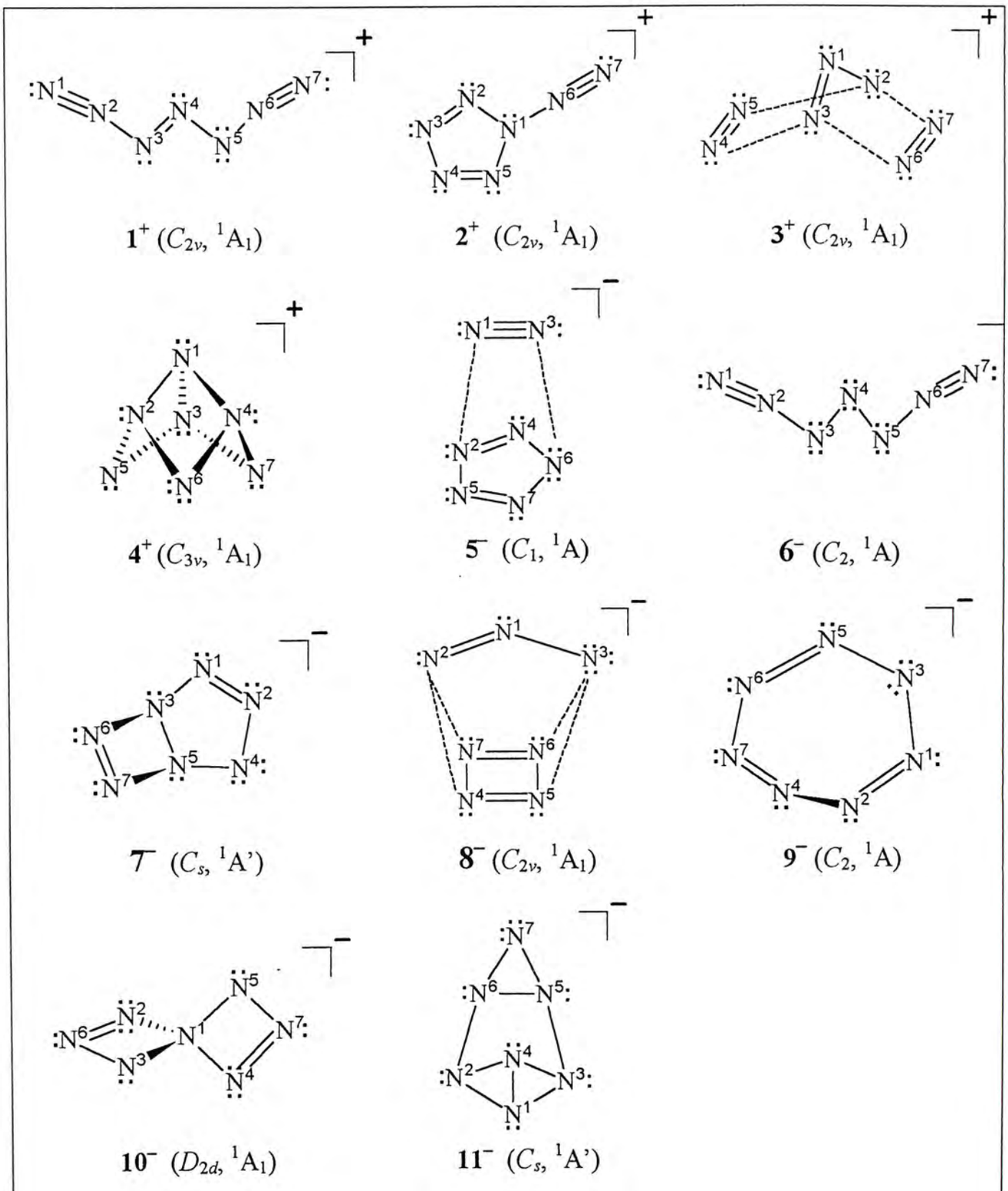

Figure 2. NBO description for the eleven N_7^+ and N_7^- isomers identified in this work.

Table 3: The G3 IEs and EAs of N_7 isomers[a]

N_7 isomer	IE (eV)	Process	EA (eV)	Process
I	9.38	**I** → $\mathbf{2}^+$	6.57	$\mathbf{5}^-$ → **I** + e^-
II	7.45	**II** → $\mathbf{1}^+$	1.82	$\mathbf{6}^-$ → **II** + e^-
III	—	—	3.04	$\mathbf{7}^-$ → **III** + e^-
IV	—	—	3.29	$\mathbf{9}^-$ → **IV** + e^-
VI	—	—	4.20	$\mathbf{10}^-$ → **VI** + e^-
VII	—	—	3.88	$\mathbf{11}^-$ → **VII** + e^-
IX	7.49	**IX** → $\mathbf{3}^+$	—	—
XII	11.94	**XII** → $\mathbf{4}^+$	—	—
XIII[b]	—	—	4.77	$\mathbf{8}^-$ → **XIII** + e^-

[a] The N_7 isomers results are taken from Ref 39. [b] This N_7 isomer, which may be considered as a $N_3\cdot\cdot\cdot N_4$ complex, is reported for the first time. The G3 E_0, H_{298}, ΔH_{f0} and ΔH_{f298} values for this radical are –382.70613 hartree, –382.69997 hartree, 1311.4 kJ mol^{-1}, and 1297.5 kJ mol^{-1} respectively.

Isomer $\mathbf{2}^+$ is about 100 kJ mol^{-1} less stable than $\mathbf{1}^+$. From Figure 1, it can be seen that isomer $\mathbf{2}^+$ is a planar structure, with C_{2v} symmetry, a five-membered ring and a side-chain connected by a N–N bond (1.307 Å). This structure is similar to the N_7 isomer **I** (the most stable N_7 isomer) reported in our previous work,[39] with the G3 IE calculated to be 9.38 eV. The general shapes of $\mathbf{2}^+$ and **I** are similar, as $\mathbf{2}^+$ is formed by ionizing an nonbonding electron located at N^7 of **I**. Actually, in **I**, there are one and 1½ lone pairs on N^6 and N^7, respectively. Upon forming $\mathbf{2}^+$, one lone pair at N^7 remains and the lone pair at N^6 becomes bonding electrons shared by N^6 and N^7. As a result, the bond angle N^1–N^6–N^7 becomes 180°. In the five-membered ring, the lengths of bonds N^1–N^2 and N^3–N^4 (or N^1–N^5) are 1.435 and 1.409 Å respectively, which are slightly shorter than a N–N single bond length (1.450 Å). Meanwhile, the bond lengths of N^2–N^3 and N^4–N^5 are 1.272 Å, implying they are conjugated double bonds. As shown in Figure 2 and in Table 2, the NBO results suggest that the bonds N^2–$N^3$and N^4–N^5 are double bonds, while the bond N^6–N^7 is a triple bond. According to Table 2, the $\Delta E_{(2)}$ values for the interaction between donor π orbitals and acceptor π* orbitals are fairly large, 88.2 kJ mol^{-1}. The $\Delta E_{(2)}$ values for donor lone pair orbitals transferred to acceptor π* orbitals are even larger, 131.2 kJ mol^{-1}. So there is conjugation between the two double bonds in the five-membered ring and also there is strong donor-acceptor interactions, or negative hyperconjugation, between the lone pair orbitals on N^1 and the π* orbitals of the two

double bonds in the five-membered ring. Even stronger hyperconjugation (295.2 kJ mol^{-1}) also exists between the lone pair orbitals on N^1 and the π^* orbitals of the (N^6–N^7) triple bond. These results suggest that the stability of this isomer is also enhanced by hyperconjugation.

About 493 and 1016 kJ mol^{-1} less stable than $\mathbf{1}^+$ are, respectively, isomers $\mathbf{3}^+$ and $\mathbf{4}^+$. Isomer $\mathbf{3}^+$ has a complex like structure with C_{2v} symmetry and may be described as a complex with three fragments, two N_2 molecules ($N^4{\equiv}N^5$ and $N^6{\equiv}N^7$) and an N_3^+ cation. The distance between these fragments is 1.828 Å. The structure of N_7 isomer **IX** is a "fully bonded" version of $\mathbf{3}^+$, with the aforementioned distance between fragments becoming 1.446 Å. The ionization energy of isomer **IX** is calculated to be 7.49 eV, which is very close to the IE of isomer **II**. It is noted that, upon forming $\mathbf{3}^+$, the one-electron bond between N^2 and N^3 is destroyed. As a result, bond angle N^2–N^1–N^3 changes from 77.6° in **IX** to 81.6° in $\mathbf{3}^+$. Examining the NBO results, there is fairly strong donor-acceptor interaction between the lone pair orbital on N^2 and the π^* orbital of bond N^4–N^5 (or N^6–N^7), and the lone pair orbital on N^3 and the π^* orbital of bond N^4–N^5 (or N^6–N^7). The $\Delta E_{(2)}$ values for these interactions are in the range of 95–120 kJ mol^{-1}. Isomer $\mathbf{4}^+$ is a highly symmetric species with C_{3v} symmetry, which is the most unstable N_7^+ cation found so far. The structure of $\mathbf{4}^+$ is similar to the structure of N_7 isomer **XII**. The G3 ionization energy of **XII** is determined to be 11.94 eV, which is much higher than the IEs of the other isomers. The two unique bond lengths of this molecule are 1.429 and 1.567 Å, implying they all are N–N single bonds. It is noted that there is one lone pair on N^2, N^3 and N^4, while four lone pairs are equally shared by N^5, N^6 and N^7. In addition, there appears to be no significant conjugation or hyperconjugation in this isomer.

4.3.2 The N_7^- isomers

The most stable N_7^- isomer is $\mathbf{5}^-$, which, as suggested by its structure shown in Figure 1, may be considered as a weak complex between fragments N_5^- and N_2, with distances between fragments (N^3–N^6 and N^1–N^2) being longer than 3 Å. At the G3 level, the dissociation energy for $\mathbf{5}^-$ to fragment into N_5^- and N_2 is 8.2 kJ mol^{-1}. This value arises from the fact that geometry optimization and energy calculation were not

carried out at the same theoretical level. In order to get a better estimate of this dissociation energy, we preformed geometry optimization at the MP2(FU)/6–311+G(3df,2p) level and the dissociation was then calculated to be 17.7 kJ mol^{-1}. Hence, it is safe to say that this complex is a weak one, both structurally (at the MP2(FU)/6–311+G(3df,2p) level) and energetically (G3). Also, the separation (3.0–3.1 Å) between N^3 and N^6 (or N^1 and N^2) is very close to the van der Waals distance (~3.08 Å) for two nitrogen atoms. Therefore, the interaction between the two fragments appears to be of the van der Waals type. Adding an electron to the structure of neutral N_7 isomer **I**, geometry optimization would yield anion $\mathbf{5}^-$. At the G3 level, the electron affinity of isomer **I** is calculated to be 6.57 eV, which is much higher than the EAs of other N_7 isomers. In the five-membered ring of $\mathbf{5}^-$, the lengths of the five bonds are between 1.340 and 1.345 Å, indicating a high degree of conjugation. The experimental N=N double bond has a length of 1.252 Å (in diimide). The aromatic bond length between two nitrogen atoms is about 1.340 Å. These results indicate that there is strong conjugation in the fragment of N_5^-. As confirmed by the NBO results given in Table 2, there is strong interaction (about 155 kJ mol^{-1}) between the N^2–N^4 and N^5–N^7 π bonds. Also, there is much stronger donor-acceptor interaction (about 675–685 kJ mol^{-1}) between the out-of-plane lone pair orbital on N^6 and the π^* orbitals of the two double bonds in the five membered ring.

Isomer $\mathbf{6}^-$ has been reported by Michels et al.[36] previously. As shown in Figure1, $\mathbf{6}^-$ have a "W–shape" open-chain structure, with C_2 symmetry. The shape of $\mathbf{6}^-$ is similar to that of N_7 isomer **II**. Indeed, $\mathbf{6}^-$ is formed when **II** accepts an electron (which pairs up with the nonbonding electron located at N^4). At the G3 level, the EA is determined to be 1.82 eV. The bond length (1.174 Å) of N^1–N^2 and N^6–N^7 is only slightly longer than that (1.094 Å) of N_2, and it is very close to the bond length of N^1–N^2 (and N^6–N^7) of isomer **II** (1.111 Å). It is also significantly shorter than a typical N=N double bond (1.252 Å). The bond length (1.241 Å) of N^2–N^3 and N^5–N^6 is slightly shorter than the N=N double bond and the N^2–N^3 (and N^5–N^6) bond length of isomer **II** (1.271 Å). According to the NBO results in Table 2, there are very strong donor-accepter interactions ($\Delta E_{(2)}$ = 970.5 kJ mol^{-1}) between the lone pair orbital on N^1 (or N^7)

and the π^* orbital of bonds N^2–N^3 (or N^5–N^6). In addition, there is less interaction between the lone pair orbital on N^4 and the π^* orbital of bond N^5–N^6 (and N^2–N^3) and the lone pair orbital on N^3 (or N^5) and the π^* orbital of bond N^1–N^2 (or N^6–N^7). The $\Delta E_{(2)}$ values for these interactions are about 75.1–102.2 kJ mol^{-1}. Hence, the stability of isomer $\mathbf{6}^-$ is enhanced by both conjugation and hyperconjugation.

About 585, 587, and 592 kJ mol^{-1} less stable than $\mathbf{5}^-$ are, isomer $\mathbf{7}^-$, $\mathbf{8}^-$, and $\mathbf{9}^-$ respectively. It is noted that these three N_7^- isomers possess formal N=N double bonds. In addition, isomer $\mathbf{7}^-$ has a five-membered ring fused with a four-membered ring, which is similar to the structure of isomer **III**. The EA of **III** is 3.04 eV. In fact, in **III**, there is an one-electron bond between N^2–N^4. After forming $\mathbf{7}^-$, the one electron bond becomes a lone pair on N^4. Isomer $\mathbf{8}^-$ can be considered as a symmetric weak complex between fragments N_4 (four-membered ring) and N_3^-, with the distance between them being 2.393 Å. From isomer $\mathbf{8}^-$, we have identified a new stable high energy N_7 isomer (hereafter denoted as **XIII**), which has a similar structure with $\mathbf{8}^-$, and the G3 EA of isomer **XIII** is 4.77 eV. Since N_7 isomer **XIII** is reported for this first time in this work, its optimized structure is also included in Figure1 for reference. Isomer $\mathbf{9}^-$ has a non-planar cyclic structure of a seven-membered ring, which is similar to the structure of N_7 isomer **IV**. The calculated G3 EA of isomer **IV** is 3.29 eV. The lone electron located on N^3 of **IV** now pairs up with the additional electron to become a lone pair.

Now we turn to the bonding of isomers $\mathbf{7}^-$, $\mathbf{8}^-$, and $\mathbf{9}^-$. For $\mathbf{7}^-$, there is very strong donor-accepter interaction between the lone pair orbital on N^4 and the π^* orbital of bond N^1–N^2. The $\Delta E_{(2)}$ value of this interaction is 901.1 kJ mol^{-1}. As $\mathbf{7}^-$ has C_s symmetry, the pictorial description given in Figure 2 for this isomer may be taken as a contributing resonance structure. In another equivalent structure, we may have a π bond between N^2 and N^4 and a lone pair on N^1. For $\mathbf{8}^-$, considering the resonance structure shown in Figure 2, NBO analysis indicates that there is very strong interactions (1404.9 kJ mol^{-1}) between the lone pair orbital on N^3 and the π^* orbital of bond N^1–N^2. Conversely, the interaction between the lone pair orbital on N^2 and the π^* orbital of bond N^1–N^3 is much weaker, 89.5 kJ mol^{-1}. These results indicate there is very strong donor-accepter interaction within the N_3^- fragment. Also, NBO analysis suggests that

the fairly strong interaction between the lone pair orbital on N^3 and the π^* orbitals of bonds N^4–N^5 (or N^6–N^7), with the $\Delta E_{(2)}$ value being 56.4 kJ mol^{-1}. For $\mathbf{9}^-$, although its structure is similar to the N_7 isomer **IV**, but their bonding descriptions are totally different. All the double bonds of **IV** are isolated entities.[38] However, the NBO results of $\mathbf{9}^-$ suggest that there are strong interactions among the three double bonds around the seven-membered ring. The $\Delta E_{(2)}$ values of these interactions are in the range of 52–151 kJ mol^{-1}. So, there is strong conjugation between the three double bonds in the seven-membered ring. On the other hand, there are very strong donor-accepter interactions (about 600–700 kJ mol^{-1}) between the lone pair orbitals on N^3 and the π^* orbitals of the N^1–N^2 and N^5–N^6 double bonds. There are also interactions between the lone pair orbital on N^4 and the π^* orbital of bond N^1–N^2 and, by symmetry, between the lone pair orbital on N^2 and the π^* orbital of bond N^4–N^7. The $\Delta E_{(2)}$ values of these interactions are 53 kJ mol^{-1}. These results suggest the stability of this isomer is also enhanced by conjugation and hyperconjugation.

Isomer $\mathbf{10}^-$ is a highly symmetric anion, with D_{2d} symmetry. Its structure is very similar to the N_7 isomer **VI**, with the G3 EA calculated to be 4.20 eV. It is noted that, in the N_7 isomer **VI**, the lone electron is delocalized between N^3 and N^5, while there are 1½ bonds at N^2–N^6 and N^4–N^7 and 1½ lone pairs at N^2 and N^4. Upon adding a single electron to **VI** to form $\mathbf{10}^-$, there are now two lone pairs at N^3 and N^5, double bonds at N^2–N^6 and N^4–N^7, and only one lone pair each at N^2 and N^4. As the two rings in $\mathbf{10}^-$ are equivalent to each other, we may picture another resonance structure with two lone pair at N^2 and N^4 and the double bond located between N^5 and N^7 as well as between N^3 and N^6. According to the NBO results, there is strong interaction (944.8 kJ mol^{-1}) between the lone pair orbital on N^5 and the π^* orbital on the bond N^4–N^7 and, by symmetry, between the lone pair orbital on N^3 and the π^* orbital on the bond N^2–N^6. About 929 kJ mol^{-1} less stable than $\mathbf{5}^-$ is isomer $\mathbf{11}^-$. Isomer $\mathbf{11}^-$ has a structure similar to that of N_7 isomer **VII** and the G3 EA is calculated to be 3.88 eV. Upon forming $\mathbf{11}^-$, the additional electron is now paired with the lone electron located at N^7 of **VII**. There is no donor-acceptor interaction from the NBO analysis of this anion. In other words, all bonds in $\mathbf{11}^-$ are N–N single bonds.

4.4 Conclusion

Applying the G3 method, we have carried out an isomeric study for the N_7^+ cations and N_7^- anions. At the MP2(FU)/6–31G(d) level, four N_7^+ and seven N_7^- isomers are identified. Except $\mathbf{1}^+$ and $\mathbf{6}^-$, all of them are reported for the first time.

The most stable N_7^+ isomer is $\mathbf{1}^+$, which has a "W–shape" open-chain structure with C_{2v} symmetry. NBO analysis suggests that the stability of this cation is enhanced by conjugation and hyperconjugation. The most stable N_7^- isomer is $\mathbf{5}^-$, which is a weak $N_2 \cdots N_5^-$ complex with C_1 symmetry. The energy for dissociating $\mathbf{5}^-$ into two fragments at MP2(FU)/6–311+G(2df,p) is 17.7 kJ mol^{-1} and the interaction between the two fragments is of the van der Waals type. In addition, NBO results suggest that the stability of isomer $\mathbf{6}^-$, $\mathbf{8}^-$, and $\mathbf{9}^-$ is also enhanced by conjugation and hyperconjugation.

Furthermore, the ΔH_f values and the structures of all 11 species, as well as the IEs and EAs of the N_7 isomers are also reported.

4.5 Publication Note

An article based on the results reported in this Chapter has been written up and submitted for publication: Law, C.-K.; Li, W.-K.; Wang, X.; Tian, A.-M.; Wong, N.-B. *Chem. Phys. Lett.* (submitted).

4.6 References

(1) Lauderadle, W. J.; Stanton, J. F.; Bartlett, R. J. *J. Phys. Chem.* **1992**, *96*, 1173.

(2) Glukhovtsev, M. N.;Jiao, H.; Schleyer, P. v. R. *Inorg. Chem.* **1996**, *35*, 7124.

(3) Christe, K. O.; Wilson, W. W.; Sheehy, J. A.; Boatz, J. A. *Angew. Chem. Int. Ed. Engl.* **1999**, *38*, 2004.

(4) Klapötke, T. M. *Angew. Chem.* **1999**, *111*, 2694.

(5) Wright, J. S. *J. Am. Chem. Soc.* **1974**, *96*, 4753.

(6) Perera, S. A.; Barrlett, J. R. *Chem. Phys. Lett.* **1999**, *314*, 381.

(7) Glukhovtsev, M. N.; Schleyer, P. R. *Chem. Phys. Lett.* **1992**, *198*, 547.

(8) Klapötke, T. M. *J. Mol. Structure. (THEOCHEM)* **2000**, *499*, 99.

(9) Nguyen, M. T.; Ha, T.-K. *Chem. Phys. Lett.* **2001**, *335*, 311.

(10) Tian, A.; Ding, F.; Zhang, L.; Xie, Y.; Schaefer, H. F. *J. Phys. Chem. A* **1997**, *101*, 1946.

(11) Gagliardi, L.; Evagelisti, S.; Roos, B.O.; Widmark, P.-O. *J. Mol. Struct. (THEOCHEM)* **1998**, *428*, 1.

(12) Wang, L. J.; Li, S.; Li, Q. S. *J. Comput. Chem.* **2001**, *22*, 1334.

(13) Li, Q. S.; Wang, L. J. *J. Phys. Chem. A* **2001**, *105*, 1979.

(14) Klapötke, T. M.; Harcourt, R. D. *J. Mol. Struct. (THEOCHEM)* 2001, *541*, 237.

(15) Chen. C.; Sun, K.; Shyu. S. *J. Mol. Struct. (THEOCHEM)* 1999, 459, 113.

(16) Ren, Y.; Wang, X.; Wong, N.-B.; Tain, A.-M.; Ding, F.-J.; Zhang, L. *Int. J. Quantum Chem.* **2001**, *82*, 34.

(17) Qu, H.; Li, Q.; Zhu, H. *Chin. Sci. Bull.* **1997**, *42*, 462.

(18) Gu, J.; Chen, K.; Tian, J. A.; et al., *J. Mol. Struct. (THEOCHEM)* **1998**, *428*, 113.

(19) Bliznyuk, A. A.; Shen, M.; Schaefer III, H F. *J. Mol. Struct. (THEOCHEM)* **1998**, *428*, 183.

(20) Chen, C.; Chuang, S.; Lu, L. *J. Chin. Chem. Soc.* **1993**, *40*, 199.

(21) Balasubramanian, K. *Chem Phys. Lett.* **1993**, *202*, 271.

(22) Chen, C.; Chuang, S. *J. Mol. Struct. (THEOCHEM)* **1995**, *340*, 143.

(23) Wright, J. S.; McKay, D. J.; DiLabio, G. A. *J. Mol. Structure. (THEOCHEM)* **1998**, *424*, 47.

(24) Ha, T. K.; Suleimenov, O.; Nguyen, M. T. *Chem. Phys. Lett.* **1999**, *315*, 327.

(25) Chen, C.; Chuang, S. *J. Mol. Struct. (THEOCHEM)* **1996**, *362*, 181.

(26) Li, S.; Qu, H.; Li, Q. *J. Chin. Universitry* **1997**, *18*, 297.

(27) Cacace, F; de Petris, G.; Troiani, A. *Science* **2002**, *295*, 480.

(28) Wasilewski, J. *J. Chem. Phys.* **1996**, *105*, 10969.

(29) Gagliardi, L.; Orlandi, G.; Evagelisti, S.; Roos, B. O. *J. Chem. Phys.* **2001**, *114*, 10733.

(30) Klapötke, T. M. *Angew. Chem. Int. Ed.* **1999**, *38*, 2536.

(31) Pyykkö, P.; Runeberg, N. *J. Mol. Structure. (THEOCHEM)* **1991**, *234*, 279.

(32) Xu, W.; Li, G.; Wang, L.; Li, S.; Li, Q. *Chem. Phys. Lett.* **1999**, *314*, 300.

(33) Nguyen, M. T.; Ha, T.-K. *Chem. Phys. Lett.* **2000**, *317*, 135.

(34) Wang, X.; Hu, H.-r.; Tian, A.; Wong, N. B.; Chien, S.-H.; Li, W.-K. *Chem. Phys. Lett.* **2000**, *329*, 483

(35) Ponec, R.; Roithova, J.; Girones, X.; Jug, K. *J. Mol. Struct. (THEOCHEM)* **2001**, *545*, 255.

(36) Michels, H. H.; Montgomery Jr. J. A.; Christe, K. O.; Dixon, D. A. *J. Phys. Chem.* **1995**, *99*, 187.

(37) Li, Q.; Hu, X.; Xu, W. *Chem. Phys. Lett.* **1998**, *287*, 94.

(38) Wang, X.; Ren, Y.; Shuai, M.-B.; Wong, N.-B.; Li, W.-K.; Tian, A.-M. *J. Mol. Struct. (THEOCHEM)* **2001**, *538*, 145.

(39) Wang, X.; Tian, A.-M.; Wong, N.-B.; Law, C.-K.; Li, W.-K. *Chem. Phys. Lett.* **2001**, *338*, 367.

(40) Li, Q. S.; Wang, L. J.; Xu, W. G. *Theor. Chem. Acc.* **2000**, *104*, 67.

(41) Li, Q. S.; Wang, L. J. *J. Phys. Chem. A* **2001**, *105*, 1203.

(42) Christe, K. O.; Wilson, W. W.; Sheehy, J. A.; Boatz, J. A. *Angew. Chem. Int. Ed.* **1999**, *38*, 2004.

(43) Curtiss, L. A.; Raghavachari, K.; Redfern, P. C.; Pople, J. A. *J. Chem. Phys.* **2000**, *112*, 7374.

(44) Carpenter, J. E.; Weinhold, F. *J. Mol, Struct. (THEOCHEM)* **1998**, *169*, 41.

(45) Carpenter, J. E. Ph. D. *Thesis*, University of Wisconsin, Madison, **1987**.

(46) Frisch, M. J.; Trucks, G. W.; Schlegel, H. B.; Scuseria, G. E.; Robb, M. A.; Cheeseman, J. R.; Zakrzewski, V. G.; Montgogery, J. A.; Jr.; Stratmann, R.E.; Burant, J. C.; Dapprich, S.; Millam, J. M.; Daniels, A. D.; Kudin, K. N.; Strain, M. C.; Farkas, O.; Tomasi, J.; Barone, V.; Cossi, M.; Cammi, R.; Mennucci, B.; Pomelli, C.; Adamo, C.; Clifford, S.; Ochterski, J.; Petersson, G. A.; Ayala, P. Y.; Cui, Q.; Morokuma, K.; Malick, D. K.; Rabuck, A. D.; Raghavachari, K.; Foresman, J. B.; Cioslowski, J.; Ortiz, J. V.; Baboul, A. G.; Stefanov, B. B.; Liu, G.; Liashenko, A.; Piskorz, P.; Komaromi, I.; Gomperts, R.; Martin, R. L.; Fox, D. J.; Keith, T.; Al-Laham, M. A.; Peng, C. Y.; Nanayakkara, A.; Gonzalez, C.; Challacombe, M.; Gill, P. M. W.; Johnson, B.; Chen, W.; Wong, M. W.; Andres, J. L.; Gonzalez, C.; Head-Gordon, M.; Replogle, E. S.; Pople, J. A. *GAUSSIAN 98*, Revision A.7; Gaussian, Inc., Pittsburgh PA, 1998.

(47) Reed, A. E.; Curtiss, L. A.; Weinhold, F. *Chem. Rev.* **1988**, *88*, 899.

(48) Lin, J.-F.; Wu, C.-C.; Lien, M.-H. *J. Phys.Chem.* **1995**, *99*, 16903.

Chapter 5

Thermochemistry of Chlorine Fluorides ClF_n, n = 1–7, and Their Singly Charged Cations and Anions: A Gaussian–3 and Gaussian–3X Study

Abstract

The Gaussian–3 (G3) and Gaussian–3X (G3X) models of theory have been used to calculate the thermochemical data for chlorine fluorides ClF_n, n = 1–7, as well as for their singly charged cations and anions. The quantities calculated include the heats of formation (ΔH_f) and bond dissociation energies (DEs) of all the species, as well as the ionization energies (IEs) and electron affinities (EAs) of the neutrals. By comparing the well–established experimental data of ClF and ClF_3 with the G3 and G3X results, it is found that the G3X method yields more accurate ΔH_f values. In addition, the G3 and G3X methods give similar IEs and EAs for ClF and ClF_3. Based on these findings, the G3X results are used to assess the sometimes conflicting experimental data and a set of self–consistent thermochemcial data for ClF_n and their ions is recommended. Furthermore, the alternating patterns of the ΔH_f, DE, IE, and EA values of the chlorine fluorides and their ions are rationalized in terms of the electronic configuration around the central Cl atom for the species involved.

5.1 Introduction

For many years, attention has been drawn towards the chemistry of hypervalent species, such as ClF_n, SF_6, and PF_5 molecules.[1-5] Hypervalent species are defined as those molecules or ions with a central atom exceeding the number of valences allowed by the traditional theory of Lewis and Langmuir.[4-5]

There have been many computational studies on the thermochemical properties of chlorine fluorides ClF_n and their singly charged cations and anions at various levels of theory.[6-15] Guest et al.[6] examined the closed shell series from ClF to ClF_5 using the RHF procedure in 1973. Peterson and Woods studied the geometry of ClF using several

different methods and various basis sets.[7] The geometry and thermochemical stability of ClF_3 were investigated by Peterson et al.[8] in 1983 and Scharf et al.[9] in 1985. In 1987, Pershin and Boldyrev determined the structures, vibrational frequencies, and interconversion pathways of a series of netural, anionic and cationic chlorine fluorides ClF_k (k = 1–7).[10] The geometrical structures arrived at in these studies have now been confirmed by experiments.[15-21] In 1992, Jasien et al.[11] studied the thermochemical stabilities of ClF_3, ClF_5, and ClF_7 using the RHF and MP2 methods. Their results suggested that ClF_3 and ClF_5 were likely to be stable species while ClF_7 was probably unstable.

Ungemach and Schaefer investigated the structures of ClF_2 and ClF_4, as well as their cations and anions using the RHF method with a double-zeta (DZ) basis set in 1976.[12] Their results confirmed the experimental finding of by Mamantov et al.[17] and Morton et al.[18] Additionally, their results also supported the linear structure of ClF_2^-, which was prepared and characterized using infrared spectroscopy by Christe et al.[19,20] Futhermore, Sannigrahi et al.[13], by estimating the full configuration interaction, predicted the electron affinity (EA) of ClF_2 to be 4.76 eV. In 1990, Christe and co-workers[21] characterized ClF_6^- by spectroscopic method.

In 1996, Van Huis et al.[14] studied the structures and energies of the ClF_n, n = 1–7 and their anions using density functional theory (DFT). Three different types of prediction for electron affinities were reported. They are the adiabatic electron affinity (EA_{ad}), the vertical electron affinity (EA_{ver}) and the vertical detachment energy (VDE). And, the first Cl–F dissociation energies (DEs) for both the neutral and the anion were also calculated.

Very recently, Ricca et al.[15] have used the CCSD(T) method and DFT to study the heats of formation (ΔH_f) for ClF_n, n = 1–3. From this work, they obtained accurate result and concluded that the accuracy of the results is strongly dependent on the basis set quality and that it is crucial to add at least one tight d function to Cl.

Despite the existence of fairly extensive experimental thermochemical data for the ClF_n, ClF_n^+, and ClF_n^- systems, there is a lack of general agreement among these measurements for many of these species. In this work, we will employ high-level calculations to arrive at a set of self-consistent thermochemical data for ClF_n, ClF_n^+, and

ClF_n^-, n = 1–7. For those quantities where no experimental data are available, it is hoped that our calculated results will serve as reliable estimates.

The Gaussian–3 (G3)[22] method proposed in 1998 by Pople and his co–workers provides an improvement in accuracy and a reduction in computational time, when compared with the G2 method.[23] However, the G3 theory still does poorly for some of the larger non–hydrogen systems containing second–row atoms such as the hypervalent SF_6 and PF_5 molecules.[24] In light of this, a modification of the G3 theory, called Gaussian–3X (G3X)[24], has been developed. This method shows an improvement for the energetics of the non–hydrogen systems over the G3 theory: the G3 mean absolute deviation is 2.11 kcal mol^{-1} (8.8 kJ mol^{-1}) for the 47 non–hydrogen species in the G3/99 test set[25], while the corresponding deviation for the G3X method is 1.49 kcal mol^{-1} (6.2 kJ mol^{-1}). Previously, we applied both G3 and G3X methods to hypervalent systems $PF_n^+/PF_n/PF_n^-$.[3] It was found that the G3X model was superior to the G3 and, based on the G3X results, a self-consistent set of thermochemical data for these species was obtained. In this work, again the G3 and G3X methods are used to calculate the thermochemical properties, including the ΔH_f, ionization energy (IE), EA, and DE values of chlorine fluoride neutrals, cations, and anions. By comparing the experimental data with the two sets (G3 and G3X) of calculated quantities, an assessment on the relative merits of the two methods can then be made.

5.2 Methods of Calculations

All calculations were carried out on DEC 500au, COMPAQ XP900 and COMPAQ XP1000 workstations, as well as on an SGI Origin 2000 High Performance Server, using the Gaussian 98[26] packages of programs. The computational models employed were the aforementioned G3[23] and G3X[24] levels of theory.

In the G3 model, the MP2(Full)/6–31G(d) harmonic vibrational frequencies, scaled by 0.9661[27], are applied for the zero–point vibrational energy (ZPVE) correction at 0 K ($E_0 = E_e$ + ZPVE). While, in the G3X model[24], the vibrational frequencies calculated at the B3LYP/6–31G(2df,p) level, scaled by 0.9854.[27]

5.3 Results and Discussion

The equilibrium structures of ClF_n, ClF_n^+, and ClF_n^-, n = 1–7, optimized at the MP2(Full)/6–31G(d) and B3LYP/6–31G(2df,p) levels are shown in Figure 1. The G3 and G3X ΔH_f at 0 K and 298 K of the neutrals, cations, and anions are summarized in Tables 1–3, respectively, while the G3 and G3X IEs and EAs are listed in Table 4.

5.3.1 Comparison of the G3 and G3X methods. Since the experimental data for ClF and ClF_3 in the literature are the most well–established among the chlorine fluorides, the comparison between the calculated and the experimental results for these two molecules are most significant in order to assess the relative merits of the G3 and G3X methods. The experimental ΔH_{f0} for ClF is -55.6 ± 0.4 [30] kJ mol^{-1}, while the G3 and G3X results are –52.4 and –53.8 kJ mol^{-1}, respectively. For ClF_3, the experimental, G3, and G3X results are -154.7 ± 2.9,[28] –147.0, and –153.1 kJ mol^{-1}, respectively. Hence in both instances the G3X method gives a better results; this is expected for the non–hydrogen systems.[24] Meanwhile, as shown in Table 4, the G3 and G3X IEs for ClF are exactly the same, 12.67 eV. The experimental IEs for ClF found in the literature range from 12.65 ± 0.01 [31] to 12.66 ± 0.01 [32] eV, and the calculated results are in excellent agreement with the latter. For ClF_3, the G3 IE (12.70 eV) and G3X IE (12.58 eV) are fairly close to each other; and the experimental values range from 12.65 ± 0.05 [32] to 13.00 ± 0.02 [33] eV. On the other hand, the G3 EA (2.31 eV) and G3X EA (2.07 eV) for ClF are not in good agreement with the experimental EAs for ClF found in the literature, 1.50 ± 0.30 eV [34] and 2.86 ± 0.20 eV;[35] it is noted that these two values are not in agreement at all. Apparently, the calculated EA of ClF depends greatly on the computational method adopted. For instance, as shown by Van Huis et al.,[14] for ClF, the calculated EAs range from 1.94 eV (BLYP/DZP) to 2.96 eV (B3LYP/DZP^{++}). For ClF_3, the EA found in the literature is only a lower bound ($>2.40 \pm 0.10$ eV),[36] and both the G3 EA (3.43 eV) and G3X EA (3.32 eV) are consistent with this value. On the basis of the above findings, we may conclude that the G3X method is more reliable to predict the ΔH_{f0} values of the ClF_n systems. However, both the G3 and G3X methods give similar IEs and EAs for ClF and ClF_3 (as noted earlier, the G3 and G3X EAs for

ClF are not very close to each other). These results suggest that the G3 method underestimates the ΔH_{f0} values of the neutral and singly charged species simultaneously, and these errors cancel each other when the IEs and EAs are calculated. In the following discussion, the G3X results will thus be given more emphasis.

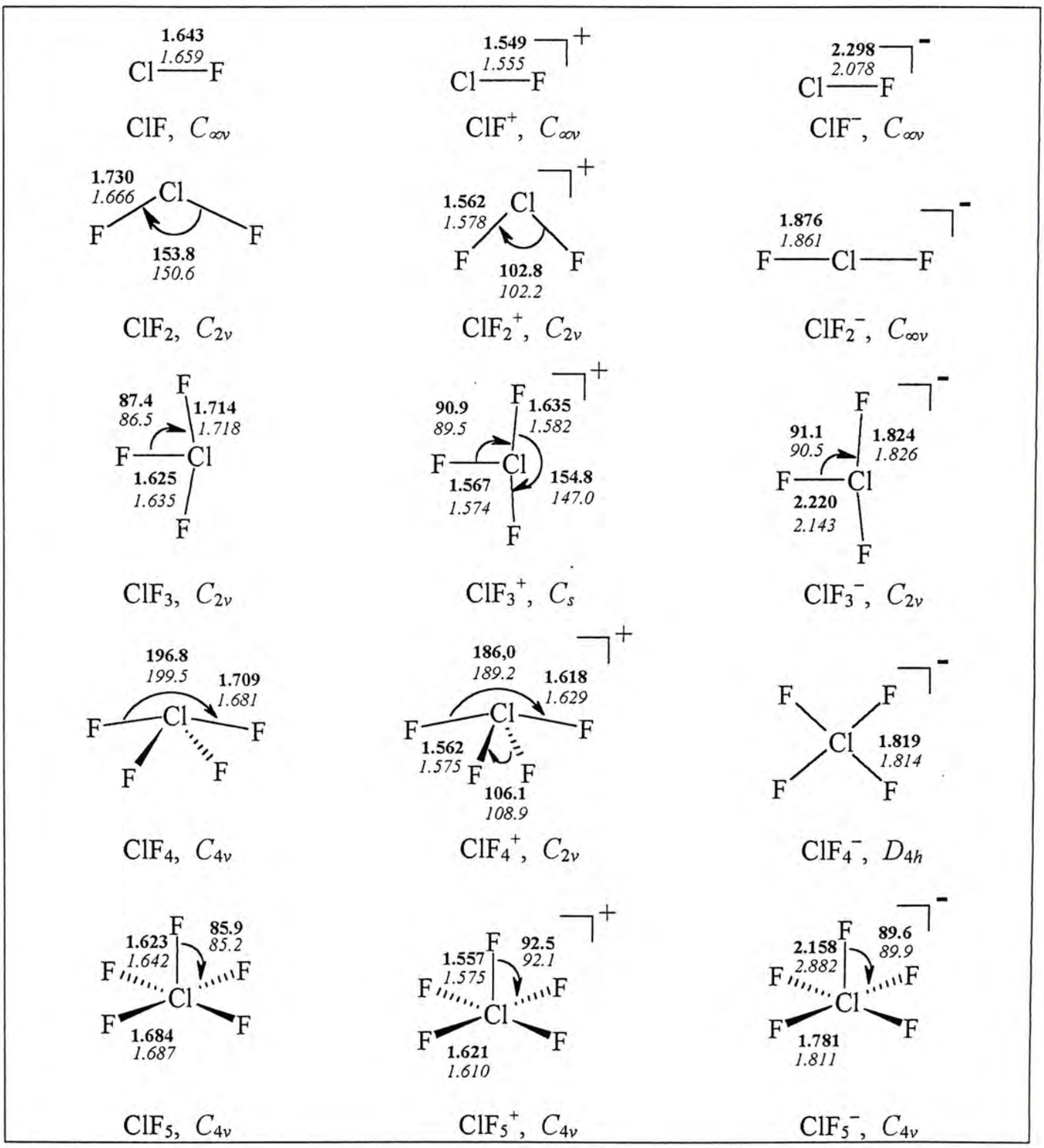

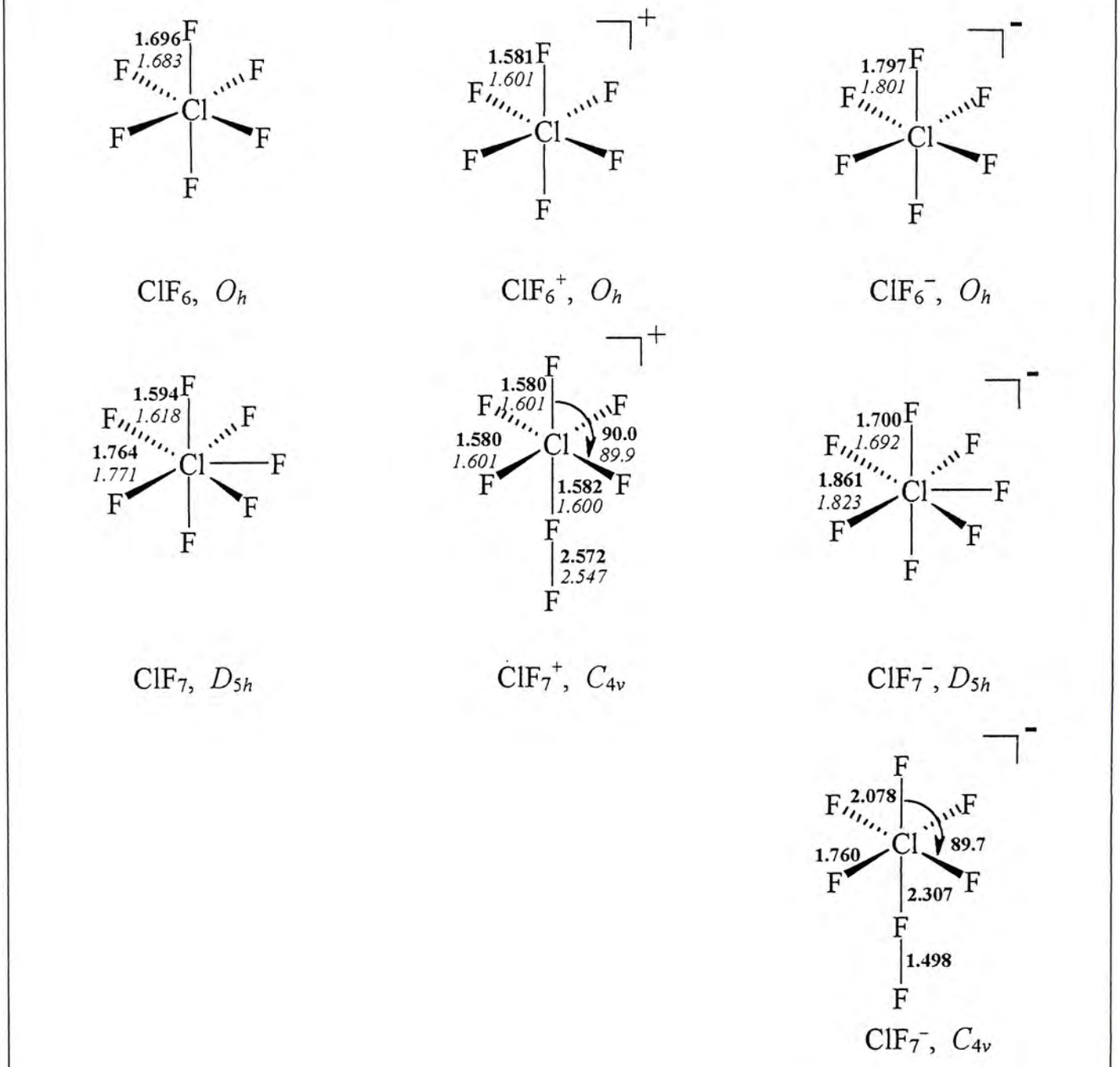

Figure 1. Theoretical equilibrium structures of chlorine fluorides and their singly charged cations and anions optimized at the levels of MP2(Full)/6–31G(d) (normal font) and B3LYP/6–31G(2df,p) (bold font).

Table 1: G3 and G3X total energies[a] (E_0), enthalpies (H_{298}), standard heats of formation at 0 K (ΔH_{f0}), and 298 K (ΔH_{f298}) of chlorine fluoride

Species	E_0 (hartrees)	H_{298} (hartrees)	ΔH_{f0} (kJ mol^{-1})	ΔH_{f298} (kJ mol^{-1})
ClF	*–559.77016*	*–559.76677*	*–52.4*	*–52.2*
	–559.77456	**–559.77069**	**–53.8**	**–52.3**
			[–55.6 ± 0.4][d]	[–55.7 ± 0.3][d]
			(–50.2 ± 0.4)[b]	(–50.3 ± 0.4)[b]
ClF_2	*–659.47480*	*–659.47053*	*–28.6*	*–30.3*
	–659.48734	**–659.48268**	**–46.3**	**–46.9**
ClF_3	*–759.23358*	*–759.22833*	*–147.0*	*–150.3*
	–759.24367	**–759.23837**	**–153.1**	**–156.3**
			[–154.7 ± 2.9][b]	[–158.9 ± 2.9][b]
			(–159.0)[c]	(–163.0)[c]
			(–160.5)[d]	(–164.6 ± 5.0)[d]
ClF_4	*–858.93072*	*–858.92488*	*–103.6*	*–109.5*
	–858.94627	**–858.93964**	**–118.9**	**–122.8**
ClF_5	*–958.68237*	*–958.67552*	*–203.2*	*–210.7*
	–958.69864	**–958.69168**	**–215.4**	**–222.6**
			[–229.3][d]	[–238.0 ± 7.0][d]
			(–229.8 ± 63.0)[b]	(–238.5 ± 63.0)[b]
ClF_6	*–1058.37241*	*–1058.36500*	*–141.1*	*–151.4*
	–1058.39211	**–1058.38305**	**–157.2**	**–163.1**
ClF_7	*–1157.99680*	*–1157.98776*	*93.3*	*83.2*
	–1158.01702	**–1158.00805**	**81.0**	**70.7**

[a] G3X results are shown in bold font, and G3 results are in italic font. Experimental values are given in brackets; those given in square brackets are the recommended values. [b] Ref 28. [c] Ref 29. [d] Ref 30.

Table 2: G3 and G3X total energies[a] (E_0), enthalpies (H_{298}), standard heats of formation at 0 K (ΔH_{f0}), and 298 K (ΔH_{f298}) of chlorine fluoride cations

Species	E_0 (hartrees)	H_{298} (hartrees)	ΔH_{f0} (kJ mol^{-1})	ΔH_{f298} (kJ mol^{-1})
ClF^+	*–559.30454*	*–559.30119*	*1170.1*	*1170.2*
	–559.30902	**–559.30519**	**1168.5**	**1169.9**
			(1170.0)[b]	(1170.0)[b]
ClF_2^+	*–659.07908*	*–659.07479*	*1010.3*	*1008.7*
	–659.08731	**–659.08302**	**1004.0**	**1002.4**
ClF_3^+	*–758.76689*	*–758.76200*	*1078.3*	*1074.0*
	–758.78134	**–758.77601**	**1060.7**	**1057.6**
			(1061.0)[b]	(1057.0)[b]
ClF_4^+	*–858.52266*	*–858.51681*	*967.8*	*961.9*
	–858.53768	**–858.53184**	**953.8**	**947.9**
ClF_5^+	*–958.20894*	*–958.20267*	*1039.8*	*1030.7*
	–958.22697	**–958.22014**	**1023.0**	**1015.4**
$ClF6^+$	*–1057.98088*	*–1057.97393*	*886.8*	*875.4*
	–1057.99883	**–1057.99198**	**875.4**	**863.7**
ClF_7^+	*–1157.66887*	*–1157.65940*	*954.3*	*945.3*
	–1157.68941	**–1157.67998**	**941.1**	**932.0**

[a] G3X results are shown in bold font, and G3 results are in italic font. Experimental values are given in brackets; those given in square brackets are the recommended values.
[b] Ref 29.

Table 3: G3 and G3X total energies[a] (E_0), enthalpies (H_{298}), standard heats of formation at 0 K (ΔH_{f0}), and 298 K (ΔH_{f298}) of chlorine fluoride anions

Species	E_0 (hartrees)	H_{298} (hartrees)	ΔH_{f0} (kJ mol^{-1})	ΔH_{f298} (kJ mol^{-1})
ClF^-	*–559.85510*	*–559.85153*	*–275.4*	*–274.7*
	–559.85063	**–559.84639**	**–253.5**	**–251.0**
			(–200 ± 29)[b]	
ClF_2^-	*–659.65639*	*–659.65178*	*–505.4*	*–506.2*
	–659.66318	**–659.65847**	**–507.9**	**–508.5**
ClF_3^-	*–759.35972*	*–759.35326*	*–478.2*	*–478.3*
	–759.36560	**–759.35929**	**–473.3**	**–473.8**
ClF_4^-	*–859.14291*	*–859.13592*	*–660.7*	*–663.6*
	–859.15404	**–859.14693**	**–664.4**	**–667.0**
ClF_5^-	*–958.83198*	*–958.82418*	*–596.0*	*–601.0*
	–958.84729	**–958.83848**	**–605.7**	**–608.0**
ClF_6^-	*–1058.58936*	*–1058.57984*	*–710.7*	*–715.4*
	–1058.60593	**–1058.59597**	**–718.6**	**–722.1**
ClF_7^-				
D_{5h}	*–1158.19675*	*–1158.18765*	*–431.6*	*–441.6*
D_{5h}	**–1158.22633**	**–1158.21546**	**–468.6**	**–473.9**
C_{4v}	**–1158.27403**	**–1158.26172**	**–593.8**	**–595.3**

[a] G3X results are shown in bold font, and G3 results are in italic font. Experimental values are given in brackets; those given in square brackets are the recommended values.
[b] Ref 32.

Table 4: G3 and G3X IEs[a] and EAs[a] of chlorine fluorides

Species	IE (eV)	EA (eV)
ClF	*12.67*	*2.31*
	12.67	**2.07**
	[12.66 ± 0.01][b]	(1.50 ± 0.30)[e]
	(12.65 ± 0.01)[c]	(2.86 ± 0.20)[f]
ClF_2	*10.77*	*4.94*
	10.89	**4.78**
	[12.77 ± 0.05][f]	(>3.23 ± 0.19)[g]
	(12.80 ± 0.30)[d]	(>0.9 ± 0.2)[f]
ClF_3	*12.70*	*3.43*
	12.58	**3.32**
	(12.65 ± 0.05)[b]	(>2.40 ± 0.10)[g]
	(13.00 ± 0.02)[d]	
ClF_4	*11.10*	*5.77*
	11.12	**5.65**
ClF_5	*12.88*	*4.07*
	12.84	**4.05**
ClF_6	*10.65*	*5.90*
	10.70	**5.82**
ClF_7	*8.92*	*5.44*
	8.91	**5.70**

[a] G3X energies are shown in bold font, and G3 energies are in italic font. Experimental values are given in brackets; those given in square brackets are the recommended values. [b] Ref 31. [c] Ref 32. [d] Ref 33. [e] Ref 34. [f] Ref 35. [g] Ref 36.

5.3.2 Assessments of the experimental results. In this part, with the help of the G3X results, we will appraise some widely scattered experimental results for various species in order to obtain a set of self-consistent thermochemical data for the ClF_n molecules and their ions.

Energetics of ClF, ClF^+, and ClF^-. The two experimental values reported for ΔH_{f0}(ClF) are –55.6 ± 0.4 [30] and –50.2 ± 0.4 [28] kJ mol^{-1}. The former value is closer to the G3X result of –53.8 kJ mol^{-1} and is hence recommended, even though the value of –50.2 ± 0.4 kJ mol^{-1} is well within the error bar of the G3X method. The experimental ΔH_{f0} value for ClF^+ is 1170.0 kJ mol^{-1},[29] which is in very good agreement with our G3X result, 1168.5 kJ mol^{-1}. As shown in Table 4, there are two experimental IEs (12.66 ±

0.01 eV [31] and 12.65 ± 0.01 eV [32]) for ClF. While both are consistent with the G3X value, 12.67 eV, the one reported by DeKock et al.[30] (12.66 ± 0.01 eV) is in excellent agreement and hence is our recommended value. The experimental ΔH_{f0} value for ClF^- is –200 ± 29 [32] kJ mol^{-1}, which is fairly close to the G3X value, –253.5 kJ mol^{-1}. However, it is stressed that the experimental uncertainty for this quantity is exceedingly large. Therefore, it may be believed that the G3X result gives a more reliable estimate. The two EAs for ClF found in the literature are 1.50 ± 0.30 [34] and 2.86 ± 0.20 [35] eV. While the G3X result is calculated to be 2.07 eV and is in agreement of neither, it falls almost right in the middle of the range spanned by the two experimental values. Clearly, the EA of ClF deserves further examination, both experimentally and computationally.

Energetics of ClF_2, ClF_2^+, and ClF_2^-. There are no experimental data reported for the ΔH_f of ClF_2, ClF_2^+, and ClF_2^-. The G3X $\Delta H_{f0}(ClF_2)$ and $\Delta H_{f0}(ClF_2^+)$ are –46.3 kJ mol^{-1} and –1004.0 kJ mol^{-1}, respectively. In the literature, there are only two experimental IEs found for the ClF_2, which are 12.77 ± 0.05 [35] and 12.80 ± 0.30 [33] eV. Both of them are fairly close with our G3X values, 10.89 eV. Considering the former result has a smaller experimental uncertainty, it is therefore our recommended value. In addition, the G3X $\Delta H_{f0}(ClF_2^-)$ and $EA(ClF_2)$ are –507.9 kJ mol^{-1} and 4.78 eV. While the two experimental EAs for ClF_2 (>3.2 ± 0.2 [36] eV and >0.9 ± 0.2 [35] eV) are lower bounds and are rather disparate, it is difficult to assess the accuracy of our G3X result. In fact, our result is greater than 3.2 eV and is reasonably close to the Sannigrahi's computational estimate of 4.67 eV.[13] According to this result, it may be claimed that the lower limit given by Dudlin et al. (0.9 ± 0.2 eV)[34] is well below the computational EAs and hence can be considered meaningless.

Energetics of ClF_3, ClF_3^+, and ClF_3^-. As mentioned before, there is a very good agreement between experimental and the G3X results for $\Delta H_{f0}(ClF_3)$ and $IE(ClF_3)$. Therefore, no further discussion is required here. The experimental $\Delta H_{f0}(ClF_3^+)$ value is 1061.0 [29] kJ mol^{-1}, which is in excellent agreement with the G3X value of 1060.7 kJ mol^{-1}. The G3X $\Delta H_{f0}(ClF_3^-)$ and $EA(ClF_3)$ are calculated to be 1057.6 kJ mol^{-1} and 3.32 eV, respectively. The experimental $\Delta H_{f0}(ClF_3^-)$ and $EA(ClF_3)$ reported in the literature are 1057.0 [29] kJ mol^{-1} and >2.40 ± 0.10 [36] eV, respectively. The experimental

$\Delta H_{f0}(ClF_3^-)$ is in excellent agreement with our calculated result. Clearly, the G3X EA for ClF_3 is much greater than the experimental lower bound.

Energetics of ClF_4, ClF_4^+, and ClF_4^-. Experimental thermochemical data are not available for any of these three species. Our calculated G3X results show that $\Delta H_{f0}(ClF_4)$ and $\Delta H_{f0}(ClF_4^+)$ are –118.9 and 953.8 kJ mol^{-1}, respectively. Hence, the G3X IE(ClF_4) is calculated to be 11.12 eV. Meanwhile, The G3X $\Delta H_{f0}(ClF_4^-)$ is calculated to be –664.4 kJ mol^{-1}, while the G3X EA(ClF_4) is 5.65 eV. The excellent agreement between the experimental and G3X values in the previous discussion can support our results, even though there are no experimental data available for ClF_4 and its ions.

Energetics of ClF_5, ClF_5^+, and ClF_5^-. The two experimental values for $\Delta H_{f0}(ClF_5)$ are –229.3 [30] and –229.8 ± 63.0 [28] kJ mol^{-1}; both are in agreement with the G3X result, –215.4 kJ mol^{-1}. But we should note the very large uncertainty of the experimental result. Unfortunately, there are no experimental studies for the ions of ClF_5, as well as for its IE and EA. The G3X $\Delta H_{f0}(ClF_5^+)$ is calculated to be 1023.0, while the IE(ClF_5) is 12.84 eV. Meanwhile, the G3X results of $\Delta H_{f0}(ClF_5^-)$ and the EA(ClF_5) are –605.7 kJ mol^{-1} and 4.05 eV, respectively.

Energetics of ClF_6, ClF_6^+, and ClF_6^-. Again there are no experimental thermochemical data for ClF_6, ClF_6^+, and ClF_6^-. The G3X $\Delta H_{f0}(ClF_6)$ and $\Delta H_{f0}(ClF_6^+)$ are calculated to be –157.2 and 875.4 kJ mol^{-1}, respectively. Hence, the G3X IE(ClF_6) is determined to be 10.70 eV. Similarly, at the G3X level, $\Delta H_{f0}(ClF_6^-)$ and EA(ClF_6) are –718.6 kJ mol^{-1} and 5.82 eV, respectively. In addition, the equilibrium structures identified for ClF_6 and its anion (both with O_h symmetry) are in agreement with the finding of Van Huis et al.[14] and Pershin et al.[10]. It is noted that the lone pair electrons in ClF_6^- may be deemed as "structurally inert," as in the cases of $TeCl_6^{2-}$, $TeBr_6^{2-}$, and $SbBr_6^{3-}$.[37] In these species, all with regular octahedral symmetry, the lone electron pair is forced inside the valence shell into a spherical orbital. As a result, the observed bond length would be longer than expected.[37] Take ClF_6^- as an example. The calculated Cl–F bond length in ClF_6^- is about 1.8 Å, which is longer than the sum of the covalent radii of Cl and F, 1.63 Å.[38]

Energetics of ClF_7, ClF_7^+, and ClF_7^-. There are again no experimental thermochemical data available for any of these three species. Our calculated G3X results show that $\Delta H_{f0}(ClF_7)$ and $\Delta H_{f0}(ClF_7^+)$ are 81.0 and 941.1 kJ mol^{-1}, respectively. Hence, the G3X IE(ClF_7) is calculated to be 8.91 eV. On the other hand, at the G3X level, $\Delta H_{f0}(ClF_7^-)$ and EA(ClF_7) are –468.6 kJ mol^{-1} and 5.70 eV, respectively. For ClF_7^-, as shown in Figure 1, two equilibrium structures with D_{5h} and C_{4v} symmetry were identified at the B3LYP/6–31G(2df,p) level (with the latter being more stable), while only one structure with D_{5h} symmetry was identified at the MP2(Full)/6–31G(d) level. In the report of Van Huis et al.,[14] only the structure of C_{4v} symmetry was found in the eight levels of theory they employed. For ClF_7, only a structure with D_{5h} symmetry was identified, in agreement with the finding of Van Huis et al.[14] and Pershin et al.[10]

5.3.3 Bond dissociation energies of ClF_n, ClF_n^+, and ClF_n^-. The G3 and G3X bond dissociation energies (DEs) of ClF_n, ClF_n^+, and ClF_n^- are summarized in Table 5.

Table 5: G3X and G3 bond dissociation energies (in kJ mol^{-1}) at 0 K for chlorine fluorides and their ions [a]

Bond	Neutral	Cation	Anion
Cl–F	*249.4*	*270.6*	*124.2*
	250.8	**262.0**	**100.4**
	(252.5 ± 0.06)[b]		
FCl–F	*53.6*	*237.2*	*307.4*
	69.9	**241.9**	**331.8**
F_2Cl–F	*195.8*	*9.4*	*50.2*
	184.2	**20.7**	**42.8**
F_3Cl–F	*34.0*	*187.9*	*259.9*
	43.2	**184.3**	***268.5***
F_4Cl–F	*177.0*	*5.4*	*12.7*
	173.9	**8.2**	***18.7***
F_5Cl–F	*15.3*	*230.4*	*192.1*
	19.2	**225.0**	***190.3***
F_6Cl–F	*–157.0*	*9.9*	*–201.7*
	–160.8	**11.7**	**–172.6**

[a] G3X energies are shown in bold font, and G3 energies are in italic font. Experimental value for Cl–F is given in brackets. [b] Ref 28.

Only the experimental DE of Cl–F (252.5 ± 0.06 kJ mol^{-1})[28] is available in the literature and included in the table for comparison. The G3 DE (249.4 kJ mol^{-1}) and G3X DE (250.8 kJ mol^{-1}) are close to each other and both are in good agreement with the experiment. It is of interest to note that the value of the DEs of ClF_7 and ClF_7^- are negative. This would indicate that the molecule is thermodynamically unstable with respect to its neutral fragments. Similar finding (for ClF_7) has been reported by Van Huis et al.[14]. They suggested that, for ClF_7, the D_{5h} structure is a minimum on the potential energy surface, and there is an energy barrier that must be crossed for the molecule to dissociate.[14] Similar rationalization applies for ClF_7^-.

5.3.4 Summary of the thermochemical data. The G3X IEs, EAs, and DEs of ClF_n, ClF_n^+, and ClF_n^- are summarized in Figure 2. Examining these results, it is seen that there is an alternating pattern for these three sets of data. Take the DEs as an example. The larger DE values correspond to the Cl–F bond energies (in kJ mol^{-1}) for ClF_2^+ (241.9), ClF_4^+ (184.3), ClF_6^+ (225.0), ClF_3 (184.2), ClF_5 (173.9), ClF_2^- (331.8), ClF_4^- (268.5), and ClF_6^- (190.3). In all of these cases, the dissociation involves the transformation from a higher and more stable species to a lower and less stable species plus a fluorine atom. Each of the stable species has a closed–shell configuration with even number of valence electrons around the central atom, whereas the unstable species do not. Similarly, a smaller DE corresponds to the transformation from a higher and less stable species to a lower and more stable species plus a fluorine atom: ClF_3^+ (20.7), ClF_5^+ (8.2), ClF_7^+ (11.7), ClF_2 (69.9), ClF_4 (43.2), ClF_6 (19.2), ClF_3^- (42.8), and ClF_5^- (18.7), where the DEs given in brackets are in kJ mol^{-1}. Referring to the other data summarized in Figure 2, IE is a measure of the transition energy from the neutral to its cation, whereas EA measures the transition from an anion to its corresponding neutral. The processes $ClF \rightarrow ClF^+ + e^-$, $ClF_3 \rightarrow ClF_3^+ + e^-$ and $ClF_5 \rightarrow ClF_5^+ + e^-$ correspond to ionization from a stable neutral to a less stable cation, and thus the IEs (in eV) of ClF (12.67), ClF_3 (12.58), and ClF_5 (12.84) have large values. The smaller IEs for ClF_2 (10.89), ClF_4 (11.12), and ClF_6 (10.70) are due to ionization from a less stable neutral to a more stable cation. Correspondingly, the electron detachment processes $ClF_2^- \rightarrow ClF_2$

+ e^-, $ClF_4^- \rightarrow ClF_4 + e^-$ and $ClF_6^- \rightarrow ClF_6 + e^-$ involve the formation of a less stable species from a more stable one. Therefore, we expect the EAs (in eV) for ClF_2 (4.78), ClF_4 (5.65), and ClF_6 (5.82) to be larger than those for ClF (2.07), ClF_3 (3.32), and ClF_5 (4.05), which correspond to detachment processes from a less stable anion to a more stable neutral. The alternating patterns for the IEs, EAs, and DEs of chlorine fluorides and their ions discussed here have also been observed for the corresponding data of sulfur fluorides, phosphorus fluorides and their ions.[2,3]

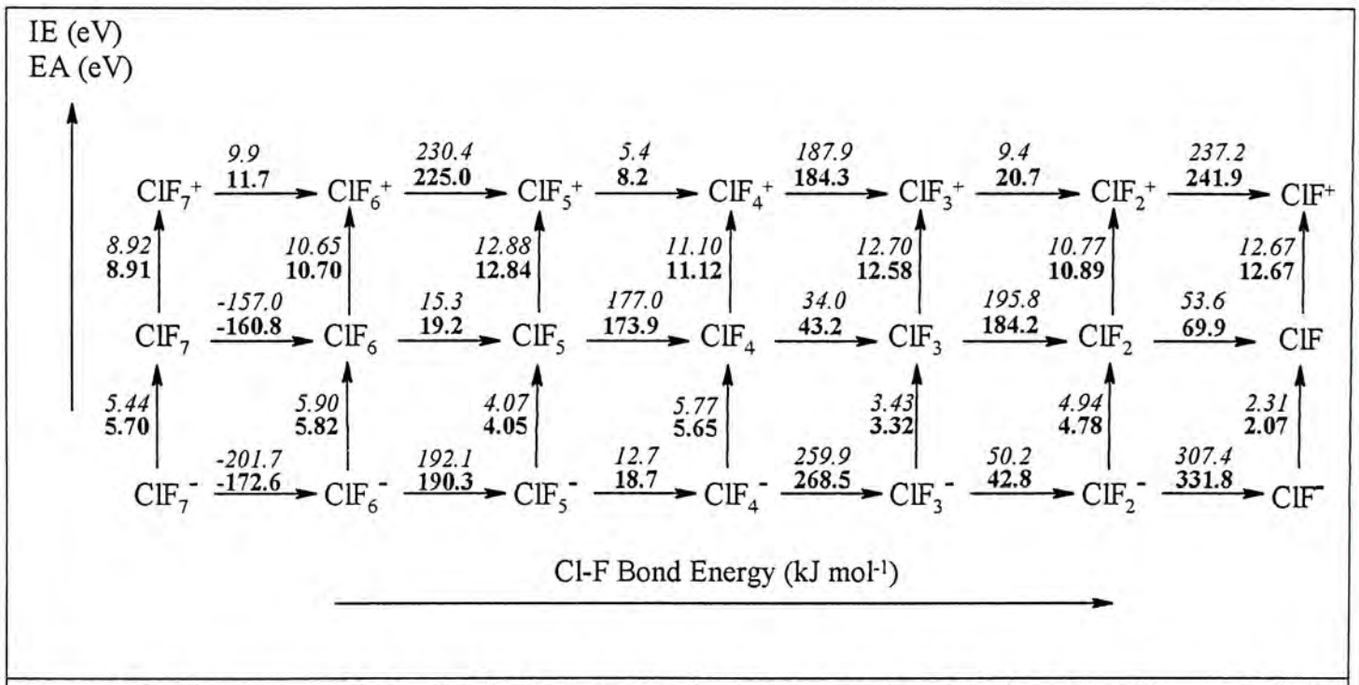

Figure 2. Summary of the G3X thermochemical data of the chlorine fluorides and their ions, illustrating the alternating patterns of the data.

5.4 Conclusion

We have applied the G3 and G3X methods to study the thermochemistry of chlorine fluorides ClF_n, as well as for their singly charged cations and anions. Specifically, we have obtained the ΔH_f values and the DEs of all the species, and the IEs and EAs of all the neutrals. When we compare the G3 and G3X ΔH_f results with the experimental data for ClF and ClF_3, it is found that G3X is more reliable method for this type of non–hydrogen systems. For the IEs or EAs of ClF_n, both the G3 and G3X method give similar results and these results are in good agreement with the available literature values. Based on the G3X results, a set of self-consistent experimental

thermochemical data for ClF_n, ClF_n^+, and ClF_n^- is recommended. The experimental bond dissociation energies are only available for Cl–F, which is consistent with our G3X result. The fair to excellent agreement between the known experimental values and the G3X results lends support to our predictions for the missing thermochemical data of chlorine fluorides. The general trends of the thermochemical data of the chlorine fluorides and their ions may be rationalized in terms of the electronic configurations of the species involved.

5.5 Publication Note

An article based on the results reported in this Chapter has been written up and submitted for publication: Law, C.-K.; Chien, S.-H.; Li, W.-K *J. Phys. Chem. A* (submitted).

5.6 References

(1) Pietro, W. J.; Francl, M. M.; Hehre, W. J.; Defrees, D. J.; Pople, J. A.; Binkley, J. S. *J. Am. Chem. Soc.* **1982**, *104*, 5039.

(2) Cheung, Y.-S.; Chen, Y.-J.; Ng, C.Y.; Chiu, S.-W.; Li, W.-K. *J. Am. Chem. Soc.* **1995**, *117*, 9725.

(3) Lau, J. K.-C.; Li, W.-K. *J. Mol. Struct. (THEOCHEM)* **2002**, *578*, 221.

(4) Lewis, G. N. *J. Am. Chem. Soc.* **1916**, *38*, 762.

(5) Langmuir, I. *J. Am. Chem. Soc.* **1919**, *41*, 868.

(6) Guest, M. F.; Hall, M. B.; Hillier, I. H. *J. Chem. Soc., Faraday Trans*, **1973**, *69*, 1829

(7) Peterson, K. A.; Woods, R. C. *J. Chem. Phys.* **1992**, *92*, 7412.

(8) Peterson, L. G. M.; Gropen, O.; Siegbahn, P. E. M. *Mol. Phys.* **1983**, *48*, 871.

(9) Scharf, P.; Ahlrichs, R. *Chem. Phys.* **1985**, *100*, 237.

(10) Pershin, V. L.; Boldyrev, A. I. *J. Mol. Struct. (THEOCHEM)* **1987**, *150*, 171.

(11) Jasien, P. G. *Chem. Phys. Lett.* **1992**, *188*, 135.

(12) Ungemach, S.R.; Schaefer, H. F. *J. Am. Chem. Soc.* **1976**, *98*, 1658.

(13) Sannigrahi, A. B.; Peyerimhoff, S. D. *Chem. Phys. Lett.* **1985**, *119*, 119.

(14) Van Huis, T. J.; Galbraith, J. M.; Schaefer, H. F. *Mol. Phys.* **1996**, *89*, 607.

(15) Ricca, A. *Chem. Phys. Lett.* **2000**, *323*, 498.

(16) Huber, K. P.; Herzberg, G. *Molecular Spectra and Molecular Structure. Constants of Diatomic Molecules*, Prentice Hall, New York, **1979**.

(17) Mamantov, G; Vickroy, D. G.; Vasini, E. J.; Maekawa, T.; Moultom, M. C. *Inorg. Nucl. Chem. Lett.* **1970**, *6*, 701.

(18) Morton, J. R.; Preston, K. F. *J. Chem. Phys.* **1973**, *58*, 3112.

(19) Christe, K. O.;Guertin, J. P. *Inorg. Chem.* **1965**, *4*, 905.

(20) Christe, K. O.;Sawodny, W.; Guertin, J. P. *Inorg. Chem.* **1967**, *6*, 1195.

(21) Christe, K. O.; Wilcom, W. W.; Chirakal, R. V.; Sanders, J. C. P.; Schrobilgen, G. J. *Inorg. Chem.* **1990**, *29*, 3506.

(22) Curtiss, L. A.; Raghavachari, K.; Redfern, P. C.; Rassolov, V.; Pople, J. A. *J. Chem. Phys.* **1998**, *109*, 7764.

(23) Curtiss, L. A.; Raghavachari, K.; Truck, G. W.; Pople, J. A. *J. Chem. Phys.* **1998**, *109*, 7764.

(24) Curtiss, L. A.; Redfern, P. C.; Raghavachari, K.; Pople, J. A. *J. Chem. Phys.* **2001**, *114*, 108.

(25) Curtiss, L. A.; Raghavachari, K.; Redfern, P. C.; Pople, J. A. *J. Chem. Phys.* **2000**, *112*, 7374.

(26) Frisch, M. J.; Trucks, G. W.; Schlegel, H. B.; Scuseria, G. E.; Robb, M. A.; Cheeseman, J. R.; Zakrzewski, V. G.; Montgogery, J. A.; Jr.; Stratmann, R.E.; Burant, J. C.; Dapprich, S.; Millam, J. M.; Daniels, A. D.; Kudin, K. N.; Strain, M. C.; Farkas, O.; Tomasi, J.; Barone, V.; Cossi, M.; Cammi, R.; Mennucci, B.; Pomelli, C.; Adamo, C.; Clifford, S.; Ochterski, J.; Petersson, G. A.; Ayala, P. Y.; Cui, Q.; Morokuma, K.; Malick, D. K.; Rabuck, A. D.; Raghavachari, K.; Foresman, J. B.; Cioslowski, J.; Ortiz, J. V.; Baboul, A. G.; Stefanov, B. B.; Liu, G.; Liashenko, A.; Piskorz, P.; Komaromi, I.; Gomperts, R.; Martin, R. L.; Fox, D. J.; Keith, T.; Al-Laham, M. A.; Peng, C. Y.; Nanayakkara, A.; Gonzalez, C.; Challacombe, M.; Gill, P. M. W.; Johnson, B.; Chen, W.; Wong, M. W.; Andres, J. L.; Gonzalez, C.; Head-Gordon, M.; Replogle, E. S.; Pople, J. A. *GAUSSIAN 98*, Revision A.7; Gaussian, Inc., Pittsburgh PA, 1998.

(27) Scott, A. P.; Radom, L. *J. Phys. Chem.* **1996**, *100*, 16502.

(28) Gurvich, L. V.; Veyts, I. V.; Alcock, C. B., Eds. *Thermodynamic Properties of Individual Substances*, CRC Press, Boca Raton, **1994**.

(29) Lias, S.G.; Bartmess, J. E.; Liebman, J. F.; Holmes, J. F.; Levin, R. E.; Mallard, W. J. *J. Phys. Chem. Ref. Data Suppl 1*, **1988**, 231.

(30) Chase, M. W., Jr. *JANAF Themochemical Tables*, 3rd ed.; Plenum: New York, **1985**.

(31) Dibeler, V.H.; Walker, J.A.; McCulloh, K.E. *J. Chem. Phys.* **1970**, *53*, 4414.

(32) DeKock, R.L.; Higginson, B.R.; Lloyd, D.R.; Breeze, A.; Cruickshank, D.W.J.; Armstrong, D.R. *Mol. Phys.* **1972**, *24*, 1059.

(33) Irsa, A.P.; Friedman, L. *J. Inorg. Nucl. Chem.* **1958**, *6*, 77.

(34) Dispert, H.; Lacmann, K. *Int. J. Mass Spectrom. Ion Phys.* **1978**, *28*, 49

(35) Dudlin, A.V.; Gorokhov, L.N.; Baluev, A.V. *Izv. Akad. Nauk SSR Ser. Khim.* **1979**, *11*, 2408.

(36) Baluev, A.V.; Nikitin, I.M.; Fedorova, L.I.; Rossolovskii, V.Ya. *Izv. Akad. Nauk SSR Ser. Khim.* **1980**, 487.

(37) Gillespie, R. J. *J. Chem. Educ.* **1970**, *47*, 18.

(38) Gillespie, R. J.; Popelier, P. L. A. *Chemical Bonding and Molecular Geometry*, Oxford, New York, **2001**.

Chapter 6

A Gaussian–3 Study of the Photoionization and Dissociative Photoionization Channels of Dimethyl Sulfide

Abstract

We have carried out the Gaussian–3 (G3) calculations on the energetics of dissociative photoionizations of dimethyl sulfide. Combining the G3 results with the experimental appearance energies for the photodissociation fragment ions CH_3^+, CHS^+, CH_2S^+, CH_2SH^+, CH_3S^+, and $CH_3SCH_3^+$, we have established the dissociation channels of dimethyl sulfide. The G3 energetics are generally in good agreement with the experimental results.

6.1 Introduction

There are significant concentrations of reduced sulfur compounds such as H_2S, CS_2, CH_3SH, and CH_3SCH_3 (dimethyl sulfide, DMS) arising from natural sources into the earth's atmosphere.[1] Among those reduced sulfur compounds, DMS is probably the most important one because it has been proposed that emission of DMS may provide a means of biological climate regulation.[2] Hence DMS is the major source of cloud condensation nuclei in the troposphere. Variations in the tropospheric concentrations of DMS could therefore affect the climate by altering the albedo of clouds.[2]

DMS is produced by marine phytoplankton[3] (first detected in the upper levels of the oceans by Lovelock et al.[4]), then escaped into the atmosphere from the oceans.[5] Another source of DMS is emitted out as organosulfur pollutants from the incomplete combustion of coal and oil.[6,7] It represents approximately 25% of the total flux of sulfur into the atmosphere[3] and plays an important role in the global sulfur cycle. Therefore, knowledge of the properties of DMS is important for an understanding of the chemistry of the atmosphere.

In order to understand the structures and energetics of photoionization products of dimethyl disulfide, Nourbakhsh et al.[8] performed a 193 nm laser photodissociation time-of-flight (TOF) study of the processes

$$CH_3SCH_3 + h\nu \rightarrow CH_3 + CH_3S$$

$CH_3SCH_3 + h\nu \rightarrow CH_3SCH_2 + H$

They measured the photoelectron-photoion coincidence (PEPICO) spectra and reported the appearance energies (AEs) for the five major fragment ions, $CH_3SCH_3^+$, $CH_3SCH_2^+$, CH_3S^+, CH_2SH^+, and CH_2S^+ resulting from the photoionization of CH_3SCH_3. A few years later, Lee et al.[9] studied the photodissociation processes of CH_3SCH_3 at 193 nm by translational spectroscopy. Their results have shown that, at 193 nm, only the simple dissociation channel producing CH_3 and CH_3S is observed.

More recently, Chen and his co-workers[10] have investigated the dissociation of $CH_3SCH_3^+$ by collisional activation. The appearance energies (AEs) and the E_{ex}-onset for the product ions CH_2SH^+/CH_3S^+, CH_2S^+, CHS^+, CH_3^+ formed in the collision-induced dissociation (CID) reaction have been measured. In this work, in conjunction with the experimental results obtained by Chen et al.,[10] we use the Gaussian–3 (G3)[11] method to study the structures and energetics of the fragments, including CH_3^+, CHS^+, CH_2S^+, CH_2SH^+, CH_3S^+, and $CH_3SCH_3^+$, as well as the mechanisms for the dissociations producing these fragments. Such a study would lead to a better understanding of the photodissociative processes of dimethyl sulfide.

6.2 Methods of Calculation

All calculations were carried out on DEC 500au, COMPAQ XP900 and XP1000 workstations using the Gaussian 98 packages of program.[12] The computational model we employed was the aforementioned G3 level of theory.[11]

6.3 Results and Discussion

Table 1 lists, for the fragments CH_3^+, CHS^+, CH_3S^+, CH_2SH^+, CH_2S^+, and $CH_3SCH_2^+$, the AEs determined in the CID of $CH_3SCH_3^+ + Ar$ and E_{ex}-onset (where E_{ex} denotes the maximum excitation energy and onset is the bond dissociation threshold) values measured by photoionization of CH_3SCH_3. Both sets of values were measured by Chen et al.[10] in the experiments of photoionization and dissociative photoionizations of dimethyl sulfide. Note that CID is from $CH_3SCH_3^+$ in the ground state; thus the AE observed in CID is measured with respect to the parent ion. On the other hand, photoionization is from the neutral ground state of CH_3SCH_3. The AE for dissociative photoionization process is hence not the same AE in CID. The

difference between these two AEs is the IE of CH_3SCH_3. Here E_{ex}-onset is defined as AE(Photoionization) - IE(CH_3SCH_3), which is in principle the same as AE(CID).

The structural formulas of the species involved in this work, along with their symmetry point groups, are displayed in Figure 1. The G3 standard heats of formation of various species involved in the dissociations of CH_3SCH_3 (**1**) and its cation (**2**) are summarized in Table 2.

Table 1: Appearance energies (AEs) and E_{ex}-onset values for CH_2SH^+ (CH_3S^+), CH_2S^+, CHS^+, and CH_3^+ determined in the CID of $CH_3SCH_3^+$ + Ar and photoionization of CH_3SCH_3, respectively.

Product Ions	CID AE (eV)	Photoionization [a] E_{ex}-onset (eV)
$CH_3SCH_2^+$	–	2.24 ± 0.06 (1.284 ± 0.02)[b]
CH_2SH^+/CH_3S^+	2.6 ± 0.2	2.20 ± 0.06 (2.03 ± 0.018)[b]
CH_2S^+	2.0 ± 0.2	1.90 ± 0.06 (1.814 ± 0.018)[b]
CHS^+	7.6 - 8.2	–
CH_3^+	6.8 - 7.3	–

[a] E_{ex}-onset = AE(Photoionization) - IE(CH_3SCH_3). [b] Ref 8.

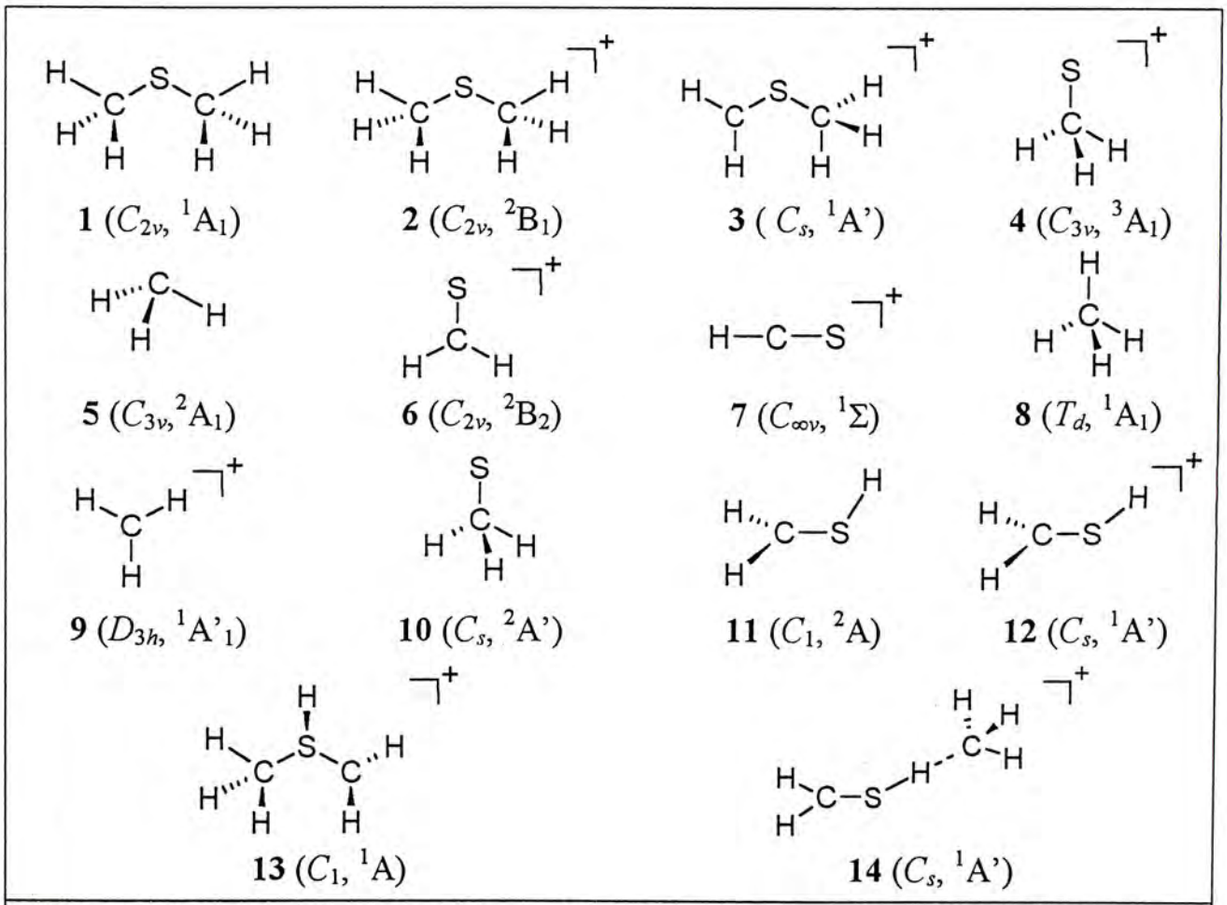

Figure 1. Structural formula of the stable species involved in the dissociation of dimethyl sulfide, along with their symmetry point groups and electronic states.

Table 2: G3 total energies (E_0), enthalpies (H_{298}), and standard heats of formation at 0 K (ΔH°_{f0}) and 298 K (ΔH°_{f298}) of the species involved in the dissociation of dimethyl sulfide and its cation[a]

Species	E_0 (hartree)	H_{298} (hartree)	ΔH°_{f0} (kJ mol^{-1})	ΔH°_{f298} (kJ mol^{-1})
CH_3SCH_3 (**1**)	–477.76744	–477.76165	–12.8	–28.1
			(–21.3)[b]	(–37.5 ± 2.0)[c]
$CH_3SCH_3^+$ (**2**)	–477.44788	–477.44174	826.2	811.9
$CH_3SCH_2^+$ (**3**)	–476.85824	–476.85285	842.9	830.8
CH_3S^+ (**4**)	–437.52523	–437.52122	1021.1	1014.5
			(1025.1 ± 2.0)[c]	
CH_3 (**5**)	–39.79144	–39.78733	149.6	147.1
			(149.0 ± 1.3)[c]	(145.8 ± 1)[b]
CH_2S^+ (**6**)	–436.94044	–436.93654	1025.1	1022.4
			(1023.0 ± 8.4)[d]	
CHS^+ (**7**)	–436.36208	–436.35810	1012.2	1013.9
			(1017.5 ± 12.1)[d]	
CH_4 (**8**)	–40.45548	–40.45167	–62.5	–70.0
			(–66.8)[c]	(–74.8)[c]
CH_3^+ (**9**)	–39.42928	–39.42548	1100.4	1097.1
			(1098.3 ± 1.3)[d]	
CH_3S (**10**)	–437.86377	–437.85966	132.3	125.9
			(131.4 ± 2.1)[d]	
CH_2SH (**11**)	–437.84986	–437.84519	168.8	163.9
			(157.7 ± 8.4)[d]	
CH_2SH^+ (**12**)	–437.57453	–437.57055	891.7	884.9
			(884.9 ± 8.4)[d]	
(**13**)	–477.41455	–477.40832	913.7	899.6
(**14**)	–477.34347	–477.36573	1021.6	1011.4
H[a]	–0.50100			
S[a]	–397.96111			
Transition structures[e]				
$\mathbf{TS_a}$	–477.37772	–477.37194	1010.4	995.1
$\mathbf{TS_b}$	–477.37404	–477.36705	1020.1	1007.9
$\mathbf{TS_c}$	–477.37834	–477.37192	1008.8	995.2
$\mathbf{TS_d}$	–477.34339	–477.33741	1100.5	1085.8

[a] Values taken from Ref 11. [b] Ref 13. [c] Ref 14. [d] Ref 15. and references cited therein.
[e] The transition structure $\mathbf{TS_a}$ to $\mathbf{TS_d}$ are defined in Figures 2–3

The G3 IE of **1** is calculated to be 8.70 eV, which is in a very good agreement with the experimental value (8.69 ± 0.02 eV) reported by Chen et al.[10] With the aid of Table 2, it can be seen that all the G3 heats of formation (ΔH°_{f0}) are in good agreement with the experimental values, except for **1**, **11**, and **12**. However, considering that the experimental uncertainty for **11** and **12** are exceedingly large, it is believed that our G3 results give a more reliable estimate.

6.3.1 Bond cleavage reactions. Dissociations of the dimethyl sulfide cation (**2**), which involve only the cleavage of bond(s), are summarized in this section.

$CH_3SCH_3^+$ (**2**) $\rightarrow$ $CH_3SCH_2^+$ (**3**)+ H $\Delta H^\circ_0 = 2.21$ eV (1)

$CH_3SCH_3^+$ (**2**) $\rightarrow$ CH_3S^+ (**4**) + CH_3 (**5**) $\Delta H^\circ_0 = 3.60$ eV (2)

$CH_3SCH_3^+$ (**2**) $\rightarrow$ CH_2S^+ (**6**) + H + CH_3 (**5**) $\Delta H^\circ_0 = 5.80$ eV (3)

$CH_3SCH_3^+$ (**2**) $\rightarrow$ CHS^+ (**7**) + H + CH_4 (**8**) $\Delta H^\circ_0 = 3.42$ eV (4)

$CH_3SCH_3^+$ (**2**) $\rightarrow$ CHS^+ (**7**) + H_2 + CH_3 (**5**) $\Delta H^\circ_0 = 3.53$ eV (5)

$CH_3SCH_3^+$ (**2**) $\rightarrow$ CHS^+ (**7**) + 2H + CH_3 (**5**) $\Delta H^\circ_0 = 7.96$ eV (6)

$CH_3SCH_3^+$ (**2**) $\rightarrow$ CH_3^+ (**9**) + CH_3S (**10**) $\Delta H^\circ_0 = 4.18$ eV (7)

$CH_3SCH_3^+$ (**2**) $\rightarrow$ CH_3^+ (**9**) + CH_2SH (**11**) $\Delta H^\circ_0 = 4.44$ eV (8)

$CH_3SCH_3^+$ (**2**) $\rightarrow$ CH_3^+ (**9**) + CH_3 (**5**) + S $\Delta H^\circ_0 = 7.23$ eV (9)

The above experimental heats of reaction, ΔH°_0, along with those calculated by the G3 method, are tabulated in Table 3 for easy comparison. From Table 3, it is seen that the G3 results are in very good agreement with the experimental values, except for reactions (1), (4), and (8).

Table 3: Experimental and calculated ΔH°_0 (eV) of the dissociation of the dimethyl sulfide

Dissociation reaction	ΔH°_0(expt)	ΔH°_0 (G3)
Simple bond cleavage reactions		
(1) $CH_3SCH_3^+$ (**2**) $\rightarrow$ $CH_3SCH_2^+$ (**3**) + H	2.21	2.41
(2) $CH_3SCH_3^+$ (**2**) $\rightarrow$ CH_3S^+ (**4**) + CH_3 (**5**)	3.60	3.57
(3) $CH_3SCH_3^+$ (**2**) $\rightarrow$ CH_2S^+ (**6**) + H + CH_3 (**5**)	5.80	5.85
(4) $CH_3SCH_3^+$ (**2**) $\rightarrow$ CHS^+ (**7**) + H + CH_4 (**8**)	3.42	3.65
(5) $CH_3SCH_3^+$ (**2**) $\rightarrow$ CHS^+ (**7**) + H + CH_4 (**8**)	3.53	3.52
(6) $CH_3SCH_3^+$ (**2**) $\rightarrow$ CHS^+ (**7**) + 2H + CH_3 (**5**)	7.96	7.96
(7) $CH_3SCH_3^+$ (**2**) $\rightarrow$ CH_3^+ (**9**) + CH_3S (**10**)	4.18	4.21
(8) $CH_3SCH_3^+$ (**2**) $\rightarrow$ CH_3^+ (**9**) + CH_2SH (**11**)	4.44	4.59
(9) $CH_3SCH_3^+$ (**2**) $\rightarrow$ CH_3^+ (**9**) + CH_3 (**5**) + S	7.23	7.24
Reactions involving reaction barriers		
(10) $CH_3SCH_3^+$ (**2**) $\rightarrow$ CH_2SH^+ (**12**) + CH_3 (**5**)	2.15	2.23
(11) $CH_3SCH_3^+$ (**2**) $\rightarrow$ CH_2S^+ (**6**) + CH_4 (**8**)	1.26	1.41

6.3.2 Dissociation channels involving transition structures. In this section, we consider the two dissociation of the dimethyl sulfide cation which involve TSs.

$CH_3SCH_3^+$ (**2**) $\rightarrow$ CH_2SH^+ (**12**) + CH_3 (**5**) $\Delta H^\circ_0 = 2.15$ eV (10)

The calculated heats of reaction is 2.23 eV, which is in good agreement with the experimental value, 2.15 eV. From Figure 2, it is seen that **2** first undergoes 1,2-hydrogen shift to form the isomeric ion $CH_2SHCH_3^+$ (**13**). This ion is calculated to be 0.91 eV less stable than **2**. This intermediate then undergoes direct cleavage of the $H_2C(H)S–CH_3^+$ bond, without another TS, to yield CH_2SH^+ (**12**) and CH_3 (**5**). The overall G3 barrier for this reaction is 1.91 eV, which is much lower than the experimental result (2.6 ± 0.2 eV). Since, at excitation energies greater than 1.91 eV, these isomeric structures **2** and **13** can interconvert and contribute to the dissociation product ions. The experimental threshold 2.6 ± 0.2 eV for the formation of CH_2SH^+ (**12**) + CH_3 (**5**) is higher than the transition barrier of 1.91 eV, so the rearrangement of the parent ion $CH_3SCH_3^+$ (**2**) via 1,2-hydrogen shift is expected to proceed prior to dissociation.

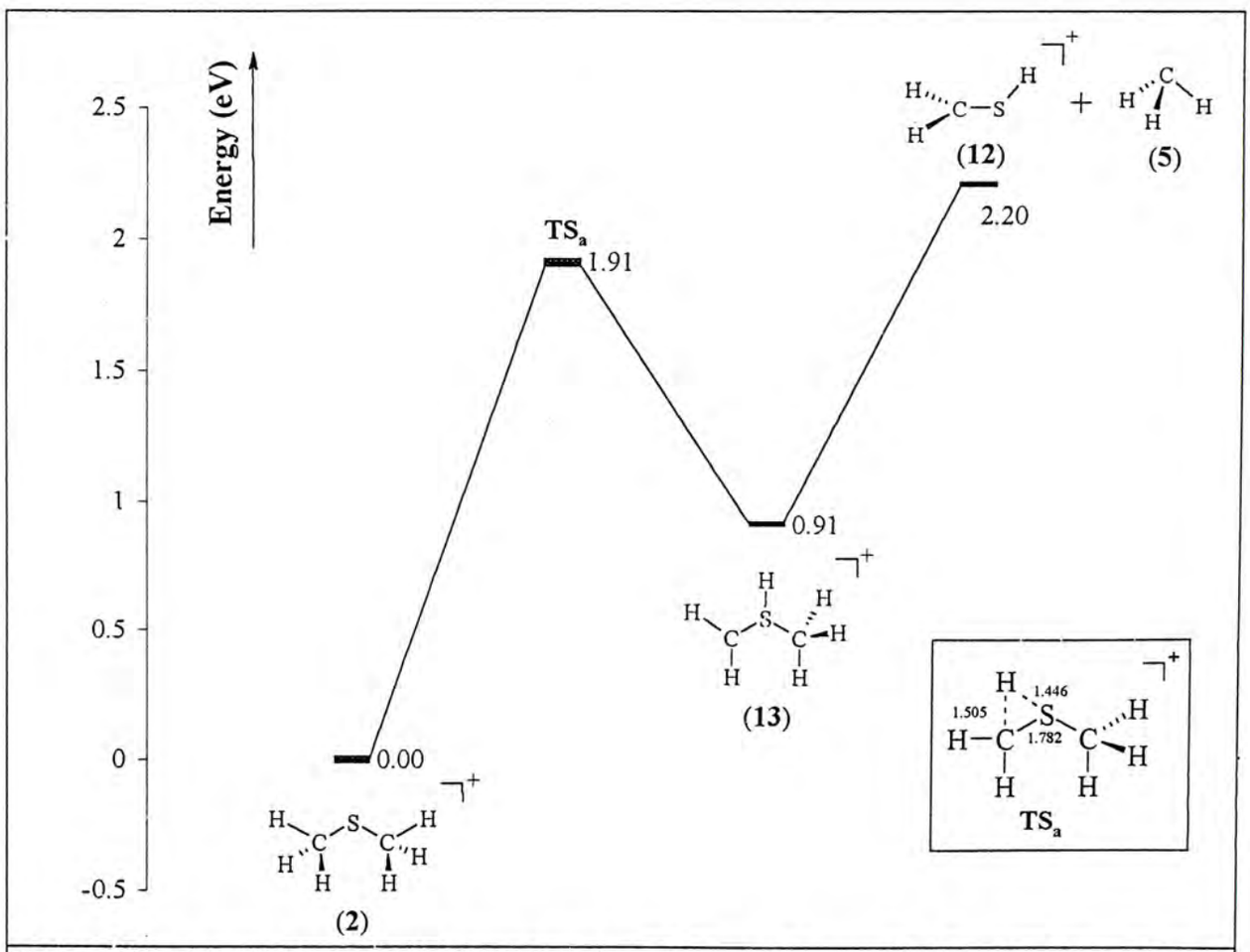

Figure 2. Potential energy surface showing the possible mechanism for dissociation $CH_3SCH_3^+ \rightarrow CH_2SH^+ + CH_3$

Another dissociation of 2 involving TS(s) is:

$CH_3SCH_3^+$ (**2**) $\rightarrow$ CH_2S^+ (**6**) + CH_4 (**8**) $\Delta H^\circ_0 = 1.26$ eV (11)

The experimental and G3 calculated ΔH°_0 are 1.26 and 1.41 eV, respectively. It can be seen that our calculated result is fairly close to the experimental measurement. The energy profile for this dissociation is summarized in Figure 3. In this reaction, both the experimental values (AE, 2.0 ± 0.2 eV, and E_{ex}, 1.9 ± 0.06 eV) for the formation of CH_2S^+ ions are higher than the thermochemical threshold of $\Delta H^\circ_0 = 1.26$ eV. It appears that a potential energy barrier of ≈ 0.75 eV may exist above the energy of CH_2S^+ (**6**) + CH_4 (**8**). As shown in Figure 3, **2** again undergo 1,2-hydrogen shift to form $CH_2SHCH_3^+$ (**13**), which can yield **6** + **8** in one step via $\mathbf{TS_d}$. Transition structure $\mathbf{TS_d}$, which involves concomitant hydrogen shift and bond breaking, is energetically 1.43 eV above **6** + **8**, leading to an overall barrier of 2.84 eV. This calculated barrier is significantly higher than the experimental value of 2.0 ± 0.2 eV, which suggests that $\mathbf{TS_d}$ may not be responsible for the dissociation and rearrangement of **13** to **6** + **8**.

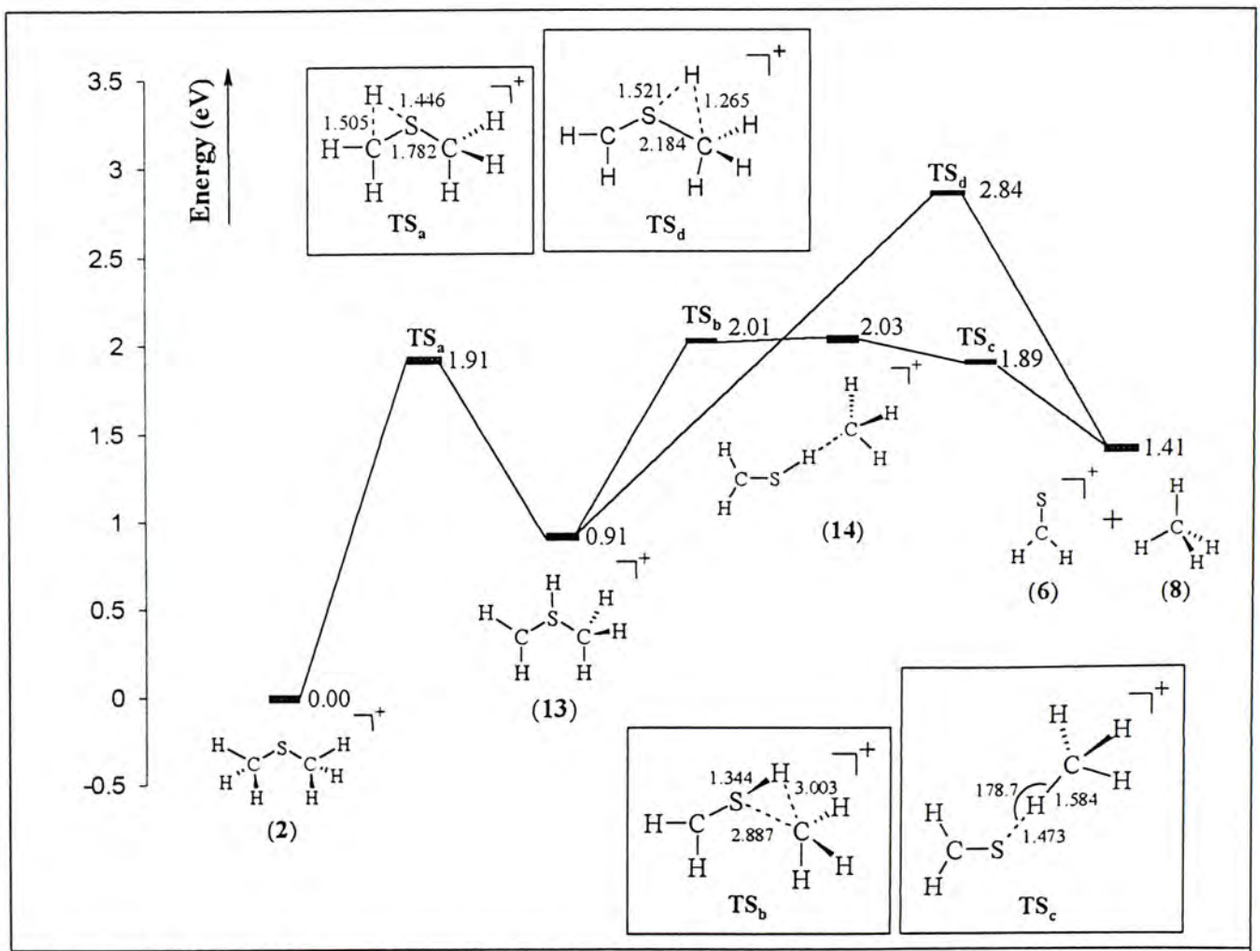

Figure 3. Potential energy surface showing the possible mechanism for dissociation $CH_3SCH_3^+ \rightarrow CH_2S^+ + CH_4$

Additionally, we have also located transition structure $\mathbf{TS_b}$ for the methyl shift across the S–H bond of **13**. This $\mathbf{TS_b}$ leads to the formation of $CH_2SH^+...CH_3$ complex (**14**), which can undergo hydrogen abstraction via $\mathbf{TS_c}$ to yield **6** + **8**. The respective methyl shift and hydrogen abstraction transition barriers are calculated to be 0.60 and 0.48 eV above **6** + **8**. Thus, the dissociation from $CH_3SCH_3^+$ to CH_2S^+ + CH_4 is governed by the transition barrier of methyl shift between $CH_2SHCH_3^+$ (**13**) and $CH_2SH^+...CH_3$ (**14**) and the overall potential barrier is 2.01 eV. This calculated result is in excellent agreement with the experimental value, 2.0 ± 0.2 eV.

All the above theoretical predictions are consistent with the experimental observation that the observed AE and E_{ex} values for these product channels agree with the corresponding thermochemical thresholds.

6.4 Conclusion

The energetics for the dissociative photoionizations of dimethyl disulfide have been carried out by the G3 method. Combining these results with the experimental photoionization spectra of various fragments reported by Chen et al, we are able to establish the dissociation channels for the formation of the following ions: CH_3^+, CHS^+, CH_2S^+, CH_2SH^+, CH_3S^+ and $CH_3SCH_3^+$. The G3 results are in good accord with the experimental values in most cases.

6.5 Publication Note

An article based on the experimental[10] and G3 results reported in this chapter has been written up and submitted for publication: Chen Y.-J.; Fenn, P. T.; Lau, K. C.; Ng, C. Y.; Law, C.-K.; Li, W.-K. *J. Phys. Chem. A* (submitted).

6.6 References

1. Wayne, R. P. *Chemistry of Atmospheres*, Clarendon, Oxford, **1991**.
2. Charlson, R. J.; Lovelock, J. E.; Andreae, M. O.; Warren, S. G. *Nature* **1987**, *326*, 655.
3. Andreae, M. O.; Raemdonck, H. *Science* **1983**, *221*, 744.
4. Lovelock, J. E.; Maggs, R. J.; Rasmussen, R. A. *Nature* **1972**, *237*, 452.
5. Badr, O.; Probert, S. D. *App. Energy* **1994**, *47*, 1.
6. Graedel, T. E. *Rev. Geophys. Space Phys.* **1977**, *15*, 421.

7. Bentley, M. D.; Douglass, I. B.; Lacadie, J. A.; Whittier, D. R. *J. Air Pollution Control Assoc.* **1972**, *22*, 359.
8. Nourbakhsh, S.; Norwood, K.; Yin, H.-M.; Liao, C.-L.; Ng, C. Y. *J. Chem. Phys.* **1991**, *95*, 5014.
9. Lee. Y. R.; Chiu, C. L.; Lin, S. M. *J. Chem. Phys.* **1994**, *100*, 7376.
10. Chen Y.-J.; Fenn, P. T.; Lau, K. C.; Ng, C. Y.; private communication.
11. Curtiss, L. A.; Raghavachari, K.; Redfern, P. C.; Rassolov V.; Pople, J. A. *J. Chem. Phys.* **1998**, *109*, 7764.
12. Frisch, M. J.; Trucks, G. W.; Schlegel, H. B.; Scuseria, G. E.; Robb, M. A.; Cheeseman, J. R.; Zakrzewski, V. G.; Montgogery, J. A.; Jr.; Stratmann, R.E.; Burant, J. C.; Dapprich, S.; Millam, J. M.; Daniels, A. D.; Kudin, K. N.; Strain, M. C.; Farkas, O.; Tomasi, J.; Barone, V.; Cossi, M.; Cammi, R.; Mennucci, B.; Pomelli, C.; Adamo, C.; Clifford, S.; Ochterski, J.; Petersson, G. A.; Ayala, P. Y.; Cui, Q.; Morokuma, K.; Malick, D. K.; Rabuck, A. D.; Raghavachari, K.; Foresman, J. B.; Cioslowski, J.; Ortiz, J. V.; Baboul, A. G.; Stefanov, B. B.; Liu, G.; Liashenko, A.; Piskorz, P.; Komaromi, I.; Gomperts, R.; Martin, R. L.; Fox, D. J.; Keith, T.; Al-Laham, M. A.; Peng, C. Y.; Nanayakkara, A.; Gonzalez, C.; Challacombe, M.; Gill, P. M. W.; Johnson, B.; Chen, W.; Wong, M. W.; Andres, J. L.; Gonzalez, C.; Head-Gordon, M.; Replogle, E. S.; Pople, J. A. *GAUSSIAN 98*, Revision A.7; Gaussian, Inc., Pittsburgh PA, 1998.
13. Lias, S.G.; Bartmess, J. E.; Liebman, J. F.; Holmes, J. F.; Levin, R. E.; Mallard, W. J. *J. Phys. Chem. Ref. Data Suppl 1*, **1988**.
14. The NIST Chemistry Webbook, http://webbook.nist.gov/chemistry/.
15. Fenn, P. T.;Chen, Y.-J.; Stimon, S.; Ng, C. Y. *J. Phys. Chem.* **1997**, *101*, 6513.

Chapter 7

Theoretical Study of the Electronic Structures of Carbon and Silicon Nanotubes, Carbon and Silicon Nanowires

Abstract

A diamond nanowire (CNW), a silicon nanowire (SiNW), a carbon nanotube (CNT), and a silicon nanotube (SiNT) were studied using the semiempirical molecular orbital PM3 method, with confirmations by ab initio calculations at the HF/3–21G and HF/3–21G(d) levels. The electronic structures of these four systems were decomposed into constituent atoms and atomic orbitals. The differences in their structures, bonding, and relative stability were elucidated. It was found that the systems with a diamond structure generally show larger band gaps than their tubular counterparts. Carbon nanotubular structure shows efficient sp^2 hybridization and π bonding, thus allowing a high stability for this structure. In contrast, silicon prefers sp^3 hybridization and favors the tetrahedral diamond-like structures, thereby forming the commonly observed nanowires. This distinction can be traced to the differences in the energetics and overlaps of the valence s and p orbitals of C against Si. Nevertheless, when the dangling bonds are properly terminated, SiNT can in principle be formed. The resulting energy minimized SiNT, however, adopts a severely puckered structure (with a corrugated surface) with Si–Si distances ranging from 1.85 to 2.25 Å.

7.1 Introduction

Since the discovery of the carbon nanotubes,[1] there has been considerable interest in their structures and electronic properties, both experimentally[2,3] and theoretically.[4,5] Carbon nanotubes are promising materials for nanotechnology because of their unique properties, such as small diameter, high aspect ratio, high mechanical strength, high thermal and chemical stabilities, excellent heat conduction, etc.[6,7] Furthermore, nanotubes can be either metallic or semiconducting, with the semiconducting band gap depending upon the tube diameter and chirality.[8,9] Even before the synthesis of single-wall carbon nanotubes (SWNTs), calculations based on the symmetry of the honeycomb lattice of graphite predicted that they could be either

semiconducting or metallic, depending upon their geometry.[10-17] The beauty and simplicity of the structures of carbon nanotubes make them excellent candidates for theoretical study.

For silicon, an element in the same group of carbon in the Periodic Table, a variety of nanostructures have also been reported and intensively studied, among which one-dimensional Si nanowires have attracted much attention recently, owing to their fundamental and technological importance.[18-20] It has been suggested that semiconductor wires finer than 100 nm in diameter may be used for developing one-dimensional (1D) quantum-wire high-speed field effect transistors and light-emitting devices with extremely low power consumption.[21] Menon and Richter have investigated the stability of quasi-one-dimensional structures of Si using a generalized tight-binding molecular-dynamics scheme.[22] They proposed a quasi-one-dimensional structure with a core of bulk-like tetrahedrally coordinated Si atoms and a surface closely resembling one of the most stable reconstruction of crystalline Si surfaces. More recently, Marsen and Sattler reported Si nanowires of 3 to 7 nm in diameter and at least 100 nm in length.[21] The wires tend to be assembled in parallel bundles. The authors proposed a one-dimensional polymeric chain structure based on a fullerene-type Si_{24} cluster for the nanowires.

Unlike carbon nanotubes, silicon nanotube has never been observed experimentally, although intensive theoretical work has been carried out, exploring the possibility of the existence of silicon nanotubes.[23,24] Nevertheless, the electronic and structural properties of a hypothetical Si nanotube similar to those of a C nanotube were compared, and similarities regarding their stereochemically dependent band structures and conducting properties have been found.[23] Some stable silicon tubular structures were also found to be similar to those of phosphorus tubes, exhibiting semiconducting properties independent of tube diameter and chirality.[24] Though the difficulty in the synthesis of silicon nanotubes is widely attributed to the property of sp^3 hybridization in silicon, how, and to what extent, such a hybridization affects the tubular structural formation still needs further clarification.

The difference in the chemistry exhibited by carbon and silicon can be traced to the difference in their π bonding capabilities. Here two components can be identified: the difference in the energetics of the valence s and p orbitals and the extent of overlaps of the π orbitals. First, the energy difference between the valence

s and p orbitals for carbon is nearly twice that for silicon. As a result, silicon tends to utilize all three of its valence p orbitals, resulting in sp^3 hybridization. In contrast, the relatively large hybridization energy for carbon implies that carbon will "activate" one valence p orbital at a time, as required by the bonding situation, giving rise, in turn, to sp, sp^2, and sp^3 hybridizations. Second, since the interatomic distance increases significantly in going from carbon to silicon, the π–π overlap decreases accordingly (by roughly an order of magnitude), resulting in much weaker π bonding for silicon in comparison with that for carbon. Hence, Si=Si bonds are in general much weaker than C=C bonds.

In the present work, we wish to compare the electronic structures of four systems: a diamond nanowire (CNW, **1**), a silicon nanowire (SiNW, **2**), a carbon nanotube (CNT, **3**), and a silicon nanotube (SiNT, **4**). Our goal is to elucidate the differences in the structures and bonding between cubic (diamond-like) and tubular nanostructures of carbon and silicon and their relative stabilities in terms of their characteristic electronic structures, with the hope of understanding the reason(s) for the hitherto unsuccessful synthesis of silicon nanotubes. However, as we shall see in this paper, when the dangling bonds on the open ends of the tubular structure are properly terminated, SiNT with a severely puckered structure can in principle be formed. Such computationally stable, energetically minimized, and geometrically optimized SiNT structures may serve as models for the design and synthesis of silicon nanotubes.

7.2 Models and Computational Methods

All calculations were carried out on DEC 500au, COMPAQ XP900 and XP1000 workstations using the GAUSSIAN 98 package of programs.[25] The PM3 parametrization[26] of the MNDO semiempirical hamiltonian[27] was used throughout the calculations for all cluster models considered here. All the structures were geometrically optimized with the PM3 method. To confirm the PM3 results, geometrical optimizations at the HF/3–21G and HF/3–21G(d) levels were further conducted for the four models. The results from the three levels of calculations were similar for **1**–**3** but rather different for **4**. As we shall see later, for **4**, PM3 and HF/3–21G(d) showed similar trends (but with different numerical values) of bond lengths and angles that are very different from those obtained with HF/3–21G. This is due to

the highly strained structure of **4**, which requires a larger and more flexible basis set (including d orbitals for Si).

The four model compounds studied in this work are shown in Figure 1. They represent a diamond nanowire $C_{54}H_{60}$ (**1**), a silicon nanowire $Si_{54}H_{60}$ (**2**), a carbon nanotube $C_{54}H_{12}$ (**3**), and a silicon nanotube $Si_{54}H_{12}$ (**4**). The carbon nanotube selected here has an armchair (3,3) structure. It is one of the smallest carbon nanotubes reported recently.[28-30] For compounds **1** and **2** shown in Figure 1, hydrogen atoms were used to saturate the boundary dangling bonds so as to stabilize the structures and to maintain the tetrahedral geometry of the diamond structures for both carbon (**1**) and silicon (**2**) nanowires. Similarly, the hydrogen atoms in compounds **3** and **4** shown in Figures 1 were used to stabilize the structures as well as to simulate the effect of a longer tube. In particular, we found that saturation of the dangling bonds with hydrogen at the ends of a silicon nanotube is crucial for the silicon tube in order to maintain the metastable structure, without which the structure first deforms and eventually collapses to form an irregularly shaped nanowire with mostly sp^3 hybridized Si atoms.

7.3 Results and Discussion

For the geometrically optimized 1-D nanostructures **1–4** considered here, there are general trends of bond length variations. As indicated in Figure 1, the C–C bonds in structure **1** are about 1.54 Å for the bonds more or less perpendicular to the wire axis and about 1.53 Å for the bonds in the other directions. In contrast, for the Si–Si bonds in structure **2**, the bonds more or less perpendicular to the wire axis are shorter (2.35 Å) than the bonds (2.36 Å) in the other directions. In the CNT **3**, the C–C bond lengths alternate between 1.40 and 1.46 Å, indicating a certain degree of C=C vs C–C bond localization. The small bond length alternation of about 0.06 Å signifies that π delocalization is extensive in **3**. We have also found that this small variation and alternation in bond lengths would be further reduced, and the delocalization further enhanced, if the length of the tube is increased. Silicon nanotube such as **4** also shows similar bond length alternation (see Figure 1), but with a much larger variation of 0.40 Å.

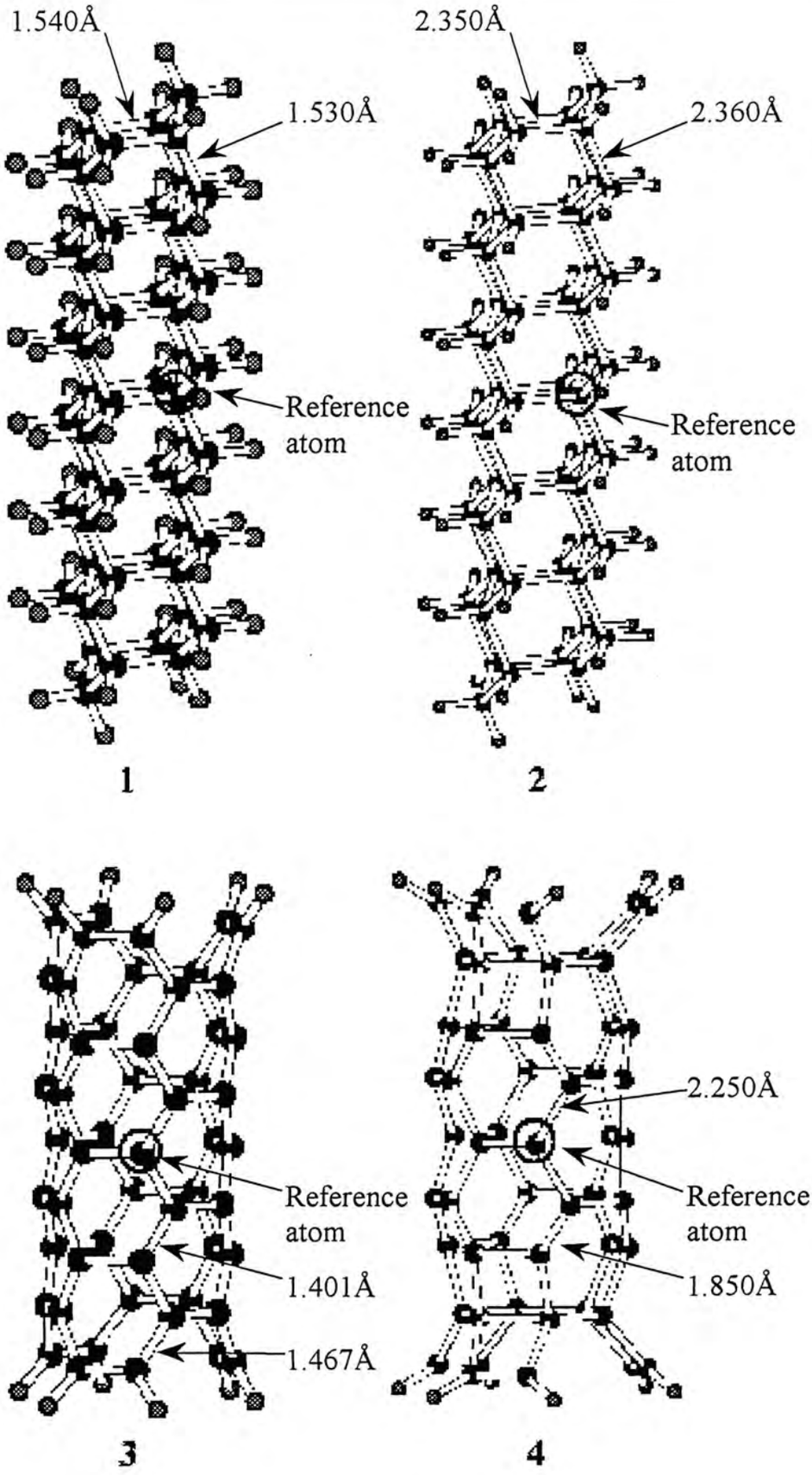

Figure 1. Four model compounds: a diamond nanowire $C_{54}H_{60}$ (1), a silicon nanowire $Si_{54}H_{60}$ (2), a carbon nanotube $C_{54}H_{12}$ (3), and a silicon nanotube $Si_{54}H_{12}$ (4).

In **4**, the shortest Si–Si bond length is only about 1.85 Å, while the longest is about 2.25 Å, showing a stronger tendency for bond localization than that found in the CNTs. In fact, as depicted in Figure 1, the "naphthalene-like" hexagonal rings in **4** exhibit strong bond alternation between 1.85 and 2.25 Å, suggesting a strong tendency for bond localization (Si=Si vs Si–Si). On the other hand, the hexagonal rings in the middle of the tube exhibit a much lesser degree of bond alternation, comprising mainly longer bonds of approximately 2.25 Å, which is close to the single Si–Si bond length of 2.35 Å. As can be seen from Figure 1, the CNT **3** has a smooth surface and a more-or-less uniform tube diameter. In contrast, the SiNT **4** has a puckered (corrugated) surface and a less uniform tube diameter. Furthermore, it should be noted that, upon geometry optimization, the ends of SiNT **4** are distorted to form 12 four-membered rings and terminated by H atoms. As a result, both ends of the SiNT **4** are capped with planar hexagonal rings rather than open-ended as in the CNT **3**.

To lend support to the structural trends described above, we performed additional Hartree–Fock calculations for the respective structures with 3–21G and 3–21G(d) basis sets. The latter basis set includes the d orbitals of Si. It was found that, except for **4**, the structural features of the other three are similar to those described above based on the PM3 calculations. The C–C bonds in **1** are about 1.54 Å, while those in **3** alternate between 1.38 and 1.45 Å; these results are similar to those obtained from the PM3 calculations. Structure **2** with HF/3–21G calculation adopts slightly longer bonds (2.38 and 2.39 Å) than those in the PM3 calculations. Considerable differences for structure **4** are found between HF/3–21G and PM3 results. The Si–Si bond length alternations are significantly reduced to 0.09 Å (alternating between 2.33 and 2.42 Å) in the ab initio calculation, comparing to the 0.40 Å variation in the PM3 calculation. However, a more accurate calculation at the HF/3–21G(d) level shows an increased Si–Si bond length alternation of 0.18 Å (between 2.16 and 2.34 Å), indicating the strong dependence on the choice of basis set for this system, probably due to its highly strained structure. The puckered feature of **4** becomes more noticeable in the Hartree–Fock calculations with both basis sets than in the PM3 calculation. We note that the trends of bond alternation in **4** determined by PM3 and HF/3–21G(d) calculations are quite similar, though the absolute values are different. In contrast, much smaller bond alternations were

obtained from the HF/3–21G calculation. Hence, for the sake of simplicity, the following discussions will be based primarily on the results of the PM3 calculations.

Table 1. Electronic energy levels for a C atom and a Si atom obtained from PM3 calculations [a]

Orbital	Energy level (eV)	Orbital	Energy level (eV)
C(2p*)	–0.82	Si(3p*)	–2.31
C(2p)	–7.23	Si(3p)	–5.08
C(2s)	–17.83	Si(3s)	–10.74

[a]C(2p*) and Si(3p*) indicate the unoccupied states from C 2p and Si 3p orbitals, respectively.

The total density of states (TDOSs) and their projections onto constituent atoms (PDOS) of **1** – **4**, depicted in Figures 2(a) – (d), respectively, were calculated by Professor R.Q. Zhang of the City University of Hong Kong based on the method reported in his previous work.[31] It is seen that the diamond nanowire **1** (Figure 2(a)) has a relatively large HOMO–LUMO (the highest occupied molecular orbital – the lowest unoccupied molecular orbital) gap of 12.2 eV. This unusually large energy gap can be attributed to the size effect of nanostructure and the deficiency of molecular orbital theory in describing the band structures.[32] The silicon nanowire **2** shows a smaller energy gap of 3.6 eV (Figure 2(b)). However, it is still too large compared with the well-known trend of energy gap as a function of structure dimension.[33] The relative trend of the HOMO–LUMO gap, however, agrees (in fact, scales properly) with the known HOMO–LUMO gaps between diamond and silicon wires of the same diameter. It is interesting to note that there is a tail at the valence band edge of the silicon nanowire (Figure 2(b)). It consists of the leftover states due to the removal of the band edge states originated from the hydrogenated silicon atoms on the surface. In contrast, there are no noticeable band tail states for the diamond nanowire, indicating the difference in the role of surface hydrogenation for carbon vs silicon nanowires. Furthermore, the valence band width of the diamond nanowire is much larger than that of the silicon nanowire. This can be rationalized in terms of the energy difference between the valence s and p states of C ($E_{2p} - E_{2s}$ = 10.60 eV) vs Si ($E_{3p} - E_{3s}$ = 5.66 eV), according to the electronic energy levels for

the respective atoms used in our PM3 calculations (see Table 1). In fact, we believe that this energetic difference is related to the pronounced difference between C and Si in terms of their tendencies in forming sp^2 vs sp^3 hybridization. We will come back to this point later.

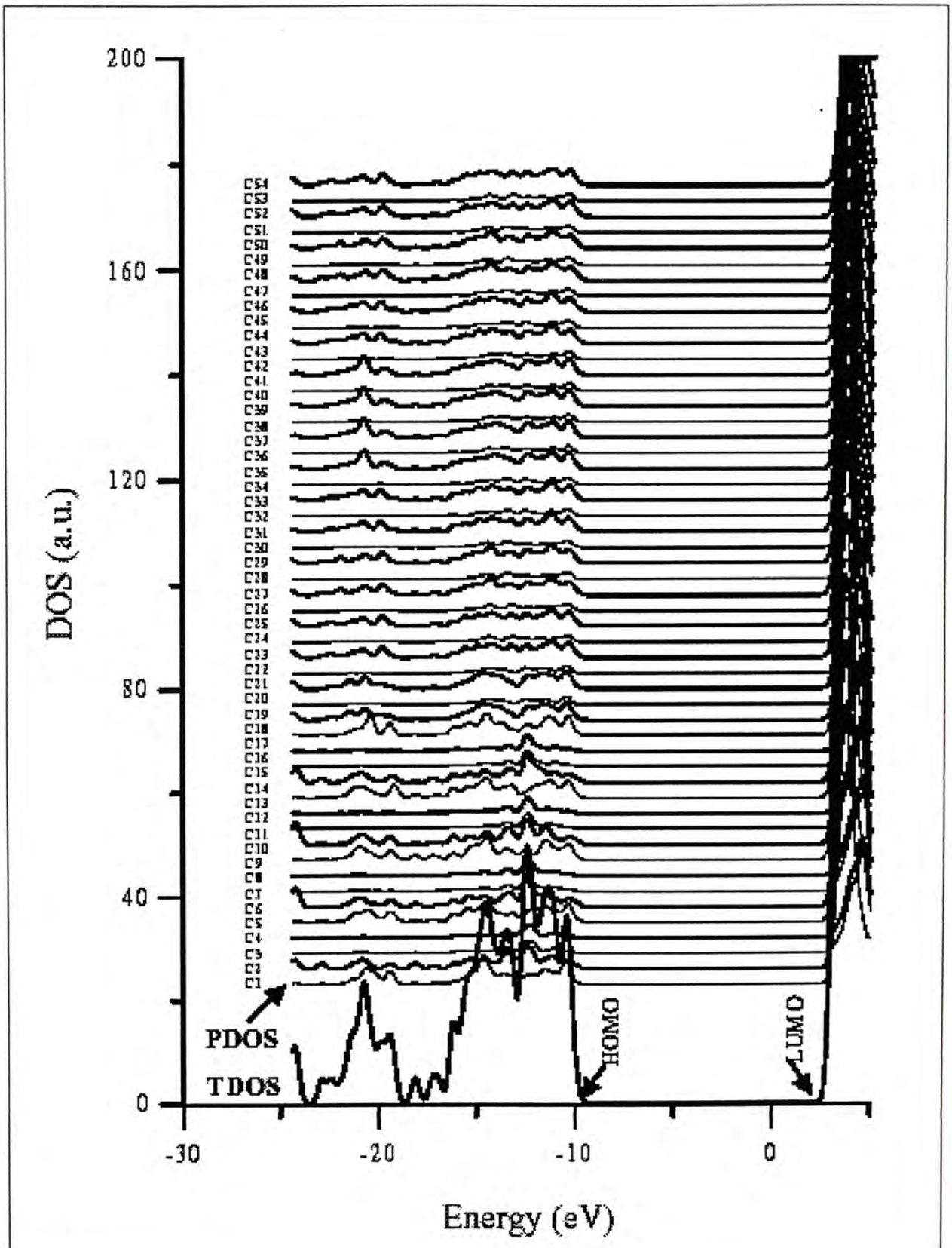

Figure 2(a). The TDOS and PDOS of diamond nanowire $C_{54}H_{60}$ (1).

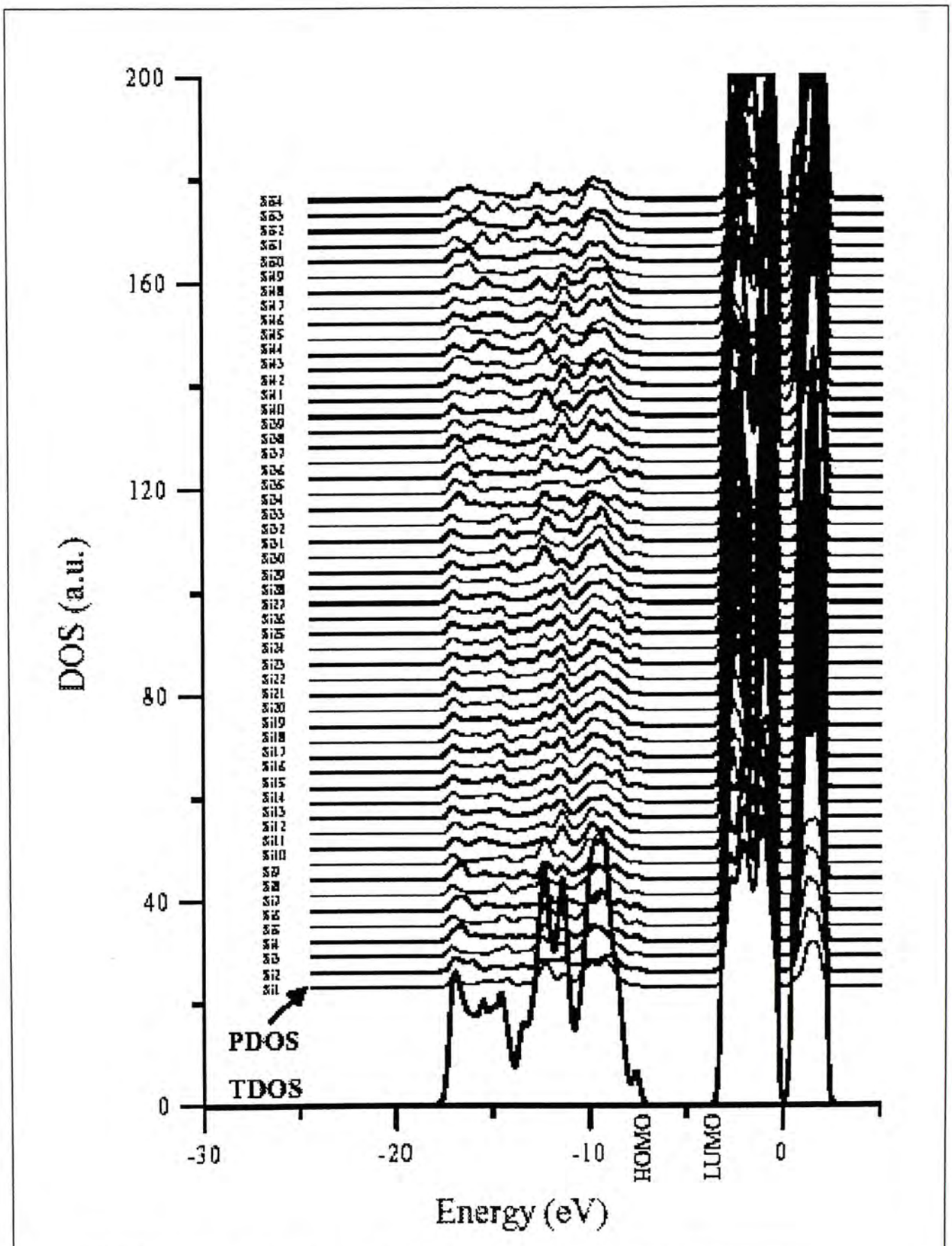

Figure 2(b). The TDOS and PDOS of silicon nanowire $Si_{54}H_{60}$ (2).

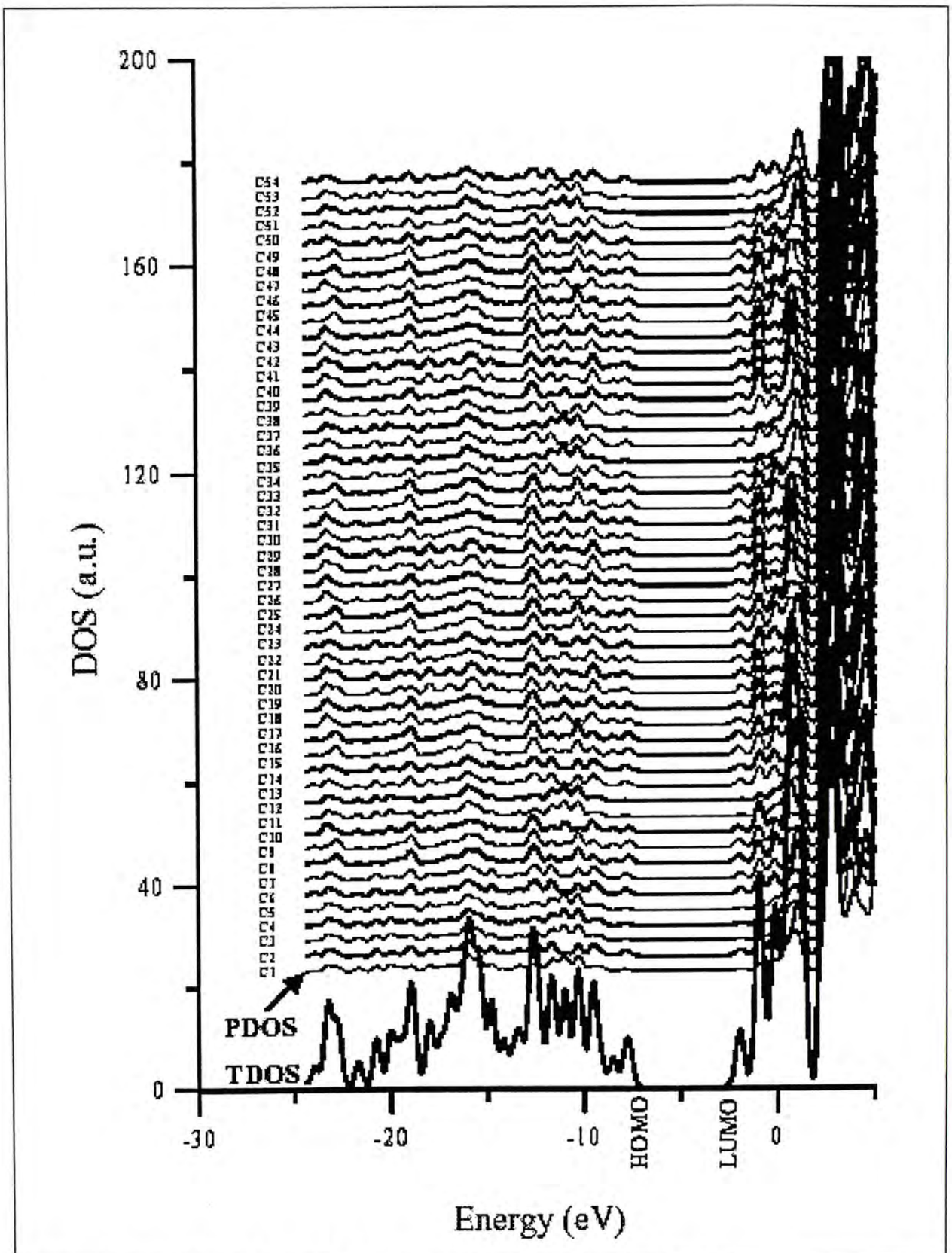

Figure 2(c). The TDOS and PDOS of carbon nanotube $C_{54}H_{12}$ (3).

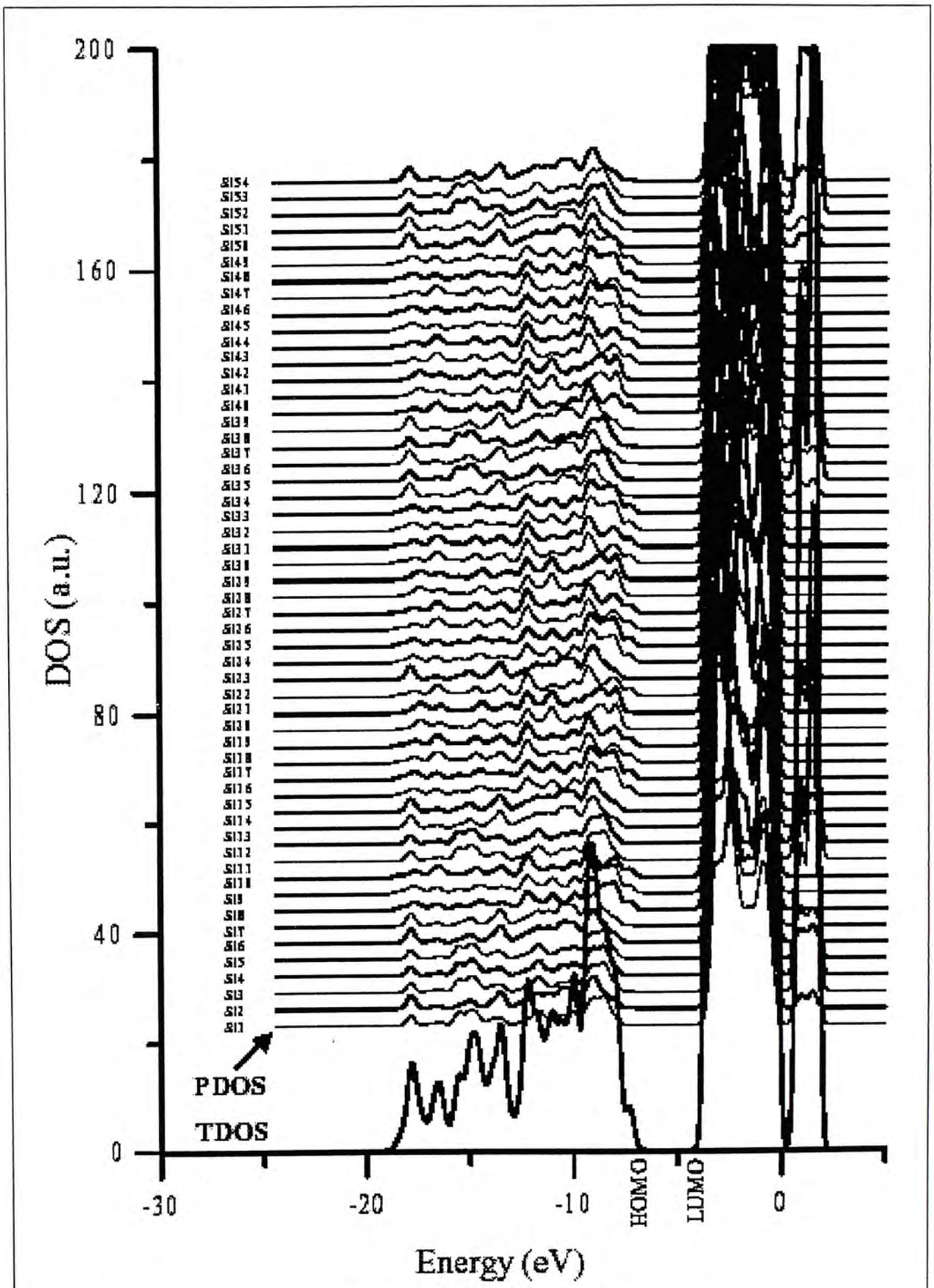

Figure 2(d). The TDOS and PDOS of silicon nanotube $Si_{54}H_{12}$ (4).

The DOS of the carbon nanotube **3** is shown in Figure 2(c). It exhibits a broadening feature compared to that of the diamond nanowire **1**. In addition, its valence band edge moves to a higher energy (i.e., a lower binding energy), while its conduction band edge drops in energy (i.e., less antibonding), mainly due to the formation of the π bonding. The resulting band gap is 4.9 eV. The DOS of the silicon nanotube **4** is shown in Figure 2(d). While it differs from that of tetrahedrally coordinated silicon nanowire **2**, shown in Figure 2(b), it retains some of the features of the valence band (especially at the top of the band) of the latter, indicating that some degree of sp^3 hybridization exists in the silicon nanotube **4**. The resulting band gap is 3.0 eV.

We now focus our attention on one representative atom (circled in Figure 1) of each of the four systems in order to reveal the distinctive features of their electronic structures. The PDOS and its decomposition into constituent atomic orbitals (ODOS) are shown in Figures 3(a) – (d) for **1** – **4**, respectively.

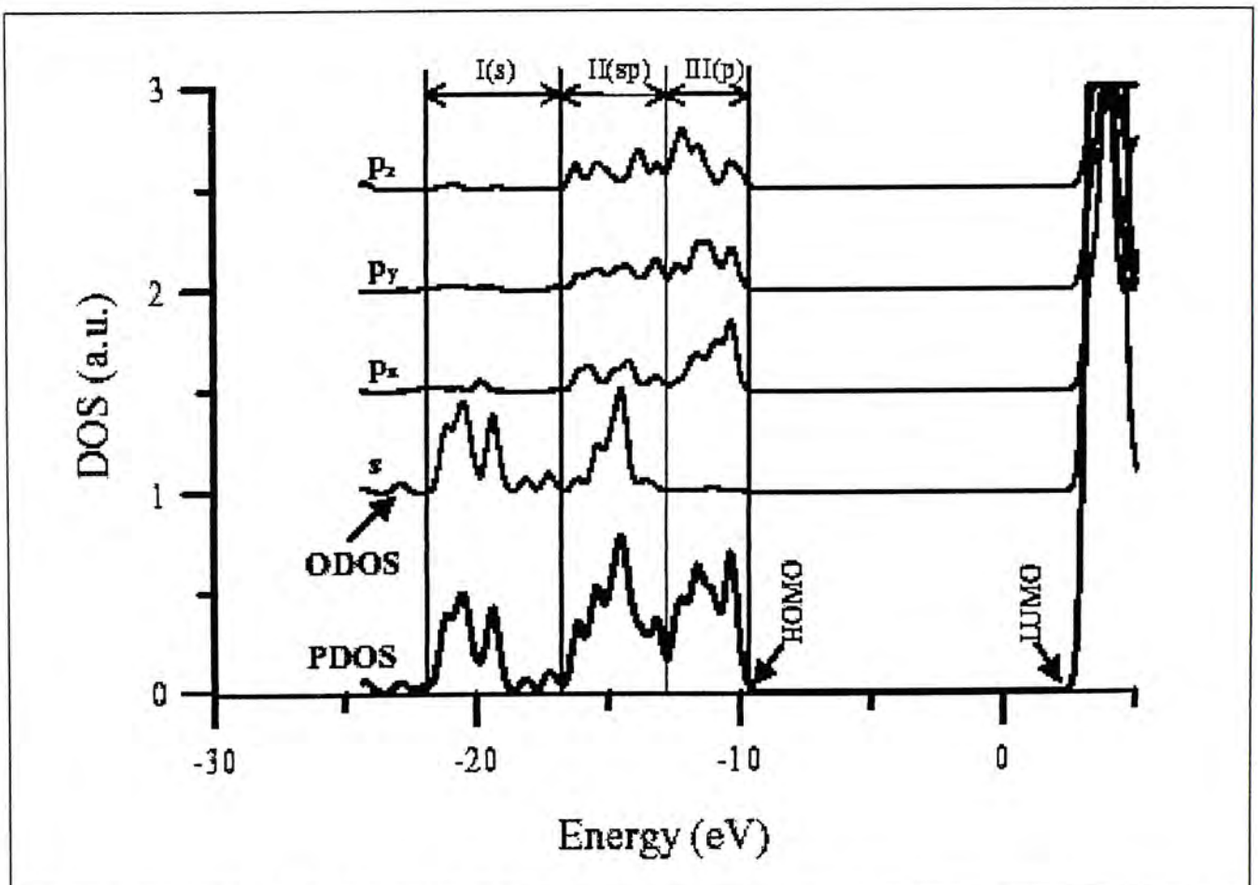

Figure 3(a). The PDOS and ODOS of one representative atom (the circled one) for each structure shown in Figure 1: diamond nanowire $C_{54}H_{60}$ (1).

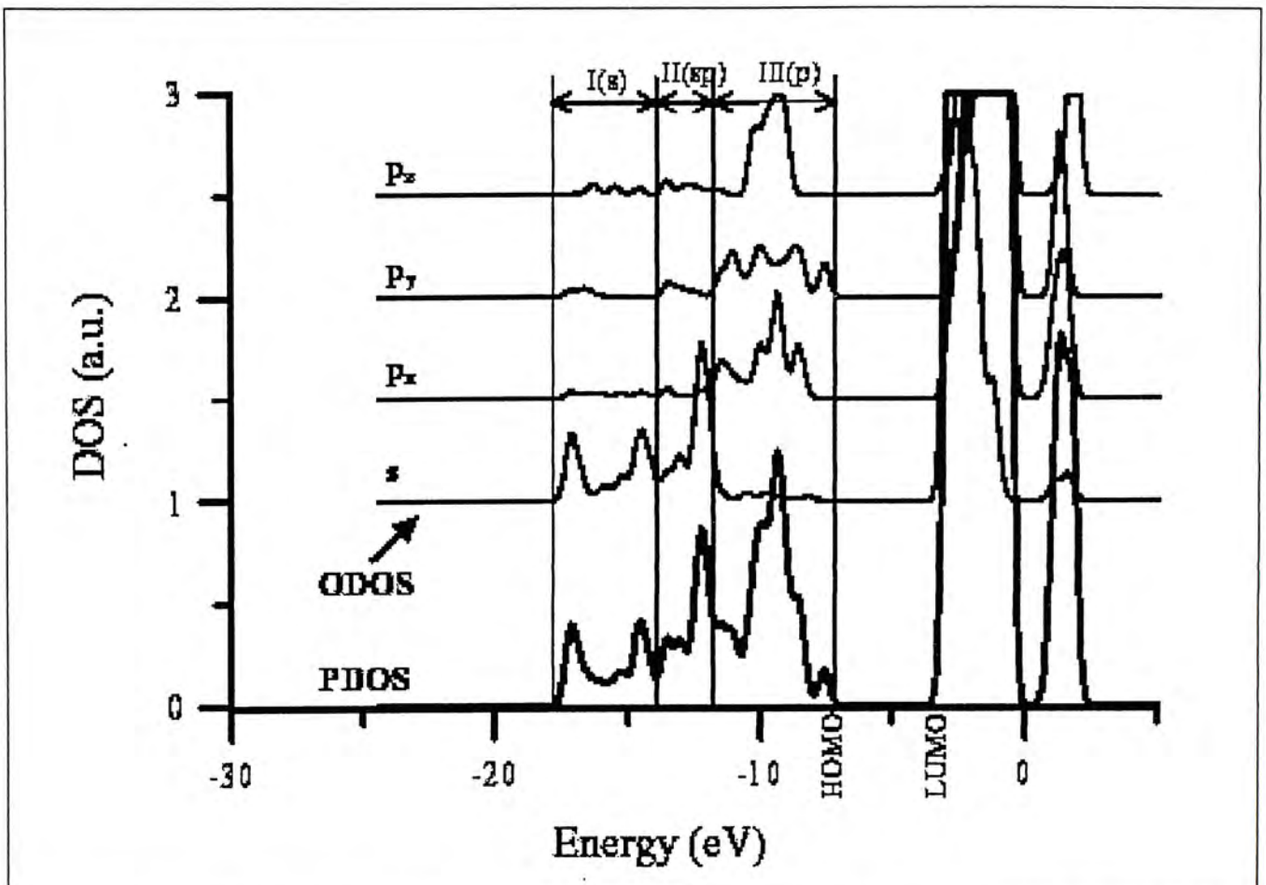

Figure 3(b). The PDOS and ODOS of one representative atom (the circled one) for each structure shown in Figure 1: silicon nanowire $Si_{54}H_{60}$ (2).

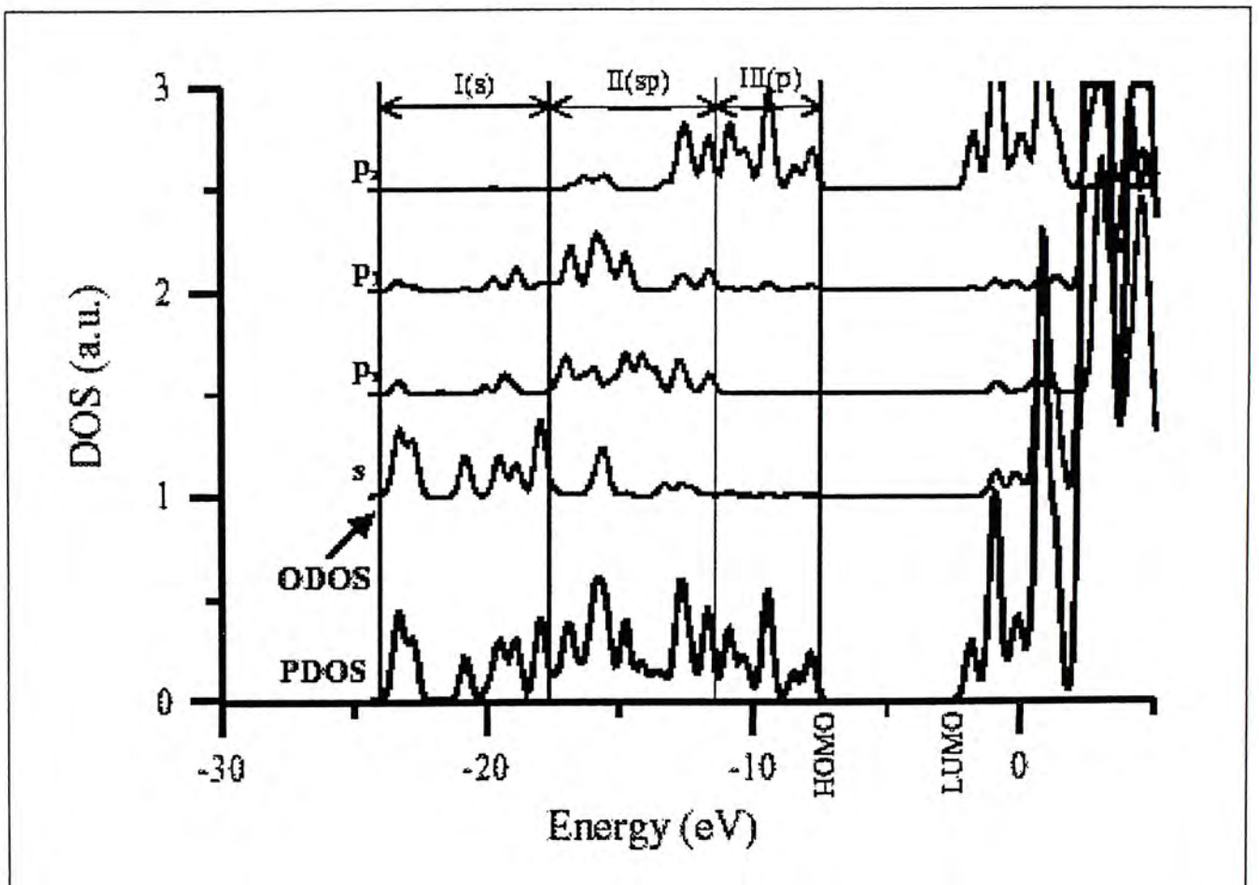

Figure 3(c). The PDOS and ODOS of one representative atom (the circled one) for each structure shown in Figure 1: carbon nanotube $C_{54}H_{12}$ (3).

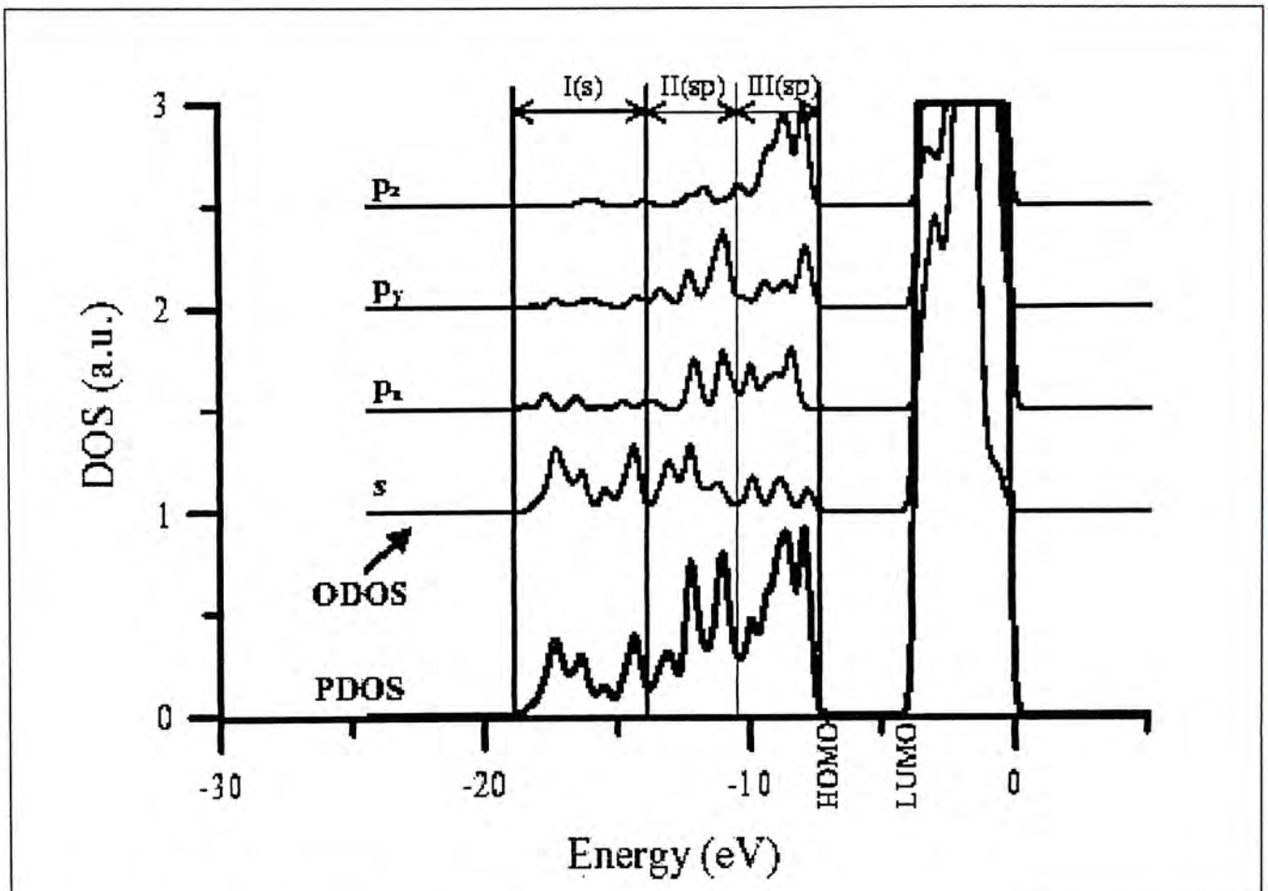

Figure 3(d). The PDOS and ODOS of one representative atom (the circled one) for each structure shown in Figure 1: silicon nanotube $Si_{54}H_{12}$ (4).

It can be seen that there are some similarities in the origin of the valence band states among the diamond nanowire **1**, silicon nanowire **2**, and silicon nanotube **4**. These similarities include: the part closest to the band gap (region III) is dominated by the three p atomic orbitals; a considerable mixing of s and p orbitals occurs in the middle part (region II) of the valence band; the s orbital (region I) located at the highest binding energy without significant mixing with the p orbitals. In contrast, for the carbon nanotube **3,** the part of valence band closest to the band gap (region III) derives mainly from one of the p orbitals, say, p_z, which participates in π bonding, while the other two components, p_x and p_y, of the p orbitals hybridize with the s orbitals, resulting in the sp^2 bonding configuration (region II), thus giving rise to the stable tubular structure. In comparison with the CNTs (**3**), silicon nanotubes (**4**), are less effective in forming sp^2 bonding configuration, due to the inherent tendency of silicon to undergo sp^3 hybridization. The three p orbitals and the s orbital efficiently hybridize in region III of Figure 3(d), with contributions of 36, 28, 22, and 14% from the p_z, p_y, p_x, and s orbitals, respectively. There is no clear separation of delocalized π bonding and the localized σ bonding formed by the sp^2 hybrid orbitals. This

feature is distinctly different from that of the carbon nanotubes such as **3**. Therefore, tubular structures for Si are, in general, less stable and tend to relax to the diamond-like structure with tetrahedral configuration, which allows for the largest extent of overlap of the sp^3 hybridized orbitals. Under appropriate conditions, such partial structural relaxation may lead to a puckered tubular structure as reported here for **4**. A complete relaxation will, of course, result in the diamond or diamond-like structures for carbon and silicon nanowires as exemplified by **1** and **2**, respectively.

As stated in the introduction, the significant difference between C and Si in their tendency to form tubular structures can be traced to the differences in the energetics and overlaps of the valence s and p orbitals of C vs Si. First, as summarized in Table 1, the energy difference between the valence s and p orbitals is $\Delta E = E_{2p} - E_{2s} = 10.60$ eV for C vs $\Delta E = E_{3p} - E_{3s} = 5.66$ eV for Si. As a result of the relatively small ΔE, Si tends to utilize all three of its valence p orbitals, thereby resulting in sp^3 hybridization and the formation of the diamond-like nanowire structure. In contrast, the relatively large ΔE for C implies that carbon will "activate" one valence p orbital at a time, as required by the bonding situation, giving rise, in turn, to sp, sp^2 (tube), sp^3 (wire) hybridizations. Second, the π–π overlap in the Si=Si bond is roughly an order of magnitude smaller than the corresponding value in C=C bond (roughly 0.01 vs. 0.10) as a result of the relatively long Si=Si distances (1.85 Å at PM3 and 2.16 Å at HF/3–21G(d)) in comparison with that of the C=C bond lengths (1.35 and 1.40 Å). The poor π–π overlaps and hence weak π bonding between silicon atoms give rise to a larger bond alternation (i.e., less electron delocalization) and a severely puckered structure for SiNTs such as **4.** By contrast, the relatively short C=C distances mean good π–π overlaps and hence strong π bonding between carbon atoms, thereby giving rise to a much smaller bond alternation (i.e., more electron delocalization) and a smooth tubular surface for CNTs such as **3**.

Finally, it is of relevance to consider the case of multi-wall tubular structures. The relatively large size of the p orbitals of silicon (in comparison with that of carbon) also means that the p orbital, say, p_z, responsible for π bonding in a tubular structure (or a planar, graphite-like structure), can extend into adjacent layers, resulting in partial sp^3 hybridization and hence a multi-wall tubular structure with a

corrugated surface. A full sp^3 hybridization will eventually turn the multi-wall tubular silicon structure into a close-packed diamond-like silicon nanowire structure.

7.4 Conclusion

In conclusion, the decomposition of DOS is a highly useful tool in revealing the details of the electronic structures of large systems such as the nanowires and nanotubes consisting of carbon and silicon atoms, as exemplified by **1** – **4**. The diamond structures show larger band gaps than the tubular structures. Carbon nanotubular structures are very stable primarily due to of the efficient sp^2 hybridization and delocalized π bonding exhibited by carbon. On the other hand, silicon tubular structures are much less stable due to the strong tendency of silicon to undergo sp^3 hybridization, thereby favoring the formation of tetrahedral diamond-like structure, rather than the tubular one. However, the results for the energy-minimized, computationally stable silicon nanotube **4** suggest that, under appropriate conditions, silicon nanotubes with puckered surface structures may be formed.

7.5 Publication Note

An article based on the results reported in this Chapter has been written up and submitted for publication: Zhang, R. Q.; Lee, S.T.; Law, C.-K; Li, W.-K.; Teo, Boon K. *Chem. Phys. Lett.* (submitted).

7.6 References

(1) Iijima, S. *Nature* **1991**, 354, 56.

(2) Wildoer, J. W. G.; Venema, L. C.; Rinzler, A. G.; Smalley, R. E.; Dekker, C., *Nature* **1998,** 391, 59.

(3) Odom, T. W.; Huang, J.-L.; Kim, P.; Lieber, C.M. *Nature* **1998**, 391, 62.

(4) J.-C. Charlier, J.-C.; Lambin, Ph. *Phys. Rev. B* **1998**, 57, R15037.

(5) Zhou, G.; Duan, W.H.; Gu, B. L. *Chem. Phys. Lett,* **2001**, 333, 344.

(6) Hamada, N.; Sawada, S. I.; Oshiyama, A. *Phys. Rev. Lett.* **1992**, 68, 1579.

(7) Saito, R.; Dresselhaus G.; Dresselhaus, M. S. *Physical Properties of Carbon Nanotubes*; Imperial College Press: London, 1998

(8) Ouyang, M.; huang, J.-L.; Cheung, C. L.; Lieber, C. M. *Science* **2001**, 292, 702.

(9) Collins, P. G.; Arnold, M. S.; Avouris, P. *Science* **2001**, 292, 706.

(10) Odom, T. W.; Huang, J-L.; Kim, P.; Lieber, C.M.; *Nature* **1998**, 391, 62.

(11) Thess A.; Lee R.; Nikolaev P.; Dai H. J.; Petit P.; Robert J.; Xu C. H.; Lee Y. H.; Kim S. G.; Rinzler A. G.; Colbert D. T.; Scuseria G. E.; Tomanek D.; Fischer J. E.; Smalley R. E., *Science* **1996**, 273, 483-487.

(12) Journet C.; Maser W. K.; Bernier P.; Loiseau A.; delaChapelle M. L.; Lefrant S.; Deniard P.; Lee R.; Fischer J.E., *Nature* **1997**, 388, 756-758.

(13) Mintmire, J. W.; Dunlap, B. I.; White, C. T. *Phys. Rev. Lett.* **1992** 68, 631.

(14) Hamada, N.; Sawada, S. I.; Oshiyama, A. *Phys. Rev. Lett.* **1992**, 68, 1579.

(15) Saito, R.; Fujita, M.; Dresselhaus, G.; Dresselhaus, M. S. *Appl. Phys. Lett.* **1992**, 60, 2204.

(16) Saito, R.; Fujita, M.; Dresselhaus, G.; Dresselhaus, M. S., *Phys. Rev. B.* **1992**, 46, 1804.

(17) R Saito, R.; Dresselhaus, G.; Dresselhaus, M. S., *Phys. Rev. B* **2000**, 61, 2981.

(18) Wang, N.; Tang, Y. H.; Zhang, Y. F.; Lee, C. S.; Lee, S. T. *Phys. Rev. B* **1998**, 58, R16024.

(19) Hu, J.; Ouyang, M.; Yang, P.; Lieber, C.M. *Nature* **1999**, 399, 48.

(20) Landman, U.; Barnett, R. N.; Scherbakov, A. G.; Avouris, P. *Phys. Rev. Lett.* **2000**, 85, 1958.

(21) Marsen, B.; Sattler, K. *Phys. Rev. B* **1999**, 60, 11593.

(22) Menon, M.; Richter, E. *Phys. Rev. Lett.* **1999**, 83, 792.

(23) Fagan, S. B.; Barierle, R. J.; Mota, R.; da Silva, A. J. R.; Fazzio, A. *Phys. Rev. B* **2000** 61, 9994.

(24) Seifert, G.; Köhler, Th.; Urbassek, H. M.; Hernández, E.; Frauenheim, Th. *Phys. Rev. B* **2001**, 63, 193409.

(25) Frisch, M. J.; Trucks, G. W.; Schlegel, H. B.; Scuseria, G. E.; Robb, M. A.;.Cheeseman, J. R.; Zakrzewski, V. G.; Montgomery, Jr. J. A.; Stratmann, R. E.; Burant, J. C.; Dapprich, S.; Millam, J. M.; Daniels, A. D.; Kudin, K. N.; Strain, M. C.; Farkas, O.; Tomasi, J.; Barone, V.; Cossi, M.; Cammi, R.; Mennucci, B.; Pomelli, C.; Adamo, C;.Clifford, S.; Ochterski, J.; Petersson, G. A.; Ayala, P. Y.; Cui, Q.; Morokuma, K.; Malick, D. K.; Rabuck, A. D.; Raghavachari, K.; Foresman, J. B.; Cioslowski, J.; Ortiz, J. V.; Baboul, A. G.; Stefanov, B. B.; Liu, G.; Liashenko, A.; Piskorz, P.; Komaromi, I.; Gomperts,

R.; Martin, R. L.; Fox, D. J.; Keith, T.; Al-Laham, M. A.; Peng, C. Y.; Nanayakkara, A.; Gonzalez, C.; Challacombe, M.; Gill, P. M. W.; Johnson, B.; Chen, W.; Wong, M. W.; Andres, J. L.; Gonzalez, C.; Head-Gordon, M.; Replogle, E. S.; Pople, J. A. Gaussian 98, Revision A.7, Gaussian, Inc., Pittsburgh PA, 1998.

(26) Stewart, J. J. P. *J. Comput. Chem.* **1989**, 2, 209.

(27) Dewar, M. J. S.; Thiel W. J.; *J. Am. Chem. Soc.* **1977**, 99, 4899.

(28) Peng, H. Y.; Wang, N.; Zhang, Y. F.; Lifshitz, Y.; Kulik, J.; Zhang, R. Q.; Lee, C. S.; Lee, S. T. *App. Phys. Lett.* **2000**, 77, 2831.

(29) Qin, L. C.; Zhao, X.; Hirahara, K.; Miyamoto, Y.; Ando, Y.; Iijima, S. *Nature* **2000**, 408, 50.

(30) Wang, N.; Tang, Z. K.; Li, G. D.; Li, J. S. *Nature* **2000**, 408, 50.

(31) Zhang, R. Q.; Lee, C. S.; Lee, S.-T.; Lee *J. Chem. Phys.* **2000**, 112, 8614.

(32) Zhang, R. Q.; Costa, J.; Bertran, E. *Phys. Rev. B* **1996**, 53, 7847.

(33) Delley, B.; Steigmeier, E. F. *Phys. Rev. B* **1993**, 47, 1307.

Chapter 8
Conclusion

Since conclusions have been made in each Chapter, we will not comment on each chemical system individually here. On the other hand, different models of theory, namely, the G3 method, as well as its variants, and other theoretical methods have been employed to study the structures, bonding, and energetics of several interesting systems. We will now remark on the relative merits of these models.

In this thesis, we have employed the G3 method to study the heats of formation of $(CH)_6$ isomers and the structures, stability, and nature of bonding of isomeric N_7 nitrogen clusters and their singly charged cations and anions. We also study the dissociation mechanisms of dimethyl sulfide with this method. In general, good to excellent agreement between the G3 results and experimental data are obtained in most cases. In addition, both the G3 and G3X methods have been used to study the thermochemistry of chlorine fluorides, ClF_n, n = 1–7, and their singly charged cations and anions. We found that G3X gives more accurate results than G3 in the heats of formation calculations of hypervalent molecules. However, it is noted that the G3X method is computationally more expensive than the G3 method. Furthermore, we have applied the PM3 and rather crude ab initio methods such as HF/3–21G and HF/3–21G(d) to investigate the electronic structures of carbon and silicon nanotubes, carbon and silicon nanowires.

Since most of the calculated results obtained in this work are in good agreement with the available experimental data, and, based on the previous successes for the G2 and G3 methods, the unexpected large discrepancies between experimental and calculated results for some quantities reported in this thesis may not be due to the failure of the theoretical model. Rather, these discrepancies suggest that the experimental results may be inaccurate and deserve re–examination.

Appendix A

The Gaussian–3 Theoretical Models

The mathematical details of the Gaussian–3 (G3) methodology as well as the variant of the G3 method, G3(MP2) and G3X, are presented below.

A.1 The G3 Theory

The G3 energy is an approximation of the energy calculated at the ab initio QCISD(T)/G3large level. It involves geometry optimization at the MP2(Full)/6–31G(d) level. Also, vibrational frequency calculations at the MP2(Full)/6–31G(d) level for the zero–point vibrational energy (ZPVE), thermal corrections, and a semi–empirical higher–level correction (HLC) are required. Based on the optimized geometry, several single–point energy calculations are performed, and the G3 energy E(G3) is given as follows.

$$E(G3) = E_{base} + \Delta E(QCI) + \Delta E(+) + \Delta E(2df,p) + \Delta E(G3large) + \Delta E(SO) + 0.9661 \times ZPVE_{MP2} + HLC_{G3}, \quad (1)$$

where E_{base} = E[MP4SDTQ/6–31G(d)],

$\Delta E(QCI)$ = E[QCISD(T)/6–31G(d) – MP4SDTQ/6–31G(d)],

$\Delta E(+)$ = E[MP4SDTQ/6–31+G(d) – MP4SDTQ/6–31G(d)],

$\Delta E(2df,p)$ = E[MP4SDTQ/6–31G(2df,p) – MP4SDTQ/6–31G(d)],

$\Delta E(G3large)$ = E[MP2(Full)/G3large – MP2/6–31G(2df,p) – MP2/6–31+G(d) + MP2/6–31G(d)],

$ZPVE_{MP2}$ = ZPVE at MP2(Full)/6–31G(d),

$HLC_{G3} = -6.386\times10^{-3}n_\beta - 2.977\times10^{-3}(n_\alpha - n_\beta)$ and

$-6.219\times10^{-3}n_\beta - 1.185\times10^{-3}(n_\alpha - n_\beta)$

for molecular and atomic species, respectively. Here $n_\alpha \geq n_\beta$ and n_α and n_β are the numbers of α and β valence electrons, respectively.

$\Delta E(SO)$ is spin–orbit correction for atomic species, and is taken from experiment or accurate theoretical calculations in the case where no experimental data are available.

A.2 The G3(MP2) Theory

In the G3(MP2) procedure, the basis–set–extension corrections is obtained at the MP2 level, instead of the MP4 level in G3, thus eliminating the MP4 single-point calculations. The G3(MP2) energy E(G3(MP2)) is given as follows.

$$E(G3(MP2)) = E[QCISD(T)/6\text{–}31G(d)] + \Delta E_{MP2} + \Delta E(SO) + 0.9661 \times ZPVE_{MP2} + HLC_{G3MP2}, \quad (2)$$

where $\Delta E_{MP2} = E[MP2/G3MP2large - MP2/6\text{–}31G(d)]$,

$HLC_{G3MP2} = -9.729\times10^{-3}n_\beta - 4.471\times10^{-3}(n_\alpha - n_\beta)$ and

$-9.345\times10^{-3}n_\beta - 2.021\times10^{-3}(n_\alpha - n_\beta)$

for molecules and atoms, respectively.

A.3 The G3X Theory

The G3X method involves geometry optimization and vibrational frequency calculations at the B3LYP/6–31G(2df,p) level. In the energy calculations, apart from the five single–points carried out in the G3 model, an additional one, HF/G3Xlarge, is required. The G3X energy E(G3X) is given as follows.

$$E(G3X) = E_{base} + \Delta E(QCI) + \Delta E(+) + \Delta E(2df,p) + \Delta E(G3Xlarge) + \Delta E(SO) + 0.9854 \times ZPVE_{B3LYP} + HLC_{G3X}, \quad (3)$$

where $\Delta E(G3Xlarge) = E[MP2(Full)/G3large - MP2/6\text{–}31G(2df,p) - MP2/6\text{–}31+G(d) + MP2/6\text{–}31G(d) + HF/G3Xlarge - HF/G3large]$,

$ZPVE_{B3LYP}$ = ZPVE at B3LYP/6–31G(2df,p),

$HLC_{G3X} = -6.783\times10^{-3}n_\beta - 3.083\times10^{-3}(n_\alpha - n_\beta)$ and

$-6.877\times10^{-3}n_\beta - 1.152\times10^{-3}(n_\alpha - n_\beta)$

for molecules and atoms, respectively.

Appendix B

Calculation of Enthalpy at 298 K, H_{298}

The theoretical energies obtained with the Gaussian–n methods refer to isolated molecules at 0 K with stationary nuclei, while thermochemical measurements are carried out with vibrating molecules at finite temperature, usually 298 K. Hence, comparison of theoretical results with experimental data normally requires zero–point vibrational energy and thermal corrections. From statistical mechanics, and assuming ideal gas behavior, the difference between the enthalpy at finite temperature (H_T) and the energy at 0 K (E_0) is given by

$$H_T - E_0 = E_T^{trans} + E_T^{rot} + \Delta E_T^{vib} + RT$$

where $E_T^{trans} = (3/2)RT$,

$E_T^{rot} = (3/2)RT$ (for a non–linear molecule)

$E_T^{rot} = RT$ (for a linear molecule) or 0 (for an atom)

$$\Delta E_T^{vib} = E_T^{vib} - E_0^{vib}$$

$$= \sum_i^{3n-6} \frac{h\nu_i}{\exp(h\nu_i / kT) - 1}$$, where ν_i's are scaled harmonic frequencies.